



Technische Universität München

The role of inflammation and the intestinal microbiome in a mouse model of Barrett esophagus

Jonas Ingermann

Vollständiger Abdruck der von der Fakultät TUM School of Life Sciences der Technischen Universität München zur Erlangung des akademischen Grades eines

Doktors der Naturwissenschaften

genehmigten Dissertation.

Vorsitzender: Prof. Dr. rer. nat. Martin Klingenspor

Prüfer der Dissertation:

1. Prof. Dr. rer. nat. Dirk Haller
2. Prof. Dr. med. Michael Quante

Die Dissertation wurde am 29.06.2020 bei der Technischen Universität München eingereicht und durch die Fakultät TUM School of Life Sciences am 15.09.2020 angenommen.

Dedicated to my family and my lab family

Table of contents

Table of contents.....	I
Publications and Presentations.....	IV
Abstract.....	V
Zusammenfassung.....	VII
List of Figures.....	IX
List of tables.....	XI
1. Introduction.....	1
1.1 Anatomy and pathophysiology of the esophagus	1
1.1.1 Anatomy of the esophagus.....	2
1.1.2 Reflux disease and esophagitis	2
1.1.3 Barrett’s esophagus and esophageal adenocarcinoma	2
1.1.4 Incidence and prognosis of esophageal adenocarcinoma	4
1.1.5 Origin of Barrett’s esophagus and esophageal adenocarcinoma	6
1.1.6 Models of Barrett’s esophagus and esophageal adenocarcinoma.....	9
1.2 Inflammation and esophageal adenocarcinoma	11
1.2.1 Inflammation and the development of cancer.....	11
1.2.2 The role of inflammation in BE and EAC	15
1.3 The microbiome’s role in tumor development.....	17
1.3.1 Microbiome: Definition and core concepts	17
1.3.2 The role of the gastrointestinal microbiome in health and disease.....	18
1.4 Aims of this thesis.....	20
1.4.1 Aim 1: Investigation of the influence of the microbiome on the L2-IL-1 β mouse model	20
1.4.2 Aim 2: Effects of an anti-inflammatory treatment on the L2-IL-1 β mouse model	20
2. Material and methods.....	21
2.1 Mice	21
2.1.1 Holding	21
2.1.1.1 Specific-pathogen-free (SPF) facility	21
2.1.1.2 Versuchsanlage Tierernährung (VAT)	21
2.1.1.3 Germfree facility.....	22
2.1.1.4 Diets	22
2.1.2 Genotyping of mice.....	23
2.1.3 Bedding transfer.....	24

2.1.4	Anti-inflammatory treatment	24
2.1.5	Sacrificing and preparation of mice	25
2.1.6	Macroscopic scoring	26
2.2	Histology	27
2.2.1	Generation of FFPE sections	27
2.2.2	Hematoxylin and eosin (HE) staining	28
2.2.3	Immunohistochemistry (IHC)	29
2.3	Flow cytometry of immune cells	30
2.4	16S RNA sequencing and analysis	33
2.4.1	Overview of fecal samples	33
2.4.2	Sequencing	34
2.4.3	Analysis of 16S sequencing data based on IMNGS and RHEA	35
2.5	Statistical analysis	35
3.	Results	37
3.1	Microbial differences in the gut influence the development of esophageal cancer ...	37
3.1.1	Housing conditions define the phenotype, part I: VAT	38
3.1.2	Housing conditions define the phenotype, part II: SPF	43
3.1.3	Comparison of VAT and SPF housing of L2-IL-1 β mice	48
3.1.4	SPF during aging	51
3.1.5	Germfree housing of L2-IL-1 β mice abrogates the inflammatory phenotype ...	54
3.1.6	Bedding transfer is sufficient for a phenotype transfer	55
3.1.7	Predictive functional profiling	56
3.1.8	Potential indicator species associated with the L2-IL-1 β HFD phenotype could not be detected	58
3.1.9	Inflammatory signaling leads to increased Lgr5+progenitorcells	60
3.2	Anti-inflammatory treatment affects tumor progression	62
3.2.1	Anakinra attenuates the HFD phenotype	62
3.2.2	NSAIDs change the immune phenotype	63
4.	Discussion	67
4.1	The gut microbiome is changed in tumor bearing mice	67
4.2	Anti-inflammatory treatment could be used for chemoprevention in BE/EAC	71
4.2.1	Anakinra reduces IL-1 β mediated inflammation	71
4.2.2	Sulindac inhibits tumor formation by a change in immune cell profiles	72
5.	Conclusion and outlook	75
6.	References	76
7.	Appendix	100
7.1	p-values Unifrac VAT SPF	100

7.2 Indicator species.....	101
Curriculum vitae	102
Acknowledgments.....	103

Publications and Presentations

Parts of this thesis were presented on an international conference and have been published during the course of this thesis making an overlap of the data inevitable.

Presentation(s)

The gut microbiome influences progression from Metaplasia to Dysplasia in the IL-1 β mouse model of Barrett Oesophagus. Oral presentation at UEG Week 2018, 20-24 October 2018, Vienna

Publications

CXCR4 Is a Potential Target for Diagnostic PET/CT Imaging in Barrett's Dysplasia and Esophageal Adenocarcinoma. Hsin-Yu Fang, Natasha Stephens Münch, Margret Schottelius, **Jonas Ingermann**, Haibo Liu, Michael Schauer, Stefan Stangl, Gabriele Multhoff, Katja Steiger, Carlos Gerngroß, Moritz Jesinghaus, Wilko Weichert, Anja A. Köhl, Antonia R. Sepulveda, Hans-Jürgen Wester, Timothy C. Wang, Michael Quante. Clin Cancer Res, 2018.[1]

High-Fat Diet Accelerates Carcinogenesis in a Mouse Model of Barrett's Esophagus via Interleukin 8 and Alterations to the Gut Microbiome. Natasha Stephens Münch*, Hsin-Yu Fang*, **Jonas Ingermann***, H. Carlo Maurer, Akanksha Anand, Victoria Kellner, Vincenz Sahn, Maria Wiethaler, Theresa Baumeister, Frederik Wein, Henrik Einwächter, Florian Bolze, Martin Klingenspor, Dirk Haller, Maria Kavanagh, Joanne Lysaght, Richard Friedman, Andrew J. Dannenberg, Michael Pollak, Peter R. Holt, Sureshkumar Muthupalani, James G. Fox, Mark T. Whary, Yoomi Lee, Tony Y. Ren, Rachael Elliot, Rebecca Fitzgerald, Katja Steiger, Roland M. Schmid, Timothy C. Wang, Michael Quante. Gastroenterology. 2019. *Authors share co-first authorship [2]

Anti-inflammatory chemoprevention attenuates the phenotype in a mouse model of esophageal adenocarcinoma. Theresa Baumeister*, **Jonas Ingermann***, Natasha Stevens Münch, Hsin-Yu Fang, Akanksha Anand, Julia Strangmann, Roland M Schmid, Timothy C. Wang, Michael Quante. Manuscript in preparation. * These authors contributed equally to this work.

Abstract

The incidence of Esophageal Adenocarcinoma (EAC) is increasing, with the only known precursor lesion being Barrett's Esophagus (BE). BE describes the replacement of the squamous epithelium in the esophagus with columnar epithelium, likely mediated by inflammation. BE and EAC are associated with obesity and a western style diet through currently unknown mechanisms. However, there remains no way to identify patients at risk for EAC and thus no effective surveillance programs. As a consequence no preventive programs exist either. L2-IL-1 β mice are a model of BE and EAC which show accelerated tumor formation when fed with a high fat diet (HFD) without getting obese.

The aim of this thesis was to investigate if the gut microbiome plays a role in a HFD mediated and accelerated phenotype. L2-IL-1 β mice were raised in an open-cage facility (VAT), a specific pathogen free facility (SPF) and a germfree facility. Germfree L2-IL-1 β showed reduced tumor formation and inflammation. VAT mice showed a stronger phenotype than SPF mice, meaning the phenotype was intensified with decreasing the hygiene level. This data links inflammation and tumor formation to the presence of bacterial communities. 16S sequencing was performed for the VAT and SPF fecal samples to analyze the microbiome. β -diversity analysis showed separate clustering of HFD fed L2-IL-1 β mice in comparison to all other groups, due to a unique taxonomic profile. These microbiome changes in HFD fed L2-IL-1 β mice were linked *in silico* to functionality by performing a PICRUSt analysis creating a predictive metagenome. Significant differences found in the KEGG pathways in HFD fed L2-IL-1 β suggest a functional component contributing to BE and EAC development. While the mechanisms remain unclear these results show an influence of the gut microbiome on BE and EAC development in L2-IL-1 β mice and could potentially support patients screening. Furthermore inflammatory cytokines such as IL-8 are important mediators of the observed HFD induced phenotype possibly by influencing progenitor cells by the tumor microenvironment. The elimination of this microenvironment under germfree housing conditions showed a systemic effect on inflammatory signaling of the intestinal microbiome.

To investigate the feasibility of chemopreventive approaches in BE and EAC, L2-IL-1 β mice were treated with the IL-1 receptor antagonist Anakinra and the nonsteroidal anti-inflammatory drugs (NSAIDs) Aspirin (ASS) and Sulindac. Anakinra treatment proved the

concept that the L2-IL-1 β mice can be treated with anti-inflammatory drugs to reduce tumor progression. Both Aspirin (ASS) and Sulindac act on cyclooxygenase 2, a proinflammatory enzyme. A protective effect of both NSAIDs could be observed in HFD fed L2-IL-1 β mice with a marked change in the immune cell profile of Sulindac treated mice. Considering the results of the AspECT trial, where ASS with/without Esomeprazole was reducing the incidence of EAC, chemoprevention with NSAIDs seems a highly promising treatment strategy for a specifically symptomatic population.

In summary we could demonstrate that HFD alters the microbiome composition in the gut in L2-IL-1 β mice. Our novel concept of esophageal carcinogenesis proposes that the gut microbiome affects systemic inflammatory responses that maybe abrogated under germfree conditions. In conclusion, future studies need to further analyze the systemic effects of diet or microbiome changes in order to further develop anti-inflammatory (or antibiotic) preventive strategies for human patients.

Zusammenfassung

Die Inzidenz des ösophagealen Adenokarzinoms (esophageal adenocarcinoma=EAC) steigt an, wobei die einzige bekannte Vorläuferläsion der sog. Barrett-Ösophagus (Barrett's Esophagus=BE) ist. BE beschreibt den Austausch des Plattenepithels im Ösophagus durch Säulenepithel, welcher wahrscheinlich durch Entzündung vermittelt wird. BE und EAC sind mit Adipositas und einer Ernährung im westlichen Stil mit derzeit unbekanntem Mechanismen assoziiert. Allerdings gibt es aktuell keine Möglichkeit, Patienten mit einem Risiko für EAC zu identifizieren, weswegen es keine wirksamen Überwachungsprogramme gibt. Infolgedessen gibt es auch keine präventiven Programme. L2-IL-1 β Mäuse sind ein Modell für BE und EAC, die eine beschleunigte Tumorbildung zeigen, wenn sie mit einer fettreichen Diät (high fat diet=HFD) gefüttert werden, ohne adipös zu werden.

Ziel dieser Arbeit war es zu untersuchen, ob das Darmmikrobiom bei einem HFD-vermittelten und beschleunigten Phänotyp eine Rolle spielt. L2-IL-1 β Mäuse wurden in einer offenen Käfighaltung (VAT), einer spezifisch pathogenfreien Haltung (SPF) und einer keimfreien Haltung aufgezogen. Keimfreie L2-IL-1 β zeigten eine reduzierte Tumorbildung und Entzündung. VAT-Mäuse zeigten einen stärkeren Phänotyp als SPF-Mäuse. Es zeigt sich eine Verstärkung des Phänotyps bei abnehmendem Hygieniveau. Diese Daten verbindet Entzündung und Tumorbildung mit dem Mikrobiom. Zur Analyse des Mikrobioms wurde für die VAT- und SPF-Kotproben eine 16S-Sequenzierung durchgeführt. Die β -Diversitätsanalyse zeigte separates Clustering von HFD-gefütterten L2-IL-1 β -Mäusen im Vergleich zu allen anderen Gruppen, was auf ein einzigartiges taxonomisches Profil zurückzuführen ist. Diese Mikrobiomveränderungen in HFD-gefütterten L2-IL-1 β -Mäusen wurden *in silico* mit der Funktionalität in Zusammenhang gebracht, indem eine PICRUSt-Analyse durchgeführt wurde, die ein prädiktives Metagenom errechnet. Signifikante Unterschiede in den KEGG-Pathways in HFD-gefütterten L2-IL-1 β -Mäusen weisen auf eine funktionelle Komponente, die zur Entwicklung von BE und EAC beiträgt. Während die Mechanismen unklar bleiben, zeigen diese Ergebnisse einen Einfluss des Darmmikrobioms auf die BE- und EAC-Entwicklung bei L2-IL-1 β -Mäusen und könnten möglicherweise das Patienten-Screening unterstützen. Des Weiteren sind inflammatorische Zytokine, wie IL-8, wichtige Mediatoren des beobachteten HFD-induzierten Phänotyps, möglicherweise durch die Beeinflussung von

Vorläuferzellen durch die Tumormikroumgebung. Die Eliminierung dieser Mikroumgebung unter keimfreien Haltungsbedingungen zeigt eine systemische Wirkung auf die Entzündungssignalwege durch das Darmmikrobiom.

Um die Durchführbarkeit von Chemoprävention bei BE und EAC zu untersuchen, wurden L2-IL-1 β Mäuse mit dem IL-1-Rezeptorantagonisten Anakinra und den nichtsteroidalen Antirheumatika (nonsteroidal anti-inflammatory drugs =NSAIDs) Aspirin (ASS) und Sulindac behandelt. Die Behandlung mit Anakinra bewies das Konzept, dass L2-IL-1 β -Mäuse mit entzündungshemmenden Medikamenten behandelt werden können um die Tumorprogression zu reduzieren. ASS und Sulindac beeinflussen beide die Cyclooxygenase 2, ein proinflammatorisches Enzym. Eine protektive Wirkung beider NSAIDs konnte bei HFD-gefütterten L2-IL-1 β Mäusen beobachtet werden, wobei sich das Immunzellprofil von mit Sulindac behandelten Mäusen deutlich veränderte. In Anbetracht der Ergebnisse der AspECT-Studie, bei der ASS mit/ohne Esomeprazol die Inzidenz von EAC reduzierte, scheint die Chemoprävention mit NSAR eine vielversprechende Strategie zu sein, wenn man in der Lage ist, die richtige zu behandelnde Population zu identifizieren.

Zusammenfassend konnten wir zeigen, dass HFD die Mikrobiom-Zusammensetzung im Darm von L2-IL-1 β -Mäusen verändert. Wir schlagen ein neuartiges Konzept der Karzinogenese des Ösophagus vor, in dem das Darmmikrobiom systemische Entzündungsreaktionen beeinflusst, die unter keimfreien Bedingungen aufgehoben werden konnten. Zusammenfassend lässt sich sagen, dass zukünftige Studien die systemischen Auswirkungen von Ernährungs- oder Mikrobiomveränderungen weiter analysieren müssen, um antiinflammatorische (oder antibiotische) präventive Strategien für menschliche Patienten weiterzuentwickeln.

List of Figures

Figure 1: Overview over the human gastro-intestinal tract.	1
Figure 2: Schematic representation of Barrett’s esophagus and the corresponding histology	3
Figure 3: Epidemiologic features of EAC in the USA	5
Figure 4: Only a minority of EAC patients is identified by current screening	6
Figure 5: Models of the origin of Barrett’s esophagus	7
Figure 6: The inflammatory pathway.	12
Figure 7: Molecular mechanisms involved in tumor formation and progression.....	13
Figure 8: IL-1 β regulation and expression.....	14
Figure 9: Tumorigenic properties of IL-1 β	15
Figure 10: Schematic representation of inflammation causing cellular damage via oxidative stress.....	16
Figure 11: Distribution of the gastrointestinal microbiome in humans	18
Figure 12: Treatment plan for the treatment of L2-IL-1 β mice with Anakinra.....	25
Figure 13: Schematic representation of a mouse stomach.....	26
Figure 14 Schematic representation of sectioning and embedding of a mouse stomach.....	27
Figure 15: Representative gating strategy for immune cells of the myeloid lineage.....	32
Figure 16: Representative gating strategy for immune cells of the T-cell lineage.	33
Figure 17: Weighted UniFrac analysis of the microbiome at the squamous-columnar junction	37
Figure 18: Macroscopic analysis of VAT mice	38
Figure 19: Histologic analysis of VAT samples using HE staining	39
Figure 20: α -diversity of VAT samples	39
Figure 21: Generalized UniFrac using non-metric Multi-Dimensional Scaling of VAT samples.....	40
Figure 22: Taxonomic distribution of VAT samples	42
Figure 23: Common obesity associated phyla in VAT samples	43
Figure 24: α -diversity of SPF samples.....	44
Figure 25: Generalized UniFrac using non-metric Multi-Dimensional Scaling of SPF samples.....	45
Figure 26: Taxonomic distribution of SPF samples	46
Figure 27: Common obesity associated phyla in SPF samples.....	47

Figure 28: α -diversity of VAT and SPF samples.....	48
Figure 29: Generalized UniFrac using non-metric Multi-Dimensional Scaling of VAT and SPF samples.....	49
Figure 30: Generalized UniFrac using non-metric Multi-Dimensional Scaling of VAT and SPF samples.....	50
Figure 31: α -diversity of SPF samples during aging	51
Figure 32: Generalized UniFrac using non-metric Multi-Dimensional Scaling of SPF samples during aging	52
Figure 33: Common obesity associated phyla in SPF samples during aging	53
Figure 34: Histologic analysis of germfree and conventional L2-IL-1 β mice.....	54
Figure 35: Representative Ly6G and Ly6C IHC staining and quantification	55
Figure 36: Histologic analysis of bedding transfer samples compared with L2-HFD and L2-Control mice.....	56
Figure 37: Predictive KEGG pathway enrichment of 16S data from wildtype and L2-IL-1 β mice on chow, control diet and HFD using PICRUSt	57
Figure 38: Significant predictive KEGG pathways of 16S data from wt and L2-IL-1 β mice on chow, control diet and HFD using PICRUSt.....	58
Figure 39: Results of the LDA Effect Size (LEfSe) analysis of the 26 weeks timepoint of the SPF cohort.....	59
Figure 40: Results of the LDA Effect Size (LEfSe) analysis of the 26 weeks timepoint of the SPF cohort based on diet and genotype	59
Figure 41: CXCR2 and Lgr5 expression	60
Figure 42: Histologic analysis of Anakinra treated mice samples using HE and Ki67 staining.....	62
Figure 43: Macroscopic analysis of L2-IL-1 β mice treated with ASS or Sulindac.....	63
Figure 44: Histologic analysis of L2-IL-1 β mice treated with ASS or Sulindac.....	64
Figure 45: Analysis of immune cells of the myeloid lineage in L2-IL-1 β mice treated with ASS or Sulindac.....	65
Figure 46: Analysis of immune cells of the T cell lineage in L2-IL-1 β mice treated with ASS or Sulindac.....	66
Figure 47: Results of the LDA Effect Size (LEfSe) analysis of the 26 weeks timepoint of the SPF cohort based on the diet.....	101

List of tables

Table 1: Composition of experimental diets	22
Table 2: Thermocycler settings for genotyping of mice	24
Table 3: Genotyping primers	24
Table 4: Macroscopic scoring	26
Table 5: Protocol for hematoxylin and eosin staining.	28
Table 6: Description of the histologic scoring used to grade inflammation, metaplasia and dysplasia.....	28
Table 7: Primary antibodies and their properties for IHC	29
Table 8: Digestion buffers for tissue samples for flow cytometry.....	30
Table 9: Krebs-Ringer-Solution for digestion of esophagus samples for flow cytometry. .	30
Table 10: Antibodies used for staining in flow cytometric assessment of immune cells.	31
Table 11: Overview of fecal samples from the SPF used for 16S RNA sequencing (HFD=high fat diet)	34
Table 12: Overview of fecal samples from the VAT used for 16S RNA sequencing (HFD=high fat diet)	34
Table 13: p-values for generalized UniFrac using non-metric Multi-Dimensional Scaling of VAT and SPF samples	100

1. Introduction

1.1 Anatomy and pathophysiology of the esophagus

The gastro-intestinal tract is a long hollow tube, responsible for the fragmentation, digestion and uptake of food and fluids. Briefly, the oral cavity fragments and predigests the food, which is then transferred via the esophagus into the stomach. The stomach is an intermediate storage organ which also lyses protein. Most of the digestion occurs in the duodenum, while most of the resorption happens in the jejunum and the ileum, with these 3 parts forming the small intestine. The colon and rectum are mainly responsible for recovering water and are also called large intestine [4]. An overview of the gastro-intestinal tract is depicted in Figure 1. A more detailed description of the esophagus and the sequence of cancer development to esophageal adenocarcinoma will be found below, while the central role of microorganisms in the gastrointestinal tract will be further described in 1.3.

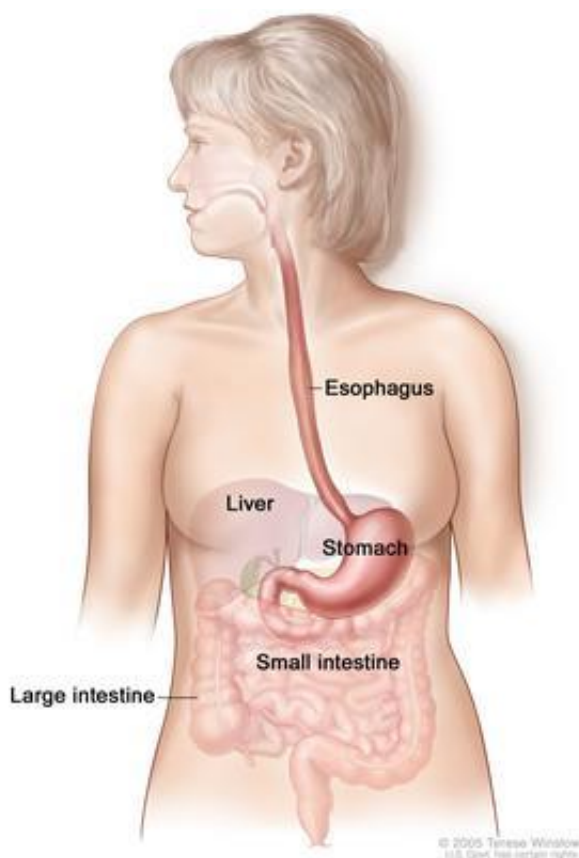


Figure 1: Overview over the human gastro-intestinal tract.
Figure taken from Pubmed Health [5]

1.1.1 Anatomy of the esophagus

The human esophagus is a 18-26 cm long muscular tube connecting the oral cavity and the stomach [6, 7]. Peristaltic movement of the esophagus transports food to the stomach [8]. The esophageal wall is made by 4 layers starting from the luminal side: mucosa, submucosa, muscularis propria, and adventitia [8]. In contrast to the rest of the gastrointestinal tract, the esophagus has no serosa [6, 8]. The esophageal mucosa is a non-keratinized squamous epithelium featuring submucosal esophageal glands [9]. At the lower esophageal sphincter the esophagus enters the stomach, above the squamous epithelium transitions to the columnar epithelium of the stomach at the so called Z-line or squamous-columnar junction [6].

1.1.2 Reflux disease and esophagitis

Gastroesophageal reflux disease (GERD) is defined as the reflux of gastric contents into the esophagus causing troublesome symptoms [10, 11]. The most common symptoms are heartburn and regurgitating, but patients may remain asymptomatic even though they have significant GERD. Chronic GERD is the main cause for esophagitis, commonly attributed to the damage caused to the esophageal epithelium by the acidic refluxate [12]. Another causative mechanism has been proposed (possibly in addition to the caustic damage by acids) where the epithelial cells of the esophagus are stimulated by the reflux to produce cytokines responsible for the tissue damage [13]. The current standard therapy for GERD and esophagitis is the treatment with proton-pump inhibitors, lowering the acidic content of the stomach and thus the refluxate [14, 15]. Bile acids originating from duodenal reflux into the stomach are another component of the refluxate damaging the mucosa [16, 17]. One possible consequence of GERD is Barrett's esophagus which can lead to esophageal adenocarcinoma.

1.1.3 Barrett's esophagus and esophageal adenocarcinoma

Barrett's esophagus (BE), a condition named after Norman Barrett, is characterized by columnar epithelium replacing regular squamous epithelium in the esophagus [18, 19]. Barrett originally suggested that the columnar epithelium represents intrathoracic stomach, however in 1953 this was contradicted, suggesting that it is gastric epithelium that lines the esophagus [18, 20]. Norman Barrett himself only agreed in 1957 to this notion [18]. Despite being described as early as 1805, the pathological relevance of columnar lined

epithelium in the esophagus has only been recognized in the 20th century [21, 22]. It is worth noting that some authors suggest that the use of columnar lined epithelium (CLE) should be preferred over the term “Barrett’s esophagus” as other authors seem to have described the condition earlier it is more descriptive and because Barrett himself never described endoscopic or histological properties of BE [21, 23]. Depending on national guidelines, the diagnosis of BE may or may not require the presence of intestinal metaplasia in histological samples, defined as the presence of goblet cells. US and German guidelines require the presence of intestinal metaplasia for BE to be diagnosed, while the British guidelines only require the presence of columnar lined epithelium [24-26]. Within this thesis the term “Barrett’s esophagus” will be used for columnar epithelium in the esophagus of mice and men with goblet (-like) cells, since it is still the most common term being used internationally and by our lab.

BE is diagnosed first by endoscopy, during which visible pink columnar epithelium is found above the gastro-esophageal junction and from which biopsies should be taken for histologic assessment, as depicted in Figure 2 [27].

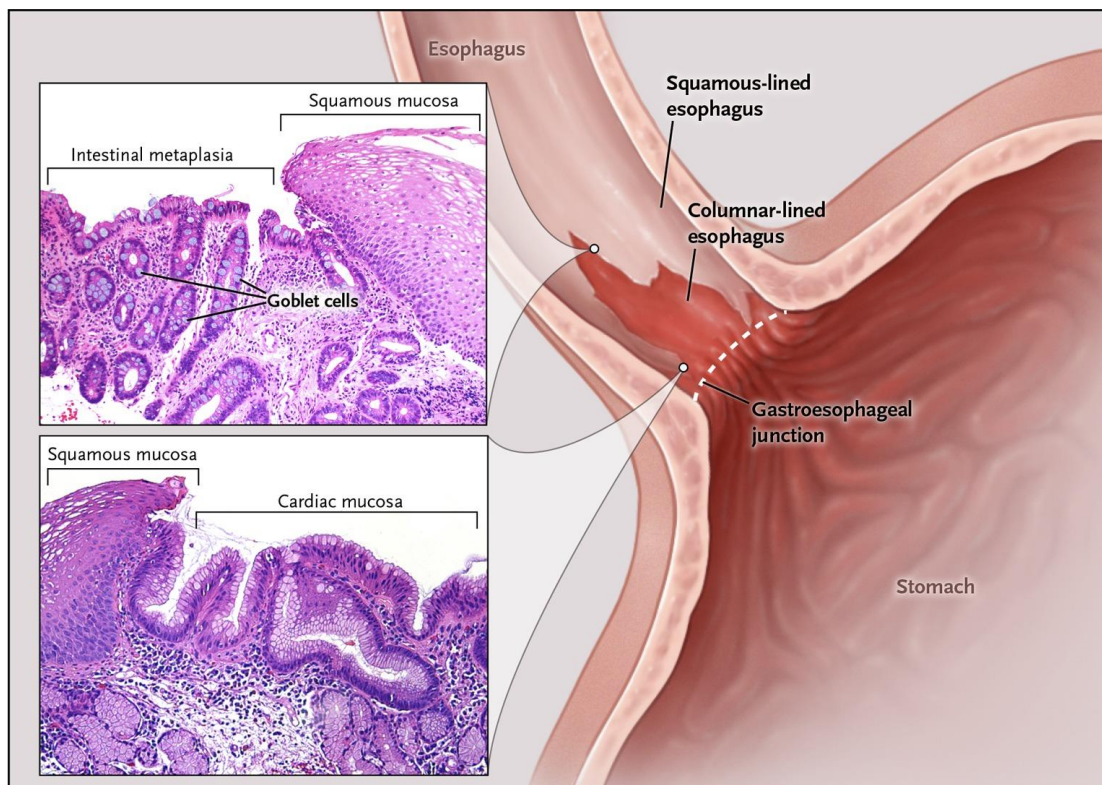
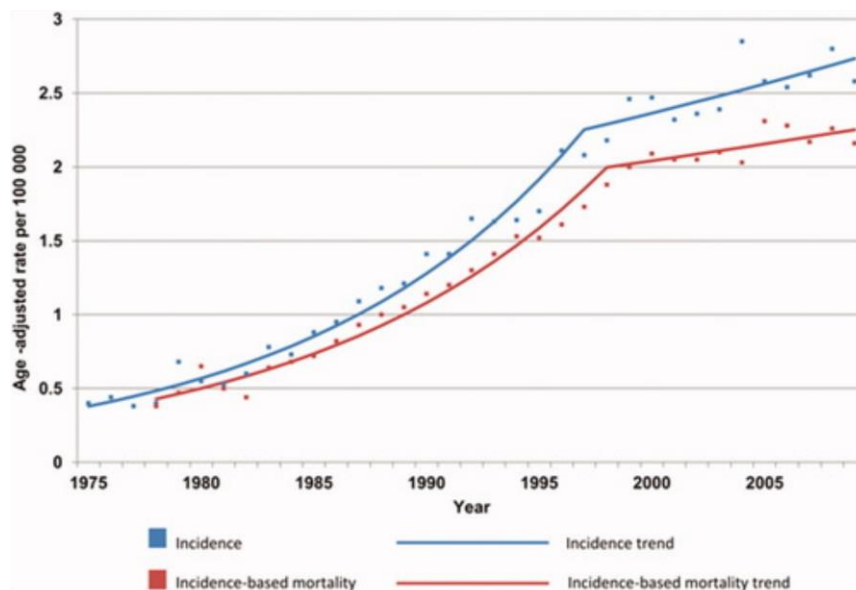
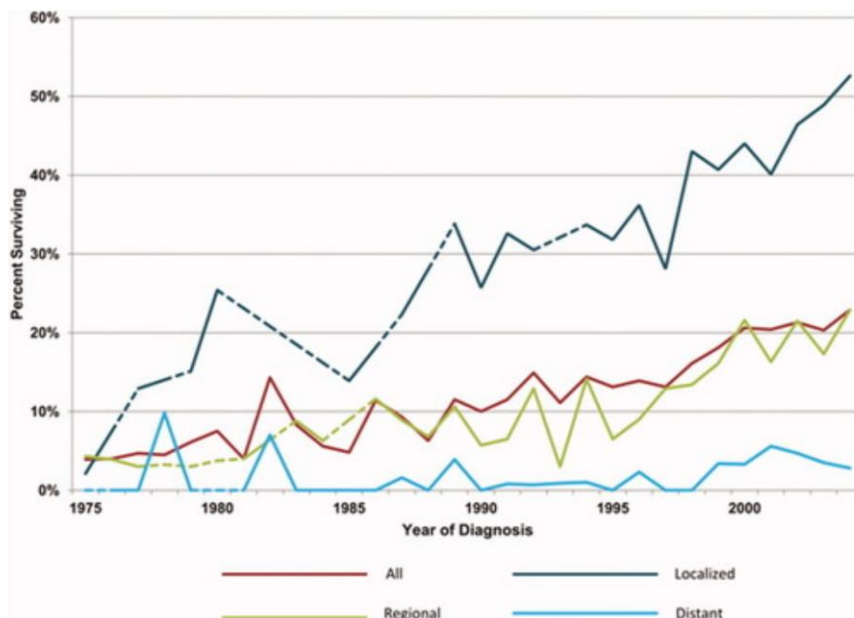


Figure 2: Schematic representation of Barrett’s esophagus and the corresponding histology
 At the dashed line the gastro-esophageal junction is defined endoscopically by the gastric folds. The HE stains show metaplasia characterized by goblet cells in the upper region and gastric mucosa in the lower region, both adjacent to normal esophageal squamous epithelium. Figure taken from [28]

Endoscopically BE is often separated into short segment BE which is less than 3 cm and long segment BE, which is longer than 3 cm [29]. BE is the only known precursor lesion for esophageal adenocarcinoma (EAC), however the progression rate is reported to be rather low in the range of 1.2-7 per 1000 person years [30-33]. This might be depending on the subgroup screened, since the progression rate seems to be related to the length of the BE segment, with very short segments (below 1 cm) rarely progressing to EAC [34, 35]. Non-dysplastic BE in general rarely progresses to EAC [35, 36]. Interestingly the length of a BE segment might be relatively stable over years, adding to the evidence that BE is only one factor for the development of EAC [37]. Currently BE is treated with proton-pump inhibitors or by endoscopic ablation [38]. Ablation can help to stop the progression of BE to EAC [39, 40].

1.1.4 Incidence and prognosis of esophageal adenocarcinoma

Currently, EAC is the most common form of esophageal cancer in the western world and has surpassed squamous cell carcinoma of the esophagus by its frequency, possibly due to the decrease in smoking, a known risk factor for squamous cell carcinoma [41]. Data from the US has shown a rising incidence of EAC in the past decades, as depicted in Figure 3 [42].

A**B****Figure 3: Epidemiologic features of EAC in the USA**

A: Incidence of EAC in the USA over the past decades **B:** Mortality of EAC in the USA over the past decades (adapted from [42])

The incidence of EAC in the western world has constantly been rising over the past decades, but a plateau effect has been suggested leading to stabilizing numbers of EAC cases [43]. The 5 year survival of EAC patients has increased, but remains poor [44]. EAC is known to be associated with age, male gender, Caucasian ethnicity, GERD, BE and obesity/dietary factors [44, 45]. Obesity in particular, is a factor that has been rising over the past decades, is easily influenced and seems to be highly relevant to the disease progression [46-48]. This might be due to increased intraabdominal pressure and thus

increased reflux, but this does not seem to be the only mechanism [49]. Current screening is limited to endoscopy and histologic analysis of BE segments, however it is unclear which patient group should be screened for EAC and how to identify that patient group which is complicating risk adapted screening for EAC. Only a minority of patients with BE progress to EAC and only a minority of patients with EAC has a history of BE, as depicted in Figure 4 [50].

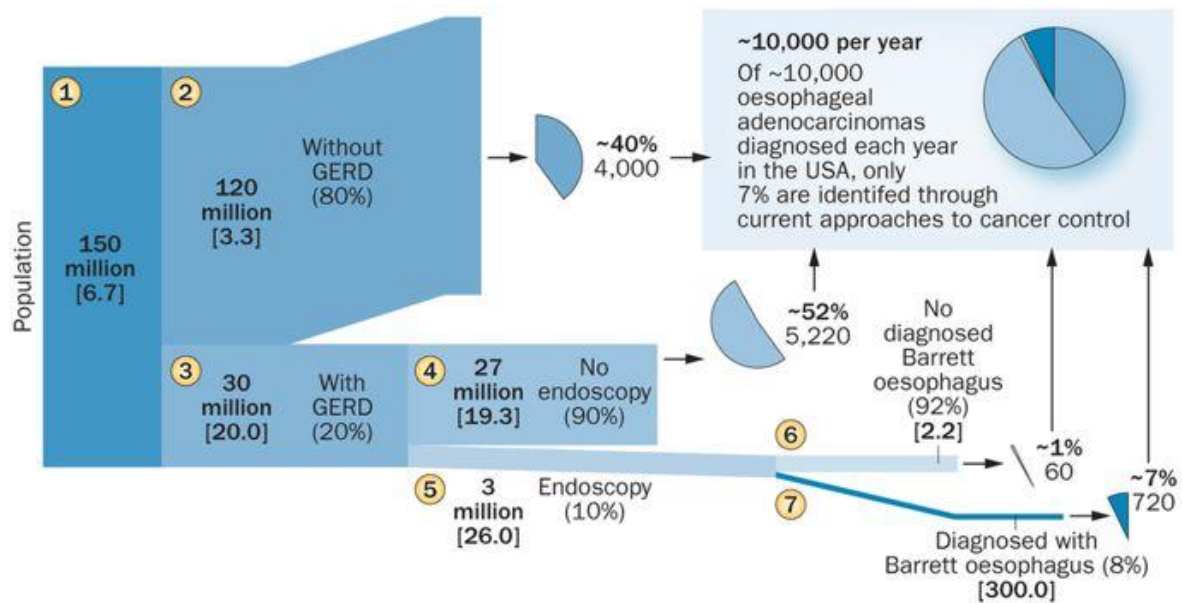


Figure 4: Only a minority of EAC patients is identified by current screening

The vast majority of EAC patients does present without a history of BE. Only 7% of all US cases have a history of GERD and BE. (Figure taken from [50])

It remains challenging to predict which patient group would benefit the most from screening for EAC due to the fact that the origin and development of BE and EAC is not fully understood and research in this field remains ongoing.

1.1.5 Origin of Barrett's esophagus and esophageal adenocarcinoma

Several hypotheses are published regarding the origin of BE and EAC, none of which have been finally proven. The commonly suggested and widely discussed concepts are depicted in Figure 5 and are discussed in more detail below.

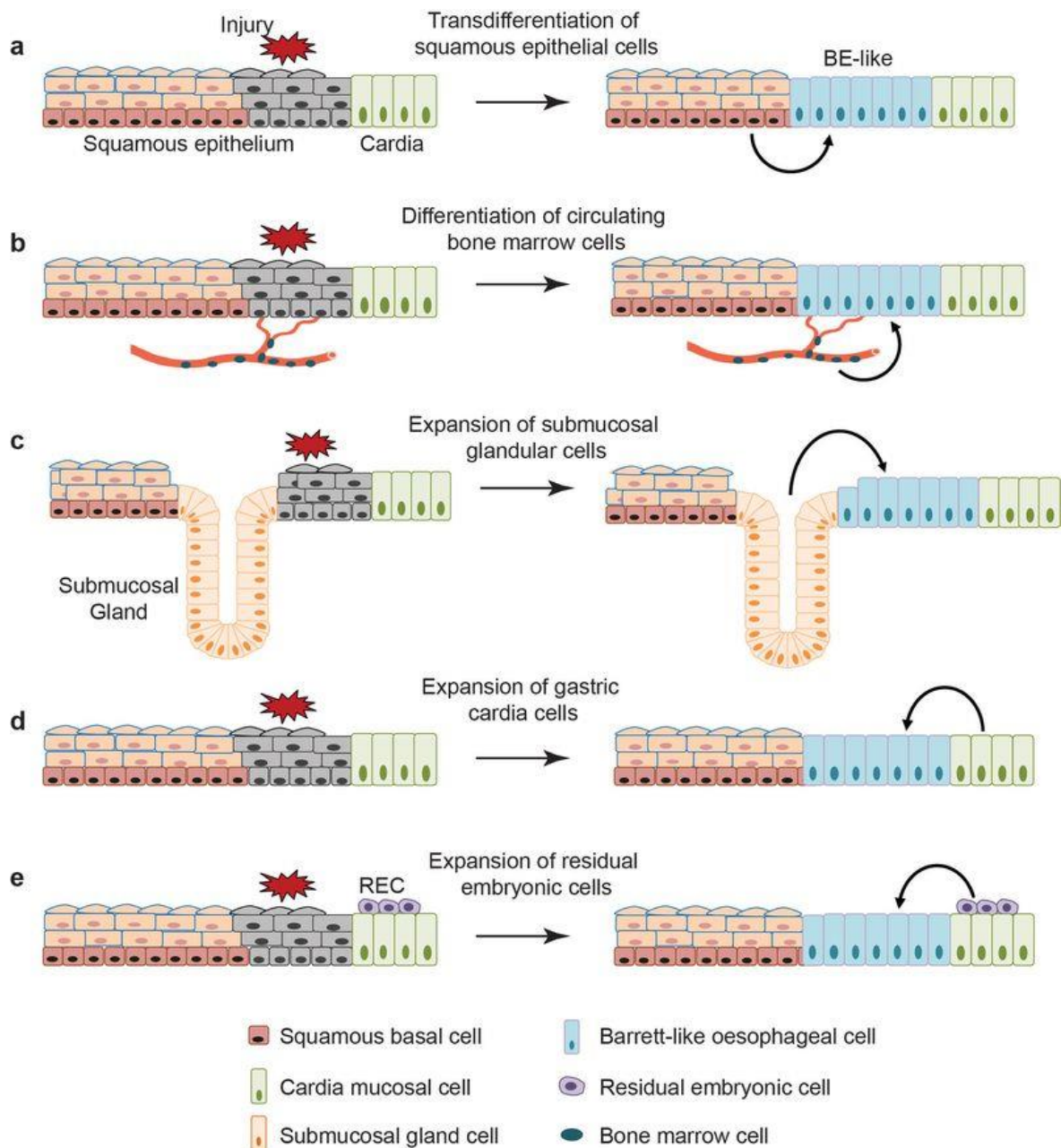


Figure 5: Models of the origin of Barrett's esophagus

A: Transdifferentiation of squamous epithelial cells **B:** Migration and transdifferentiation of bone marrow cells **C:** Expansion of submucosal glands **D:** Expansion of stem cells from the cardia **E:** Expansion of residual embryonic cells. Figure taken from [51]

One hypothesis proposes the transdifferentiation of squamous epithelial cell into columnar cells. Transdifferentiation refers to the transformation of a differentiated cell to another differentiated type of cell with or without a cell division in between [52]. The transdifferentiation of columnar epithelium of the esophagus to squamous epithelium occurs physiologically in the embryonic development of mice [53]. The inverse transdifferentiation from squamous epithelium to a (more) columnar epithelium has been shown in cell culture and in mice [54, 55].

Circulating bone marrow cells have been described to migrate across tissues, giving rise to different tissues, often in response to injury [56-59]. By now there is evidence suggesting that circulating bone marrow cells contribute to cancer development as an origin of tumor cells [60]. In a study of irradiated rats, bone marrow was transplanted and esophagojejunostomy was performed to induce BE, results showed that circulating bone marrow cells can take part in the formation of intestinal metaplasia in the esophagus [61]. Similar results could be shown in mice and also in a human case, where a male patient treated with a stem cell transplantation from a female donor later developed EAC with cells harboring two X chromosomes [62].

Submucosal glands have been proposed as an origin of BE [63]. Experiments in a canine model of BE have shown that columnar epithelium can rise after removal of the squamous epithelium, potentially from submucosal glands [64]. Following the submucosal glands into the BE epithelium has shown that a gradual morphological transition between the cells of the gland duct and the columnar epithelium can occur in humans [65]. Analysis of the genetic heterogeneity of crypts in human BE and EAC specimens has shown that BE is not a monoclonal disease and that a point mutation in a gland can be seen in adjacent BE epithelium, suggesting a contribution of submucosal glands to the development of metaplastic, columnar epithelium [66]. RNA sequencing of single cells has shown the similarity of cells from BE to cells from esophageal submucosal glands [67].

The gastric cardia is a short mucosal segment containing mucus glands at the gastro-esophageal junction, where the proximal stomach meets the distal esophagus, and seems to increase in length during inflammation [68]. It has been shown that a specific Lgr5 expressing stem cell population is present at the squamous-columnar junction in mice, which has also been described in the human cardia and BE [69-71]. This is the hypothesis on which the work presented in this thesis is based, since the mouse model used in this study has been shown to develop metaplasia originating from stem cells at the squamous-columnar junction [72].

p63 is thought to be essential for maintenance and morphogenesis of stratified epithelia and p63 deficient mice show erosion or loss of stratified epithelia due to the loss of regenerative cell populations maintained by p63 [73]. p63 deficient mice embryos present with BE like metaplasia and gene expression profiles similar to BE. Interestingly residual

embryonic stem cells are present at the squamous-columnar junction in mice and men and can migrate towards the squamous epithelium [74].

A recent publication suggests transitional basal cells as the origin of BE [51]. Briefly, the authors presented evidence for a transitional zone at the squamous-columnar junction with p63+KRT5+KRT7+ cells contributing to BE. This hypothesis is supported by lineage tracing experiments.

Even though there is a plethora of publications supporting most of the above mentioned hypothesis, none of them has been proven conclusively. This is why different models are currently being used to investigate and understand BE and EAC.

1.1.6 Models of Barrett's esophagus and esophageal adenocarcinoma

To understand the mechanisms responsible for the development of BE and EAC various models have been used. Several cell lines have been derived from BE and EAC tissues, i.e. OE33 and BAR-T, while normal esophageal cell lines like HET-1A have been established as well [75-77]. Most of the experiments performed with these cell lines were treatment experiments (e.g. with bile acids and/or different pH) to investigate the mechanism beneath the transition of normal tissue to BE and further to EAC [78-80]. In addition to these classic 2D cell culture experiments, novel techniques have been developed over the past years to expand the study of BE and EAC. Organotypic cultures try to mimic a physiological epithelium. A basal layer of fibroblasts and epithelial cells can grow to a multilayered epithelium with specific medium and the introduction of a liquid-air interface [81, 82]. This more complex system can be used for treatment with growth factors, shows a histology similar to the *in vivo* situation and allows the introduction of additional cell types, e.g. immune cells [83]. Another very promising and widely applied technology is the generation of 3D organoids. These are cells (often stem cells) embedded in a matrix and treated with growth factors to form 3 dimensional structures with spatially oriented, specialized cells [84, 85]. Organoids have been created from different tissues (e.g. stomach, kidney) and can be used for experiments with growth factors, other cell types and bacteria [86-92]. Other models, like using a porcine esophageal scaffold cultured with human epithelial cells and fibroblasts are published, but rarely used compared to the conventional cell culture techniques [93]. Given the limitations of cell culture based

approaches (limited cell types, limited interaction of different tissues, lack of the immune system), different animal models of BE and EAC have been developed and used by researchers.

While relatively rare, dogs can develop spontaneously BE and EAC [94, 95]. Most canine studies use surgical models of BE and EAC, sometimes accelerated by mimicking reflux [96, 97]. Though dog's esophagi are similar to human esophagi, the model is rarely used because of the difficulty of handling and the long progression times [98]. Interestingly baboons have naturally reflux and develop BE but not EAC [99, 100]. Those primates might be a useful model due to the close relationship to humans but primate research is cost intensive and ethically difficult [101]. Another animal model which is very similar to the human situation is the pig in which the esophagus is similarly structured as in humans [102]. Pigs would be a good model due to their evolutionary closeness to humans and the fact that recently transgenic pigs are possible e.g. by utilizing Crispr/Cas technology [103-105]. However, so far no models of BE and EAC in pigs have been reported. The most commonly used animal model in BE and EAC research are rats and mice.

Rats have been used since 1962 as a model for reflux disease, when surgical anastomosis was used to prove the importance of duodenal reflux for the development of esophagitis [106]. This surgical intervention is able to develop into a BE like phenotype via a multilayered epithelium [107, 108]. Addition of known carcinogens leads to an increase in tumor incidence and highlights the importance of duodenal reflux for the development of EAC [109]. Surgical mouse models have only been used over the last decades, likely due to the increased difficulty of performing surgery [110]. A new model drastically reducing the mortality has been recently developed, where neodymium magnets are implanted in the esophagus and the jejunum, leading to fistula formation due to pressure necrosis [111]. Similar surgical models have also been developed in mice [111-113]. Other models utilize a Zinc-deficient diet in addition to the treatment with bile acids to generate a BE like phenotype [114].

Genetic models of cancer have become available over the last years, mainly due to the sequencing of the mouse genome and the development of techniques to manipulate the mouse genome [115]. Genetic modification of mice has been combined successfully with surgical techniques. In 1999 total gastrectomy with esophagojejunostomy was performed in p53 knock-out mice, leading to 2/4 mice developing EAC [116]. A similar experiment

was performed on p27 knock-out mice, where the mice were treated with the carcinogen N-methyl-N-benzyl nitrosamine after esophagojejunostomy leading to BE and EAC formation [117]. Another approach used epithelial cells and fibroblasts grown from the esophagus of *Sonic hedgehog* transgenic mice on a decellularized rat trachea implanted beneath the skin of immunodeficient mice. This leads to a more columnar phenotype of the epithelium [118]. p63 deficient mice are embryonically lethal, but present with BE like metaplasia in the esophagus [74]. The model used in this thesis is a transgenic mouse model, in which human IL-1 β is expressed under the control of the EBV-L2 promotor. This leads to continuous inflammation in the esophagus and leads to BE and EAC, which can be accelerated by bile acids and/or nitrosamines [72]. This is highly similar to the human situation where inflammation is considered to be a central driver of BE and EAC [119-121]. A recently developed model uses doxycyclin inducible CDX2 overexpression in the transitional basal cells to investigate BE [51]. Interestingly most of the models support an involvement of inflammation in the development of EAC, highlighting the relevance of inflammatory processes and supporting the use of L2-IL-1 β mouse model for investigating the link between inflammation and EAC.

1.2 Inflammation and esophageal adenocarcinoma

While cancers are highly diverse regarding location and development, they often share the hallmarks of cancer: self-sufficiency in growth signals, insensitivity to growth-inhibitory (antigrowth) signals, evasion of programmed cell death (apoptosis), limitless replicative potential, sustained angiogenesis, and tissue invasion and metastasis [122]. In an update of these hallmarks, inflammation and avoiding immune destruction have been presented as emerging hallmarks, highlighting the importance of inflammatory processes in cancer development [123].

1.2.1 Inflammation and the development of cancer

The notion that inflammation is associated with cancer seems to be an old concept, apparently dating back to 1863 and Rudolf Virchow [124, 125]. Nowadays it is thought that chronic infection and inflammation contribute to about 25% of all cancers worldwide [126]. Inflammation is a physiological process which does not necessarily lead to a pathological outcome. A schematic representation of inducers and effectors within the inflammatory pathway is depicted in Figure 6.

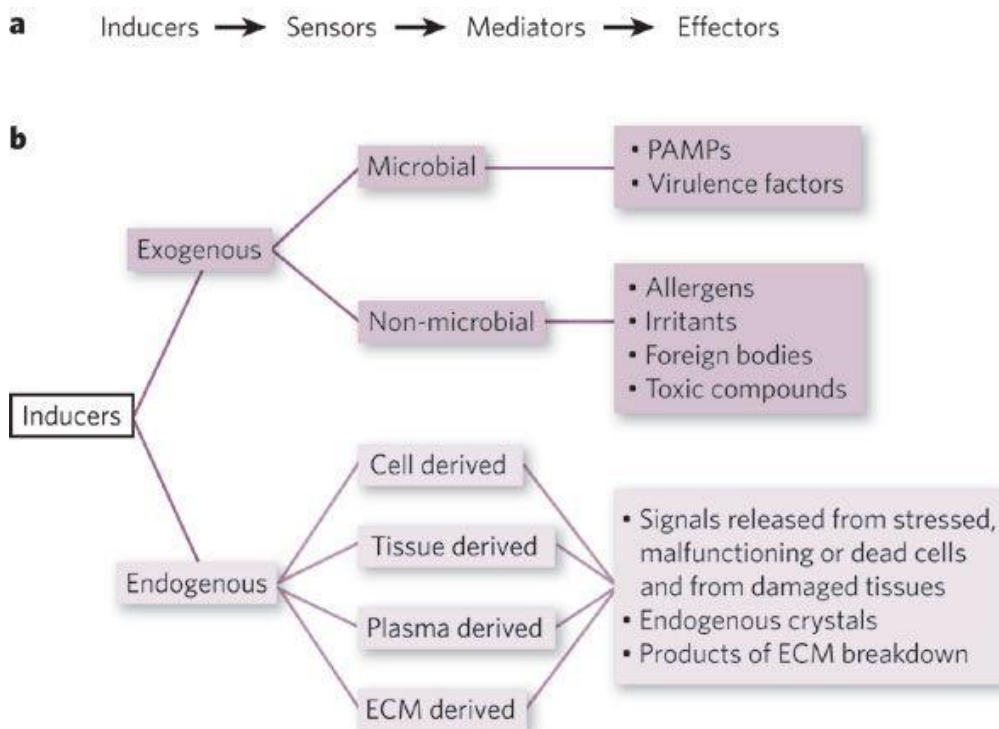


Figure 6: The inflammatory pathway.

a generic inflammatory pathway consists of inducers, sensors, mediators and effectors.. **b** Inducers of inflammation can be classified as exogenous or endogenous, and these two groups can be further classified as shown. ECM, extracellular matrix; PAMP, pathogen-associated molecular pattern. (Figure and legend from [127])

Bacterial infection leads to the activation of pattern recognition receptors, such as the Toll-like receptors mainly present on immune cells [128]. This leads to a signaling cascade involving e.g. NF- κ B which translocates to the nucleus and regulates the expression of inflammatory cytokines [129]. These cytokines recruit and activate immune cells, such as neutrophilic granulocytes (neutrophils) which target and destroy the bacteria [130]. As another example, inflammation is involved in the process of tissue repair, where after injury mainly macrophages produce important growth factors for tissue regeneration [131]. Normally the inflammatory reaction is resolved once infection has been repelled or the wound is healed, though sometimes the reaction persists and becomes chronic. Chronic inflammation is associated with a wide range of diseases such as metabolic syndrome, liver fibrosis and cancer [132-134].

Cancer is linked to chronic inflammation through various molecular mechanisms. The central player NF- κ B (as shown in Figure 7) is activated by oxidative and inflammatory

signals, leading to phosphorylation and degradation of I κ B α and a translocation of NF- κ B into the nucleus [135].

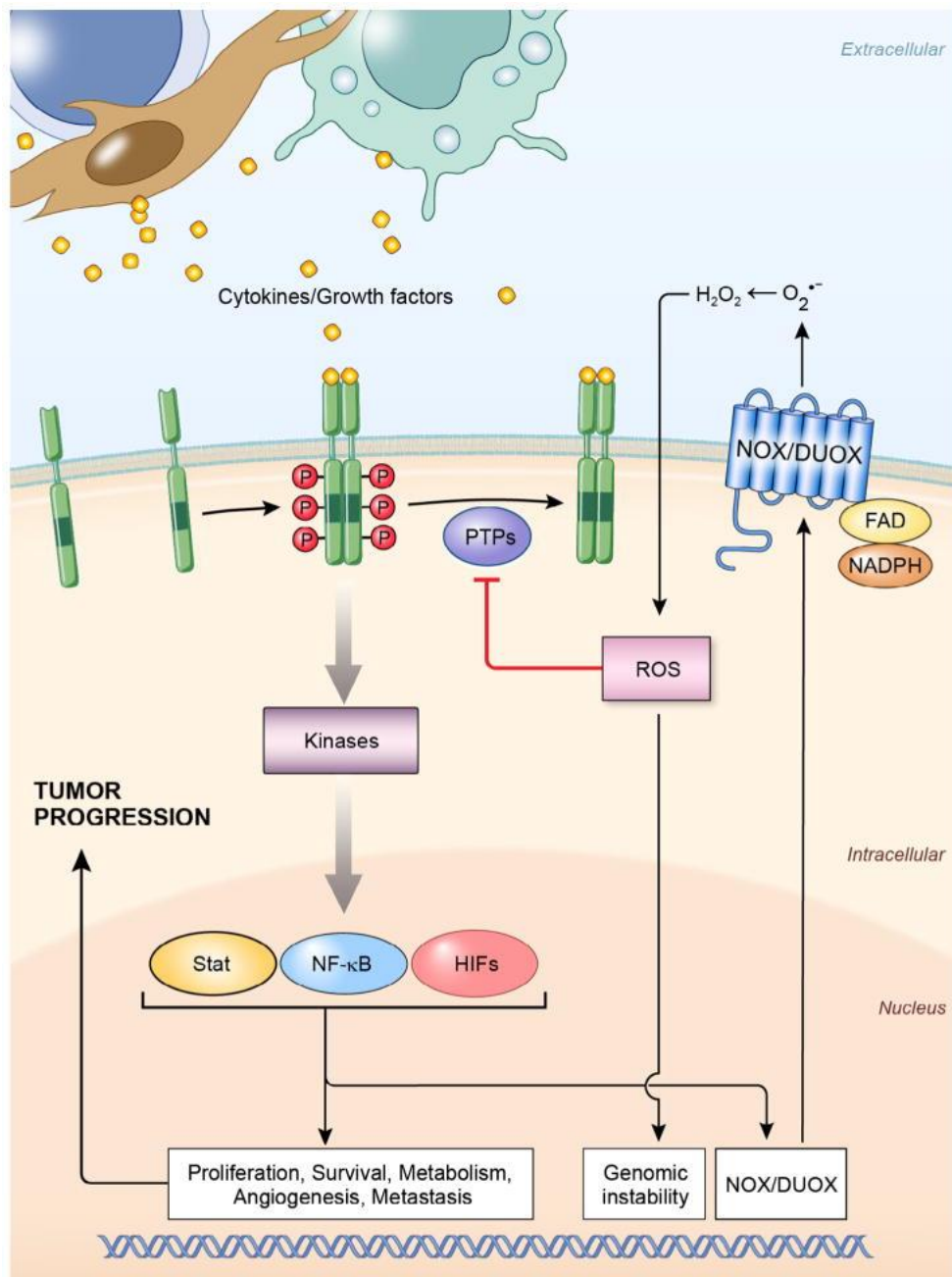


Figure 7: Molecular mechanisms involved in tumor formation and progression.

Cytokines and reactive oxygen species regulate NF- κ B signaling and regulate tumor development (Figure from [134])

NF- κ B signaling seems to be activated in most tumors and targets anti-apoptotic signaling, inflammatory mediators, regulators of invasion and DNA damage repair [136, 137]. It has to be considered though that NF- κ B signaling is not only relevant in the tumor cells, but also in immune cells, as has been shown in experimental colitis in mice, where the

inactivation of NF- κ B in the epithelium leads to less tumor formation, but the inactivation in myeloid cells leads to a reduction in tumor size [138]. This led to the conclusion that it depends on cell type and cell environment whether NF- κ B signaling has tumor supporting or tumor repressing properties.

Interleukins are a group of cytokines that consist of more than 50 different proteins, having pro- and anti-inflammatory properties depending on the involved cell types [139]. Interleukin-1 β is mainly active in immune cells, involved in NF- κ B signaling and regulated by inflammatory signals as depicted in Figure 8.

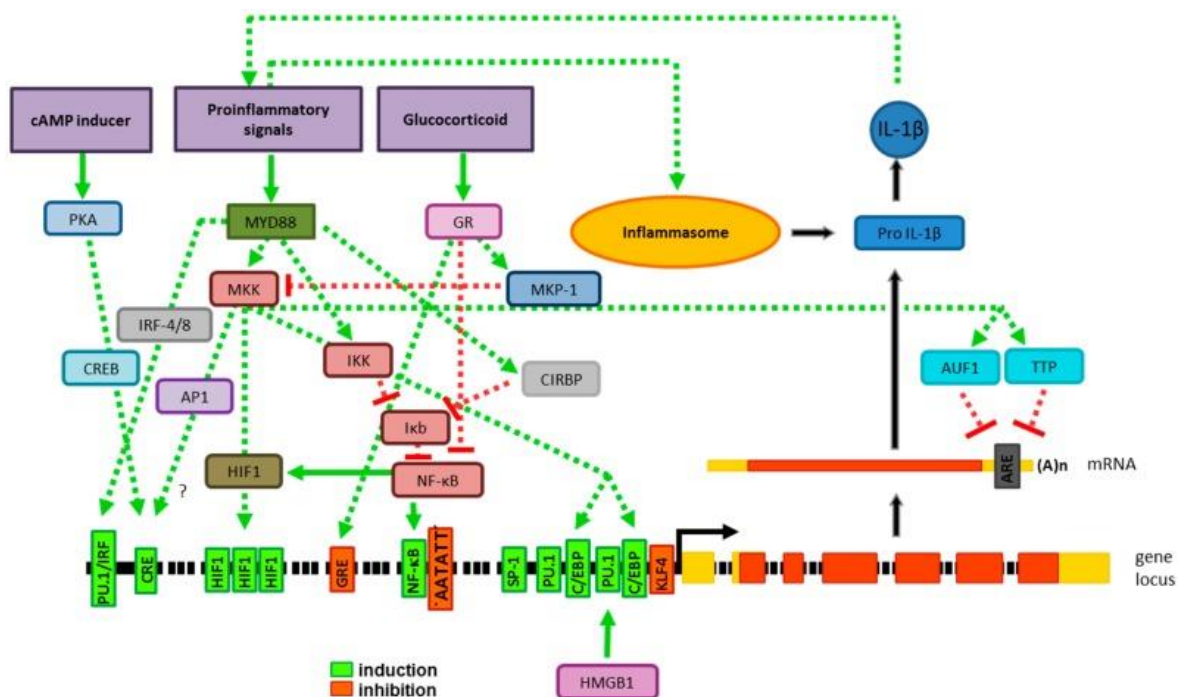


Figure 8: IL-1 β regulation and expression

Transcriptional and posttranscriptional regulation results in expression of functionally inactive pro-IL-1 β . Stimulatory (green) and inhibitory (red) activities exerted by stimuli, signaling adaptors and TF are indicated by arrows. TF binding sites (boxes) within the IL-1 β gene promoter that induce (green) or inhibit (orange) gene expression are named. The transcription start site is drawn (black arrow). Exons (boxes) encompass non-coding (yellow) and protein-coding (orange) regions. The derived IL-1 β mRNA, and the location of the AU-rich elements (ARE) engaged by RNA-binding proteins are depicted. Pro-IL-1 β is cleaved by active inflammasomes which yields bioactive IL-1 β . (Figure and Figure legend from [140])

IL-1 β expression is regulated on two levels. First mRNA expression is mainly activated by MYD88, which is downstream to receptors reacting to extracellular stimuli such as TLR, TNF α or even IL-1 β signaling [141-143]. MYD88 also interacts with NF- κ B signaling and can thus promote IL-1 β as an reaction to NF- κ B [144]. In addition it seems to be possible, that IL-1 β is not only regulated on the mRNA level by the expression, but also by changes to the half-life of the IL-1 β mRNA itself. IL-1 β and TNF- α stimulation of neutrophils can

lead to an increased half-life, while IL-4 seems to reduce it in monocytes [145, 146]. The translated pro-IL-1 β needs to be further processed. The canonical pathway starts with the activation of cytoplasmic receptors, such as NLRP3, which is activated by Lipopolysaccharides (LPS) [147]. As a consequence inflammasomes are formed and recruit Caspase-1 which cleaves pro-IL-1 β leading to the active form IL-1 β [148]. IL-1 β activates the IL-1 receptor family at the cell membrane, namely IL-1R1, which is mainly expressed on immune cells and epithelial cells and can be antagonized by IL-1 receptor antagonist (IL-1RA) [149]. While IL-1 β is considered to be a pro-inflammatory cytokine crucial in inflammation, its role in cancer development is ambiguous. IL-1 β seems to have anti-tumorigenic properties, since injection of IL-1 β into tumors has been described to have a positive effect on tumor regression [150, 151]. This is possibly due to necrosis but also leads to severe side-effects [152, 153]. On the other hand, possibly in the setting of chronic inflammation, IL-1 β has tumorigenic properties mainly by modifying the tumor microenvironment, as depicted in Figure 9.

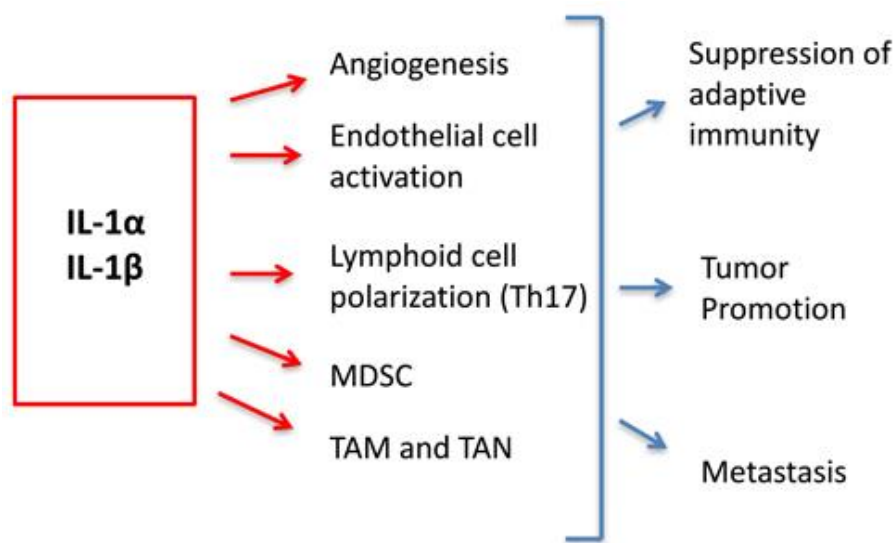


Figure 9: Tumorigenic properties of IL-1 β

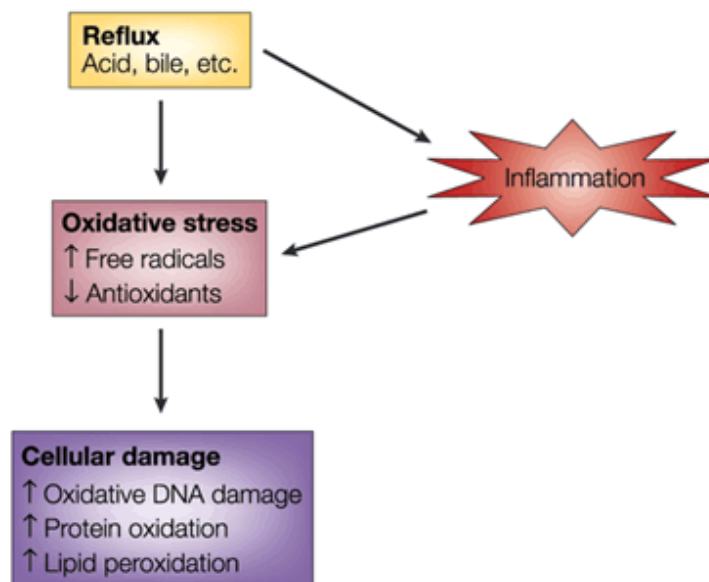
Mechanisms by which IL-1 β affects changes in the tumor microenvironment promoting tumor formation, growth and metastasis (Figure adapted from [154])

In summary the role of inflammation, often driven by IL-1 β and NF- κ B, is ambiguous and seems to be depending on the context within the local microenvironment.

1.2.2 The role of inflammation in BE and EAC

Inflammation plays a large role in the development of various malignancies. Since BE is often associated with reflux disease (both gastric and duodenal), bile acids in the reflux are

thought to support inflammation by the activation of COX and Notch signaling [72, 155]. COX signaling also plays a role in the reaction to oxidative stress and as a consequence anti-oxidative agents have experimentally shown to be protective against BE and EAC [156, 157]. This is possibly due to DNA damage and oxidative processes induced by inflammation, as depicted in Figure 10.



Nature Reviews | Cancer

Figure 10: Schematic representation of inflammation causing cellular damage via oxidative stress
 Reflux and inflammation are causing oxidative stress by free radicals which lead to DNA damage (Figure taken from [158])

Since obesity is an important factor associated with BE and EAC, various links between obesity, inflammation and BE/EAC have been established. One hypothesis states that increased reflux due to increased intraabdominal pressure supports inflammation and tumor development [159-161]. Another hypothesis is that fat, functioning as a physiologically active tissue, leads to a chronic systemic low level inflammation associated with increased serum values of pro-inflammatory cytokines such as IL-6 or TNF- α , which likely influence tumor development [162-164]. The concept of systemic inflammation is supported by data that shows increased cytokine and adipokine levels in plasma samples were associated with an increased hazard ratio to develop EAC and BE respectively [120, 165, 166]. Increased IL-8 level in the esophageal tissue have been demonstrated to be associated with esophagitis, reflux disease, BE and EAC [167, 168]. IL-1 β is also present in inflamed esophageal mucosa after acidic injury, possibly mediated by IL-6 expression

[169-171]. The inflamed area then forms a microenvironment in an interplay with immune cells, epithelial cells and mesenchymal cells, which mediate and resolve the inflammation, chronic inflammation and tumor formation [170, 172-174]. This suggests that BE and EAC formation depends on inflammation and not only on tissue damage caused by reflux [13, 72]. While epithelial cells often are in contact with bacteria, viruses and fungi (especially in the digestive tract), not much is known about the role of these microorganisms in the development of BE and EAC.

1.3 The microbiome's role in tumor development

1.3.1 Microbiome: Definition and core concepts

The microbiome is originally defined as the entirety of all microorganisms in a specific habitat, including bacteria, viruses and fungi [175]. However some authors refer to the microbiome as the collective genome of the microorganisms in a habitat and use the term microbiota to describe the organisms themselves [176]. In current literature the terms microbiome and microbiota are often used synonymously or following one of the presented definitions. In this work the term microbiome will be used to refer to the genomes, functions and products of the microbiota [177]. The human microbiome project aimed to investigate the human microbiome across the whole body, whereas most other studies focus on a particular organ of interest [176]. Both kind of studies provide valuable insight in the understanding of the role of the microbiome in health and disease. The term dysbiosis is often used to describe changes in the microbiome associated with a pathogenic phenotype [178]. Often there is no clear definition of dysbiosis due to the lack of a definition of how exactly a healthy microbiome should be composed, which is based on the lack of knowledge and lack of functional data. In studies a dysbiotic microbiome is mostly defined by its association with a pathologic phenotype. A commonly used proxy for a dysbiotic microbiome is one with a reduced microbial diversity. An extreme example is (recurrent) *Clostridium difficile* infection, where *C. difficile* often is the dominating species and the disease can be cured by the restoration of a healthy gut microbiome [179-181].

To understand functional implications, microorganism are being cultured, however due to the fact that most bacteria are not yet cultivable, genomic and transcriptomic technologies are currently being used to analyze the microbiome and its functions [182-184]. The microbiome has been shown to play various roles in health and disease in a wide range of

processes, e.g. cancer, neurobiological behavior (anxiety, depression) and metabolic phenotypes [185-189]. While some of these associations remain controversial, it is widely acknowledged that the microbiome of the gut is a highly relevant player in health and disease.

1.3.2 The role of the gastrointestinal microbiome in health and disease

While most surfaces of mammals are colonized by a microbiome, the amount of microorganisms and their relevance is most clearly described in the gastrointestinal tract [190, 191]. As depicted in Figure 11, there is an observable gradient in the microbiome density along the human gastrointestinal tract.

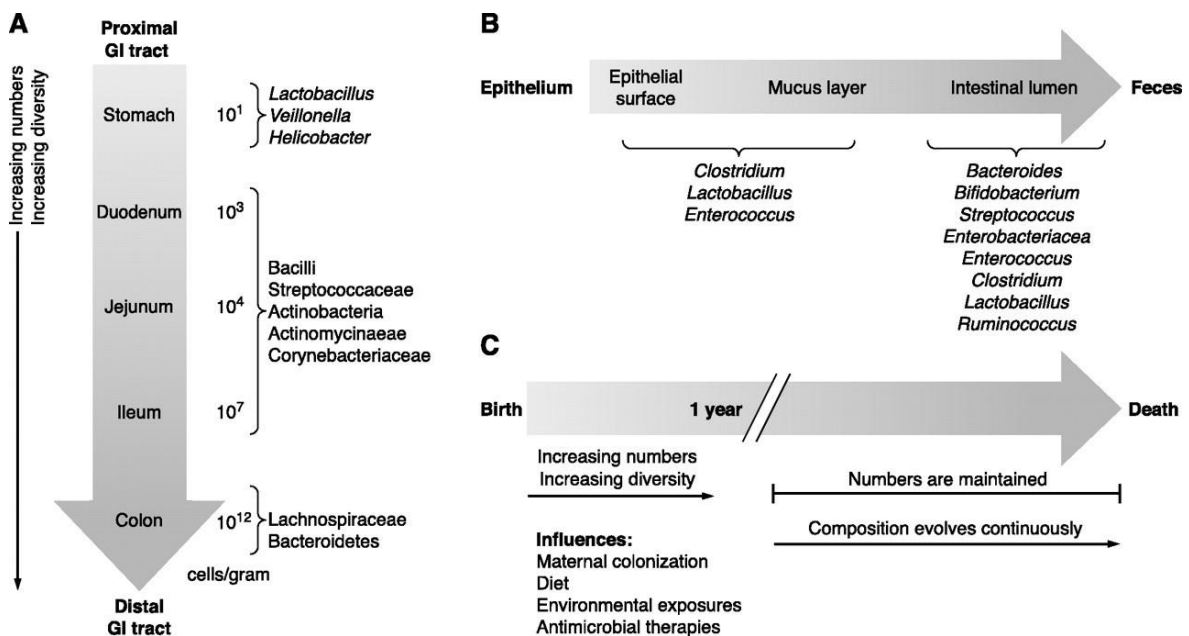


Figure 11: Distribution of the gastrointestinal microbiome in humans

A: Density and diversity of the microbiome along the gastrointestinal tract **B:** Distribution of bacterial species ranging from the epithelium to the lumen **C:** Establishment, influences on and stability of the gastrointestinal microbiome (Figure taken from [192])

The stomach is the least colonized compartment of the human gastrointestinal tract and the number of bacterial cells vastly increases distally, with a shift in the composition of the bacterial families observed. Due to changes in the local environment, there is also a gradient of bacterial families observed reaching lumenally from the epithelium. The microbiome is thought to be largely stable after weaning and the beginning of adult eating habits, though the composition might be changing due to e.g. diet, environmental influences or antibiotic treatment [193, 194].

It is widely known, that the gut microbiome is essential for the digestion and metabolizing of nutrients in the gut. It has been shown that obesity can be induced in germfree mice through the bacterial transfers from either obese men or mice with changes in the *Firmicutes:Bacteroidetes* ratio in interaction with dietary contents [195-197]. Possible mechanisms include short chain fatty acids which are produced by the microbiome and can act via the gut-brain axis [198]. While the associations with obesity and metabolic disease are highly relevant, there is also increasing evidence for the involvement of the gut microbiome in cancer. Colorectal cancer is a common cancer which is rarely inherited and is associated with a low intake of fiber and high intake of protein [199]. Additionally it has been shown that the fecal microbiome of patients with colorectal cancer is changed compared to healthy controls [200-202]. One causative mechanism might be that bacteria are able to influence the gut epithelium by causing inflammation [203, 204]. While the exact contribution of the microbiome and the interplay with other factors (e.g. genetics, nutrition) is not known in detail, it's relevance in colorectal cancer is well described [205, 206].

In contrast to the well-established relevance of the microbiome in gut disease, relatively little is known about the relevance of the microbiome in BE and EAC. The normal microbiome within the human esophagus is relatively small compared to the lower digestive tract, but possibly diverse [207]. Early studies reported changes of the local microbiome linked to BE and other risk factors such as obesity [208, 209]. A lower diversity of the microbiome or possibly single strains (such as *Fusobacterium nucleatum*) in the esophagus has been reported to be detrimental [210-212]. Interestingly the treatment of reflux disease with proton pump inhibitors also influences the local microbiome, likely due to the pH changes [209, 213, 214]. While very little is known about the microbial mechanisms influencing the formation of BE and EAC, nitric oxides and nitrosative stress have been suggested as a responsible mechanism [215, 216]. The interplay of nutrition, the microbiome and inflammation is not fully explained yet and was thus a focus of this thesis.

1.4 Aims of this thesis

1.4.1 Aim 1: Investigation of the influence of the microbiome on the L2-IL-1 β mouse model

The first aim was to investigate the role of the microbiome and purified diets in BE and EAC. While it is known that changes in the microbiome and diet are associated with intestinal disease, little is known about the microbiomes influence on esophageal disease formation. The focus of this part was about detecting differences in the microbiome between different strength of phenotypes in the L2-IL-1 β mouse and investigating possible causative links.

1.4.2 Aim 2: Effects of an anti-inflammatory treatment on the L2-IL-1 β mouse model

The second aim was to investigate the influence of anti-inflammatory prevention (such as Anakinra, Sulindac and Aspirin) on L2-IL-1 β mice. Since inflammation is likely a central driver for esophageal carcinogenesis, anti-inflammatory treatment is a potential preventive measure. While Anakinra directly inhibits IL-1 β signaling, Sulindac and Aspirin are more common anti-inflammatory drugs that act on COX signaling. The focus of this part was to observe changes in inflammation and dysplastic lesion formation to investigate which of these drugs could be of use to prevent the development of EAC in patients.

2. Material and methods

2.1 Mice

All animal experimental work performed in Germany was carried out with the approval of the Regierung Oberbayern according to the animal experimental permits (Tierversuchsanträge) 55.2.1.54-2532-125-12 and 55.2-1-54-2532-24-2016. L2-IL-1 β mice express human IL-1 β under the control of the EBV-L2 leading to continuous inflammation in the esophagus BE and EAC [72]. L2-IL-1 β mice were bred with C57BL/6J mice (wildtype=wt). Mice in the SPF and VAT were frequently backcrossed with C57BL/6J wildtype mice. The offspring was weaned at the age of 3 weeks and the ears were punched to assign a unique number. The punch biopsies (55.2-1-54-2532-24-2016) or the tips of the tail (55.2.1.54-2532-125-12) were then used for genotyping. After genotyping, the mice were assigned to experimental cohorts and treatment with experimental diets started at the age of 6 weeks. Mice were weighed every week to monitor weight gain/loss and inspected for health issues.) L2/IL8Tg mice were created by crossbreeding the L2-IL-1 β mice with mice expressing human IL8 [217].

2.1.1 Holding

2.1.1.1 Specific-pathogen-free (SPF) facility

The specific-pathogen-free (SPF) facility is an individually ventilated cage facility fulfilling the FELASA criteria. The mice were maintained in 12 hours day to night cycle, bedding and water was replaced weekly unless stated otherwise. The mice had free access to food and water. Mice were sacrificed at 3,6,9 and 12 months of age.

2.1.1.2 Versuchsanlage Tierernährung (VAT)

The Versuchsanlage Tierernährung (VAT) is an open cage facility and has a lower hygiene level than the SPF (e.g. being positively tested for *Helicobacter* spp., *Pasteurella* spp., *Trichomonas* spp., *Syphacia* spp.). The mice were maintained in 12 hours day to night cycle, bedding and water was replaced weekly. The mice had free access to food and water. Mice were sacrificed at 6 months of age.

2.1.1.3 Germfree facility

Germfree mice were generated by embryo transfer rederivation of conventional L2-IL-1 β mice into Germfree Swiss recipient mothers as previously described [218, 219]. Germfree mice were maintained in sterile isolators on autoclaved food (RMH3000, Purina) and water. Sterility of isolators was confirmed every other week by 16S PCR, aerobic, anaerobic and fungal culture as well as Gram stains of fecal smears. Germfree mice were held and bred and their paraffin sections were kindly donated by James G. Fox at the Massachusetts Institute of Technology, Cambridge, MA, USA. Mice were sacrificed at 12-14 months of age.

2.1.1.4 Diets

Mice were bred on standard lab chow. At the age of ~6 weeks the mice were then distributed to the different diet based cohorts. The composition of the diets is presented in Table 1. Chow was autoclaved before entering the mouse holding area, while the control diet and the high fat diet (HFD) were irradiated with γ radiation by the manufacturer before they were fumigated and entered the mouse area. It is important to note that the control diet is matched to the HFD, while the chow is different to both special diets. All diets were manufactured by Ssniff in Germany.

Table 1: Composition of experimental diets

	V1124-000	S5745-E712	S5745-E702
Dietary components	Standard Chow	High fat diet Palm oil	Control
Gross Energy (GE)	16.7 MJ/kg	21.9 MJ/kg	16.9 MJ/kg
Metabolizable Energy (ME)	14.0 MJ/kg	19.7 MJ/kg	15.3 MJ/kg
Protein [kJ%]	27	18	23
Fat [kJ%]	12	48	13
Carbohydrates [kJ%]	61	34	64
Crude Nutrients [%]			
Protein	22.0	21.2	21.2
Fat	4.5	25.1	5.1
Fiber	3.9	5.0	5.0
Ash	6.2	5.3	5.3
Starch	34.2	26.7	45.9
Sugar	5.1	6.1	6.1
N free extracts	51.2	37.7	56.8
Amino Acids [%]			
Lysine	1.5	1.8	1.8
Methionine	0.5	0.8	0.8
Met + Cys	0.4	1.1	1.1

	V1124-000	S5745-E712	S5745-E702
Dietary components	Standard Chow	High fat diet Palm oil	Control
Amino Acids [%]			
Threonine	0.9	0.9	0.9
Tryptophan	0.3	0.3	0.3
Minerals [%]			
Calcium	1.0	0.9	0.9
Phosphorus	0.7	0.7	0.7
Sodium	0.2	0.2	0.2
Magnesium	0.2	0.2	0.2
Vitamins [IU/kg]			
Vitamin A	25,000.00	18,000.00	18,000.00
Vitamin D ₃	1,500.00	1,800.00	1,800.00
Vitamin E	135	180	180
Fatty acids [%]			
C 12:0	-	0.01	0.01
C 14:0	0.01	0.21	0.02
C 16:0	0.54	9.18	0.58
C 18:0	0.14	1.11	0.18
C 20:0	0.02	0.1	0.02
C 16:1	0.02	0.05	0.01
C 18:1	1.03	9.19	1.29
C 18:2	2.42	4.67	2.65
C 18:3	0.28	0.35	0.29

2.1.2 Genotyping of mice

Mice tail tips/ear punch biopsies were incubated over night at 55° C in a shaker in 198/99 µl DirectPCR® Lysis Reagent Tail (31-102-T, Peqlab) supplied with 2/1 µl Proteinase K (03115828001, Roche Diagnostics) respectively. After visual inspection of the lysis process samples were heated at 85°C for 45-60 minutes. After quickly spinning down 0.5 to 1 µl of the supernatant were transferred to a fresh PCR tube. 5 µl ReadyMix™ REDTaq® PCR Reaction Mix (R2648, Sigma) were added with 1 mM of the respective Primers and filled up to 10 µl with PCR grade water. PCR was performed as shown in Table 2 using the primer pairs described in Table 3 in a Thermal Cycler (T100, BioRad). The PCR product was visualized on a 1,5% agarose gel in TAE solution (840004, Biozym) with ethidium bromide (2218.1, Roth) with a 100 bp ladder (N0467L, BioLabs). The presence of a band with the corresponding size indicates the presence of the transgene in the mouse.

Table 2: Thermocycler settings for genotyping of mice

Phase	Temperature [°C]	Time [s]	No. of cycles
Denaturation	94	180	1
Denaturation	94	30	35
Annealing L2-IL-1 β	57	30	
Annealing IL8	55	30	
Elongation	72	30	
Storage	4	∞	1

Table 3: Genotyping primers

Target	Forward/Reverse	Sequence (5' – 3')	Amplicon size
pL2-IL-1 β	Forward	CTT CCT GTT CCA TTC AGA GAC GAT	277 bp
	Reverse	CTC CAG CTG TAG AGT GGG CTT ATC	
IL-8	Forward	TGA GGT CAA GGG CTA GGA GA	300 bp
	Reverse	AAA TTT GGG GTG GAA AGG TT	

2.1.3 Bedding transfer

L2-IL-1 β mice were feed with a control diet after weaning. In contrast to the regular procedure, the bedding was removed weekly but only half of it replaced with fresh bedding. The other half was bedding from a cage of adult female L2-IL-1 β mice (9-12 months old) on HFD.

2.1.4 Anti-inflammatory treatment

The Anakinra study was performed by Dr. rer. nat. Natasha Stephens Münch and Jonas Ingermann. L2-IL-1 β mice were put on either HFD or regular lab chow at the age of 6 weeks. At the age of 18 and 24 weeks, an osmotic pump (Minipump 2006, Alzet) was implanted. Briefly the pumps were filled with 200 μ l containing 150 μ g/ μ l Anakinra (Kineret, Swedish Orphan Biovitrum AB). For implantation mice were narcotized with 0.5 mg/kg Medetomidin, 5 mg/kg Midazolam and 0,05 mg/kg Fentanyl injected intraperitoneally. Shortly before the cut 10 mg/kg Rimadyl was injected subcutaneously. After surgery the mice were woken up by 2.5 mg/kg Atipamezol, 0.5 mg/kg Flumazenil and 1.2 mg/kg Naloxon and allowed to recover on a heating plate. The treatment schedule is depicted in Figure 12.

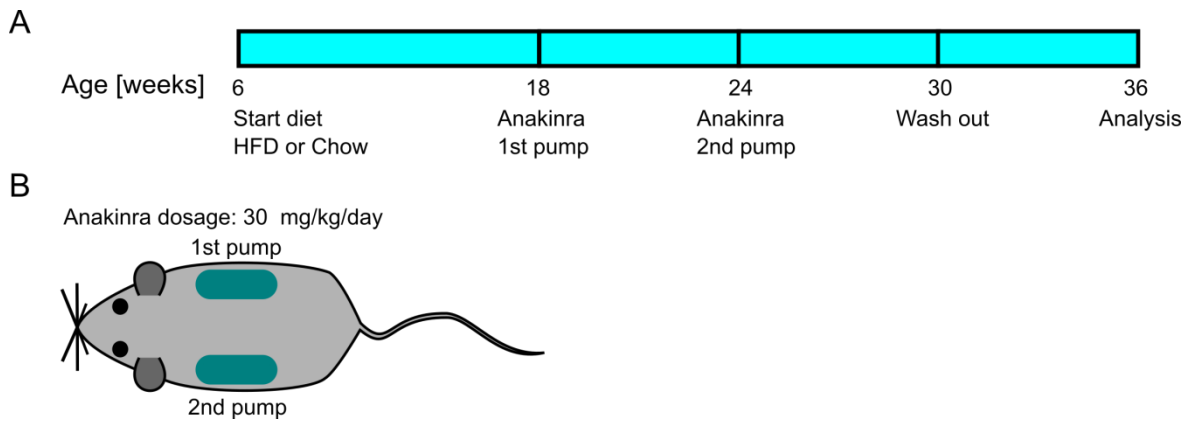


Figure 12: Treatment plan for the treatment of L2-IL-1 β mice with Anakinra

A: Time table with implantation timepoints **B:** Schematic representation of the implants position

For the treatment with nonsteroidal anti-inflammatory drugs (NSAIDs), mice were fed the HFD or Control diet enriched with 0.032% Sulindac (S8139-5G, Sigma) by the manufacturer Ssniff [220]. The Sulindac enriched diets were given from 6 weeks of age on until the time of sacrifice. Aspirin was purchased from the veterinary pharmacy at the Wissenschaftszentrum Weihenstephan (Suispirin, Animedica). Aspirin was prepared freshly 3 times a week, sterile filtrated and given *ad libitum* in the water bottles at 30 mg/L to the mice starting at the age of 6 weeks [221].

2.1.5 Sacrificing and preparation of mice

The mice were euthanized using either Isoflurane (Isofluran CP, CP-Pharma) or CO₂. Briefly, CO₂ was introduced to a chamber with a deflecting plate at a constant flow of 60% volume of the chamber per minute [222]. For Isoflurane mice were put in a locked chamber with a tissue soaked in Isoflurane. If no respiration could be observed anymore, death was verified by testing for reflexes. The mouse was then fixed on its back using needles and a careful cut opening the skin from the lower abdomen up to the head was performed. Blood was drawn directly from the heart with a syringe (305501, BD Plastipak) and transferred into a microvette (20.1344, Sarstedt). The blood was allowed to rest for ~20 minutes and then spun down at 13000g for 10 minutes. The serum was taken off and snapfrozen in liquid nitrogen. The stomach, intestine, liver, kidney and spleen were taken out and put on ice. The stomach was opened along the large curvature, washed in PBS and flattened out on Whatman paper (3030 917, Schleicher&Schuell) as depicted in Figure 13. The flattened stomach was then photographed with a ruler for scale using a compact camera (Ricoh CX6) in macro mode for macroscopic scoring of lesions.

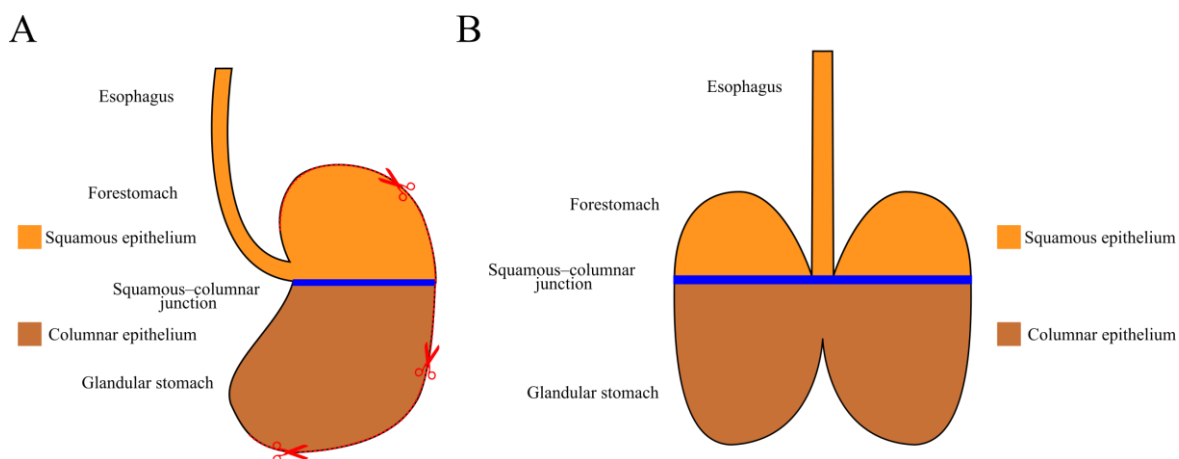


Figure 13: Schematic representation of a mouse stomach.

A: Stomach, as presented after taken out of the mouse. The stomach was then cut open along the large curvature (red dotted line) **B:** Stomach after opening and flattening out.

Parts from the esophagus, forestomach, cardia and the rest of the stomach were cut off and snap frozen in liquid nitrogen while the flattened stomach was secured with a sponge (094005, Kabe Labortechnik), put in a histologic cassette (7-0014, neoLab) and fixed in 4% paraformaldehyde (Pharmacy of the Klinikum Rechts der Isar) in PBS (A0965, AppliChem).

2.1.6 Macroscopic scoring

Photographs of the stomach were evaluated to measure a macroscopic score for evaluating the lesions. The cardia region and the esophagus were scored according to Table 4. The average of the scores for tumor size and coverage were then calculated and used as the lesion score.

Table 4: Macroscopic scoring

Tumor size		Tumor coverage	
0	No abnormalities	0	No abnormalities
1	<0.5mm	1	Focal tumors (<20%)
2	<1.0mm	2	Partial tumors (20-50%)
3	<2.0mm	3	Increased tumors (>50-80%)
4	<3.0mm	4	Continuous tumors (>80%)

2.2 Histology

2.2.1 Generation of FFPE sections

Tissue samples were fixed in 4% paraformaldehyde (Pharmacy of the Klinikum Rechts der Isar) in PBS (A0965, AppliChem) for 24h and then stored in 70% ethanol at 4° C until they were dehydrated in a Leica ASP300S overnight. After the dehydration the flattened stomachs were cut and embedded as depicted in Figure 14, allowing staining of large sections of stomach tissue in one slide.

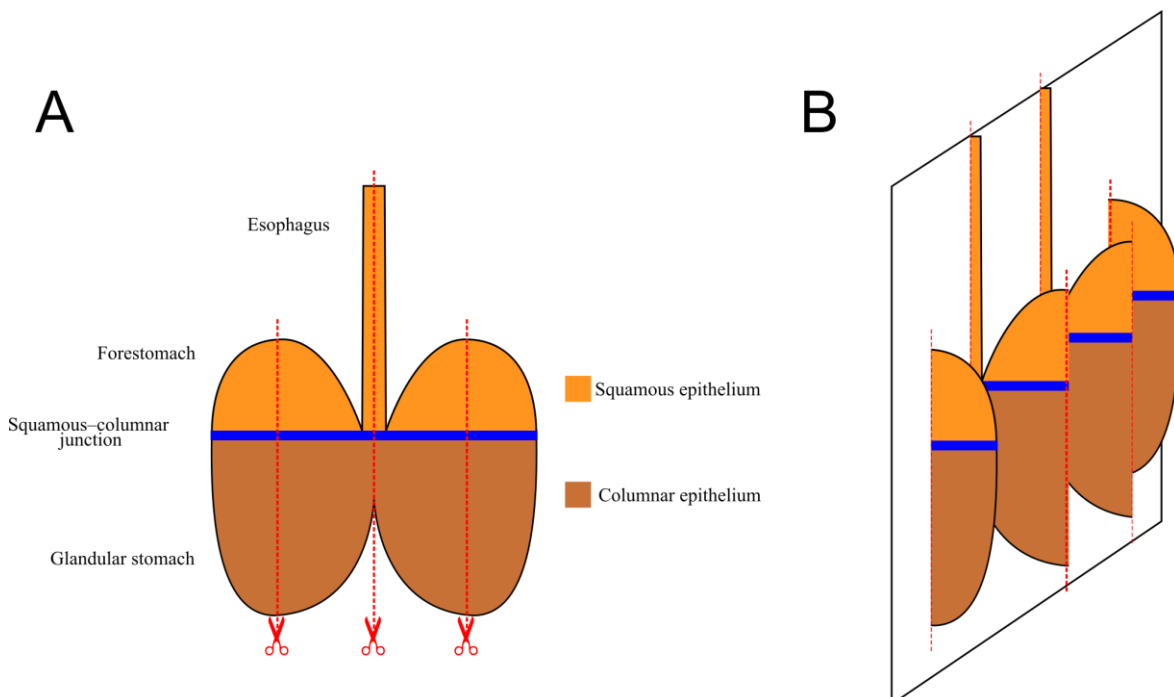


Figure 14 Schematic representation of sectioning and embedding of a mouse stomach

A: The stomach was cut in 4 pieces (red dotted line)**B:** The sections were embedded with the cut side facing the bottom of the paraffin block

All other tissues were embedded without any additional preparations. The formalin fixed paraffin embedded (FFPE) blocks were then cut to 2-3 μm thick sections on a microtome (HM 355S, Thermo Scientific). The cut sections were flattened out on ~58° C warm distilled water and pulled on microscope slides (J1800AMNZ or J3800AMNZ, Thermo Scientific). The slides were allowed to dry overnight and were then baked at 60° C for 1 hour in an incubator (UT 12, Heraeus). The slides were stored at room temperature until staining.

2.2.2 Hematoxylin and eosin (HE) staining

The slides were rehydrated and stained as described in Table 5. Slides were then mounted using Pertex (41-4010-00, Medite).

Table 5: Protocol for hematoxylin and eosin staining.

All steps were performed in glass containers, all steps which were performed twice were done using 2 glass containers.

Reagent	Time	Article number	Manufacturer
Roti-Histol	10-30 min	6640.4	Roth
Roti-Histol	5 min	6640.4	Roth
100% Ethanol	2x 3-5 min	Pharmacy of the Klinikum Rechts der Isar	
96% Ethanol	2x 3-5 min	Pharmacy of the Klinikum Rechts der Isar	
70% Ethanol	2x 3-5 min	Pharmacy of the Klinikum Rechts der Isar	
dH ₂ O (running)	3-5 min		
Mayer haemalum	3 min	1.09249.2500	Merck
Tap water (running)	10 min		
0.33% Eosin	3.5 min	Pharmacy of the Klinikum Rechts der Isar	
96% Ethanol	25 sec	Pharmacy of the Klinikum Rechts der Isar	
Isopropanol	25 sec	Pharmacy of the Klinikum Rechts der Isar	
Roti-Histol	2x 1.5 min	6640.4	Roth

HE stained slides were scored for inflammation, metaplasia and dysplasia by an experienced gastroenterologist according to Table 6.

Table 6: Description of the histologic scoring used to grade inflammation, metaplasia and dysplasia.

Score	Inflammation	Metaplasia	Dysplasia
0	no inflammation	no metaplasia	no dysplasia
1	mild inflammation	rare mucus cells	superficial epithelial atypia
2	moderate inflammation	single metaplastic glands	atypia in glandular complexity
3	severe inflammation	multiple metaplastic glands	low grade dysplasia
4			high grade dysplasia

2.2.3 Immunohistochemistry (IHC)

All steps are performed at room temperature unless specified otherwise. Rehydration of slides was performed as described in steps 1-6 in Table 5. Antigen retrieval was performed either by boiling slides for 20 minutes in Citrate Buffer pH 6.0 (2L dH₂O + 5.88g Citrate (Sigma) in a pressure cooker with a 20 minutes cool down or for 20 minutes with unmasking solution (H-3300, Vector Labs) in the microwave followed by a 15 minutes cool down or for 20 minutes with 0.3% Triton (X100, Sigma) in PBS (A0965, AppliChem) in the microwave followed by a 20 minute cool down. The tissue sections were encircled with a Dako Pen (S2002, Dako) and blocking was performed in 3% H₂O₂ (1.08597.1000, Merck) for 10 minutes followed by 3 times washing with PBS for 5 minutes. Blocking was performed using a Streptavidin/Biotin Blocking Kit (SP-2002, Vector Labs) and the matching serum (S-1000 or S-5000, Vector Labs) for 30 minutes. After 3 times washing with PBS for 5 minutes the primary antibody was allowed to bind in a wet chamber for either 2 hours at room temperature or at 4° C overnight. After 3 times washing in PBS for 5 minutes the secondary antibody (BA-1000 or BA-4000, Vector Labs) was applied for 30 minutes. After 15 minutes the ABC kit (PK-6100, Vector Labs) was prepared and added for 30 minutes after 3 times washing with PBS for 5 minutes. After 3 times washing with PBS the DAB was applied (SK-4100, Vector Labs) and the development was monitored under a microscope. The development was stopped by dipping the slides in PBS and counterstaining with haematoxylin (1.05175.2500, Merck) was performed for 1 minute. After blueing in tap water for 3-5 minutes the slides were dehydrated by following steps 1-6 in Table 5 inversely and then mounted using Pertex (41-4010-00, Medite). Analysis was performed by counting several 10x fields under a microscope for Ly6C and Ly6G staining. CXCR2/Lgr5 double staining was performed according to the RNA Scope 2.5 HD assay manual (312171, ACD) for the Lgr5 in situ hybridization followed by standard IHC procedure for CXCR2 staining.

Table 7: Primary antibodies and their properties for IHC

Antigen	Dilution	Antigen retrieval	Article number	Manufacturer
Ki67	1:500	0.3% Triton/PBS	Ab15580	Abcam
Ly6C	1:100	0.3% Triton/PBS	56-5931-82	eBioscience
Ly6G	1:100	0.3% Triton/PBS	12-5932-82	eBioscience
CXCR2	1:250	0.3% Triton/PBS	Ab14935	Abcam

2.3 Flow cytometry of immune cells

Mice were euthanized and the abdomen and thorax were opened. Blood was drawn using a disposable small volume syringe (07664163, BD) from the heart and approximately 100-200 μ l were added to 5 ml of Red Blood Cell lysing buffer (R7757, Sigma) and lysed at room temperature. Stomach, Liver, Spleen and the intestine were taken out and put into PBS (A0965, AppliChem) until further processing. The spleen was put in PBS on ice. The stomach was opened as described before (2.1.5) and dissected into esophagus, cardia and forestomach and the rest of stomach. Colon and liver pieces were also collected. Esophagus, cardia and forestomach, rest of stomach, colon and liver were put in small dishes (628161, Greiner) with 1 ml of 0.5 M EDTA (AM9260G, Invitrogen) and cut into small pieces with a fine scissor. The cut samples were transferred into 50 ml tubes (227261, Greiner) and 5 ml of the appropriate digestion buffer was added (Table 8 and Table 9).

Table 8: Digestion buffers for tissue samples for flow cytometry.
The digestion buffers were prepared fresh shortly before sacrificing the mice.

Tissue	Buffer	Contents
Esophagus	Krebs-Ringer-Solution	BSA 40 mg/ml (9418, Sigma) + Collagenase P (11213873001, Roche) 2 mg/ml
Cardia and forestomach + Rest of stomach	RPMI (11875-093, Invitrogen)	Collagenase P 2 mg/ml (11213873001, Roche) + Pronase 2 mg/ml (10165921001, Roche)
Liver + Colon	RPMI(11875-093, Invitrogen)	Collagenase P 2 mg/ml (11213873001, Roche)

Table 9: Krebs-Ringer-Solution for digestion of esophagus samples for flow cytometry.
The Krebs-Ringer-Solution was prepared in ddH₂O and adjusted to pH=7.4.

Compound	Concentration	g/L	Article number	Manufacturer
NaCl	118 mM	6.9	S3014-1KG	Sigma
NaHCO ₃	24.8 mM	2.08	1.06329.0500	Merck
KH ₂ PO ₄	1.2 mM	0.16	3904.1	Roth
KCl	4.8 mM	0.358	1.04936.1000	Merck
CaCl ₂	1.25 mM	0.139	CN93.1	Roth
MgSO ₄	1.2 mM	0.14	208094-500G	Sigma
HEPES	10 mM	2.383	9105.3	Roth

The tissue samples were digested in a shaking incubator (TH15, Edmund Bühler GmbH) at 37 °C and 150 rpm for 30 minutes. Meanwhile the spleens were passed through a 40 µm cell strainer (352340, Falcon) with the plunger of a syringe (4606108V, B Braun). The spleen samples were spun down with the blood at 400 g 4°C for 10 minutes. The supernatant was discarded and the pellet resuspended in 1 ml Red Blood Cell lysing buffer. After again being spun down at 400 g 4°C for 10 minutes spleen and blood were resuspended in ~150 µl of FACS buffer (DPBS (14190-094, life technologies) with 2% BSA (A2153, Sigma) and 2mM EDTA (AM9260G, Invitrogen)) and transferred into a conical bottom 96 well plate (650180, Greiner) which stayed on ice for the whole procedure.

After digestion the tissue samples were passed through 40 µm strainer as described before and centrifuged at 400 g 4°C for 10 minutes. The supernatant was discarded, and the liver tissue resuspended in 1 ml Red Blood Cell lysing buffer while the other samples were resuspended in FACS buffer and transferred into the 96 well plate. After spinning down the liver, the supernatant was discarded, and the liver resuspended and transferred into the 96 well plate. The whole plate was spun down at 400 g 4°C for 10 minutes, the supernatant discarded and the cells resuspended in 200 µl FACS buffer. After being spun again the supernatant was discarded and the cells resuspended in 50 µl of the appropriate staining solution (Table 10). Staining was performed for 30 minutes on ice while the whole box was covered with tin foil.

Table 10: Antibodies used for staining in flow cytometric assessment of immune cells.

All Antibodies were added at 0.5 µl and filled up to 50 µl with FACS buffer per sample. The antibodies were all purchased from eBioscience and are all anti-mouse.

Myeloid panel		T-cell panel	
Antibody	Reference number	Antibody	Reference number
CD11c FITC	11-0114-85	NK1.1 APC-eFlour 780	47-5941-82
F4/80 APC	17-4801-82	CD3e FTIC	11-0033-82
CD11b APC-eFlour 780	47-0112-82	CD8a APC	17-0081-82
CD45 eFlour 450	48-0451-82	CD4 eFlour 450	48-0041-82
Ly-6C PE	12-5932-82	γδ TCR PE	12-5711-82
Ly-6G Alexa Flour 700	56-5931-82		

After staining 150 μ l of FACS buffer were added, the plate was spun down 400 g 4°C for 10 minutes and the supernatant was discarded. The pellets were resuspended in 200 μ l FACS buffer and spun down as described before. After discarding the supernatant the pelleted cells were resuspended in 130 μ l FACS buffer and transferred to 1.4 ml tubes (MP32022, MICRONIC) containing 45 μ l of FACS buffer and 5 μ l of 7-AAD (00-6993-50, eBioscience). The cells were then immediately transferred to the flow cytometer (Gallios, Beckman Coulter). The gating strategy used to identify immune cell populations in FlowJo (BD) after applying compensation is shown in Figure 15 and Figure 16.

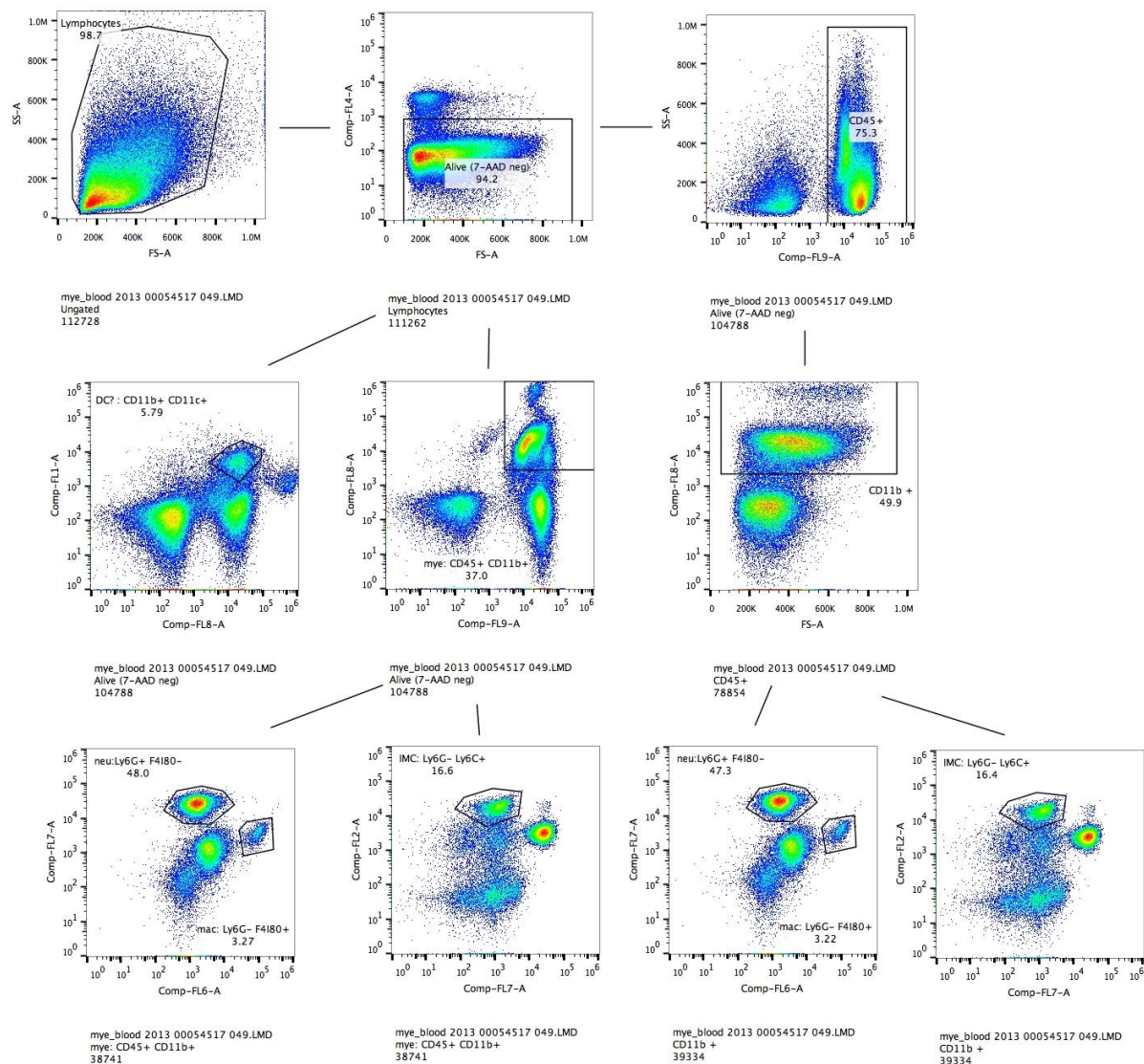


Figure 15: Representative gating strategy for immune cells of the myeloid lineage.

Living cells were either gated for CD45 and CD11b positive cells or first CD45 positivity and afterwards for CD11b positivity. Double positive cells were then used for the identification of immune cells. Cells being positive for Ly6G and negative for F4/80 were identified as neutrophils, while cells negative for Ly6G and positive for F4/80 were identified as macrophages. Ly6C negative Ly6G positive cells were identified as immature myeloid cells. Cells positive for CD11b and CD11c are putative dendritic cells.

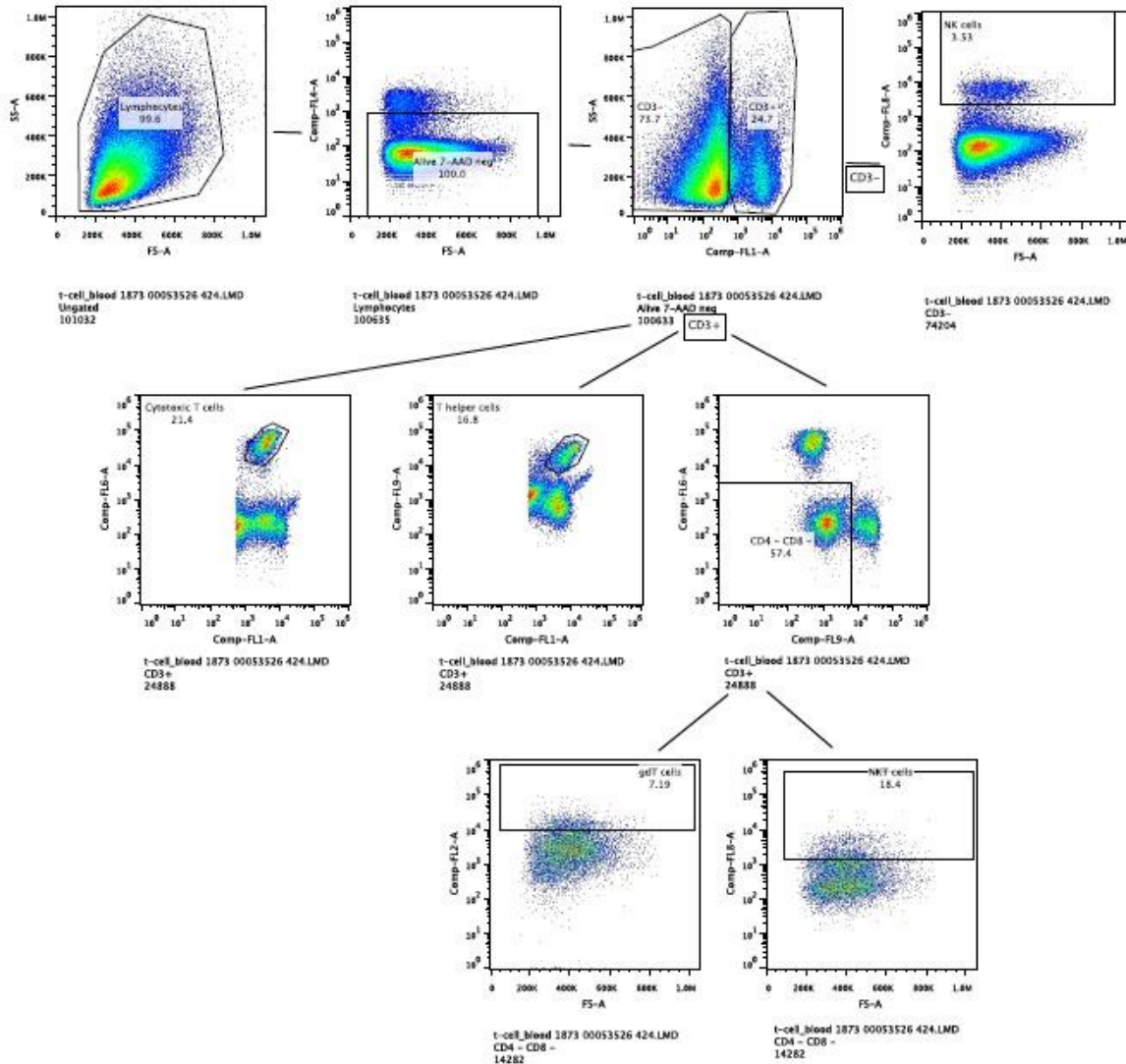


Figure 16: Representative gating strategy for immune cells of the T-cell lineage.

Living cells were either gated for CD3 positive. CD3 negative cells were gated for NK1.1 positivity and the positive population referred to as NK cells. CD3 positive cells were analyzed for CD4 and CD8 expression. CD4 positive cells were considered T helper cell and CD8 positive cells as cytotoxic T-cells. CD4 and CD8 negative cells were gated for $\gamma\delta$ TCR or NK1.1 positivity, leading to the identification of $\gamma\delta$ T-cells and NKT cells.

Blood and spleen samples were used as positive controls to identify immune cells. Samples yielding less than 25000 events were excluded from the analysis.

2.4 16S RNA sequencing and analysis

2.4.1 Overview of fecal samples

The samples used in this analysis were partially generated by Dr. Natasha Stephens Münch during her doctoral thesis [88]. Briefly fecal samples were collected at the time of sacrificing, frozen in liquid nitrogen and stored at -80°C . Fecal samples were chosen to

show the L2-IL-1 β phenotype progressing over time while using adult (6 months old) wildtype mice as a reference for an adult, matured microbiome. A detailed overview of the samples used for 16S sequencing from the SPF representing the major cohort used for the microbiome analysis is presented in Table 11.

Table 11: Overview of fecal samples from the SPF used for 16S RNA sequencing (HFD=high fat diet)

	Age [months]	3	6	9	12
L2-IL-1β-HFD	Male	5	5	5	5
	Female	5	5	5	5
L2-IL-1β-Chow	Male	5	5	5	5
	Female	5	5	5	5
L2-IL-1β-Control	Male		3		
	Female		3		
wt-HFD	Male		5		
	Female		5		
wt-Chow	Male		5		
	Female		5		
wt-Control	Male		3		
	Female		3		

Additionally a cohort of male mice from the VAT was analyzed to investigate the influence of a lower hygiene level. The samples used are depicted in Table 12.

Table 12: Overview of fecal samples from the VAT used for 16S RNA sequencing (HFD=high fat diet)

Age [months]	6
L2-IL-1β-Control	4
L2-IL-1β-HFD	5
wt-Control	5
wt-HFD	5

2.4.2 Sequencing

The whole sequencing procedure was performed as follows by TATAA Biocenter in Gothenburg, a commercial provider of sequencing services. The fecal samples were sent on dry ice to TATAA and stored at -80° C. DNA was extracted using the PowerMag Microbiome RNA/DNA Isolation Kit (27500-4-EP, MO BIO Laboratories/Qiagen). 260/280 ratios were analyzed using a Dropsense 96 (2010-64, Trinean/Unchained labs). Libraries were prepared according to 16S Metagenomic Sequencing Library Preparation as

recommended by Illumina [223]. Samples were fragmented, end repaired and ligated using Nextera XT DNA Library Preparation Kit (FC-131-1096, Illumina). Finalized libraries were quality checked with capillary electrophoresis using a Fragment Analyzer (Advanced Analytical) and the concentration was checked. The libraries were normalized and pooled before MiSeq sequencing (MiSeq, Illumina). Run specifications were MiSeq 2x300 bp v3 in a total of one run. Sequences were demultiplexed and provided to us.

2.4.3 Analysis of 16S sequencing data based on IMNGS and RHEA

The sequences were remultiplexed using remultiplexor, a Perl script provided by the creators of IMNGS [224]. IMNGS provides the user with a workflow to analyze 16S rRNA amplicon datasets using a web interface [224]. Briefly, IMNGS is based on the UPARSE pipeline [225]. Pairing, quality filtering and OTU (operational transcriptional units) clustering is done by USEARCH 8.0 [226]. Chimera filtering is done by UCHIME with the RDP set 15 as reference database, with the RDP training set 15 being used for classification with the RDP classifier 2.11 [227, 228]. Sequence alignment is performed by MUSCLE [229]. A phylogenetic tree was created using Fasttree [230]. Manual curation of the taxonomic assignment was performed by checking the OTU sequences by aligning with the Silva database via their webtool and the RDP classifier [228, 231]. Mismatches between the two classifications were resolved by identifying the OTU sequence using EzBioCloud [232]. Normalization of Sequences and further analysis was performed using Rhea in RStudio, a graphical user interface for the statistical programming language R [233-235]. To identify potential indicator species LDA Effect Size (LEfSe) analysis was performed with the default settings on the public galaxy server of the Huttenhower lab [182, 236].

2.5 Statistical analysis

Statistic testing was performed using Graphpad Prism 6 [237]. Tests were performed as indicated in the respective figure legends. Briefly, ANOVA with Tukey post-hoc testing and t-test were performed first to test for normality and variance. If the assumption of normality or equal variance was violated, Kruskal-Wallis tests with Dunn's post-hoc testing or Mann-Whitney U tests were performed. Histological scores were compared

using Kruskal-Wallis tests with Dunn's post-hoc testing or Mann-Whitney U tests due to the ordinal nature of this kind of data.

3. Results

3.1 Microbial differences in the gut influence the development of esophageal cancer

Our lab has shown that cancer progression is accelerated in L2-IL-1 β mice by feeding a HFD independent of obesity [88]. While microbial changes were suspected to be associated with this phenotype, it remained unclear whether that was an effect of local changes at the squamous-columnar junction or rather a systemic effect of the gut microbiome. The laboratory of Professor Timothy Cragin Wang at Columbia University kindly provided data regarding the microbiome localized at the squamous-columnar junction. Briefly L2-IL-1 β mice were treated with bile acids and N-methyl-N-nitrosourea and sacrificed at the age of 12 months as described before after which 16S DNA from the squamous-columnar junction was isolated, amplified, sequenced and analyzed with QIIME [72, 238].

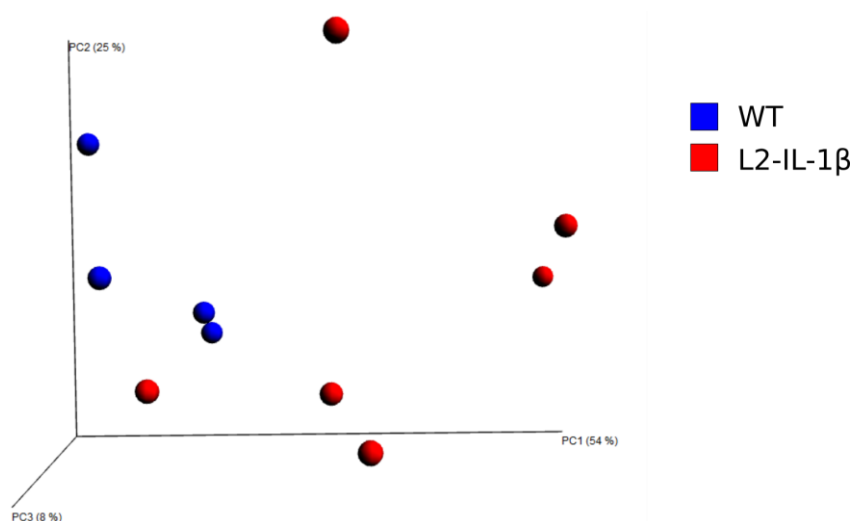


Figure 17: Weighted UniFrac analysis of the microbiome at the squamous-columnar junction (WT=wildtype)

Figure 17 shows the results of a weighted UniFrac analysis which includes not only phylogenetic distances but also abundances in a distance metric. Since no obvious clustering could be observed regarding the local microbiome, analysis performed by our lab was focusing on the gut microbiome based on our experiences regarding diet and holding facility.

3.1.1 Housing conditions define the phenotype, part I: VAT

The VAT cohort is from an open cage facility and represents the lowest hygiene level analyzed within this project.

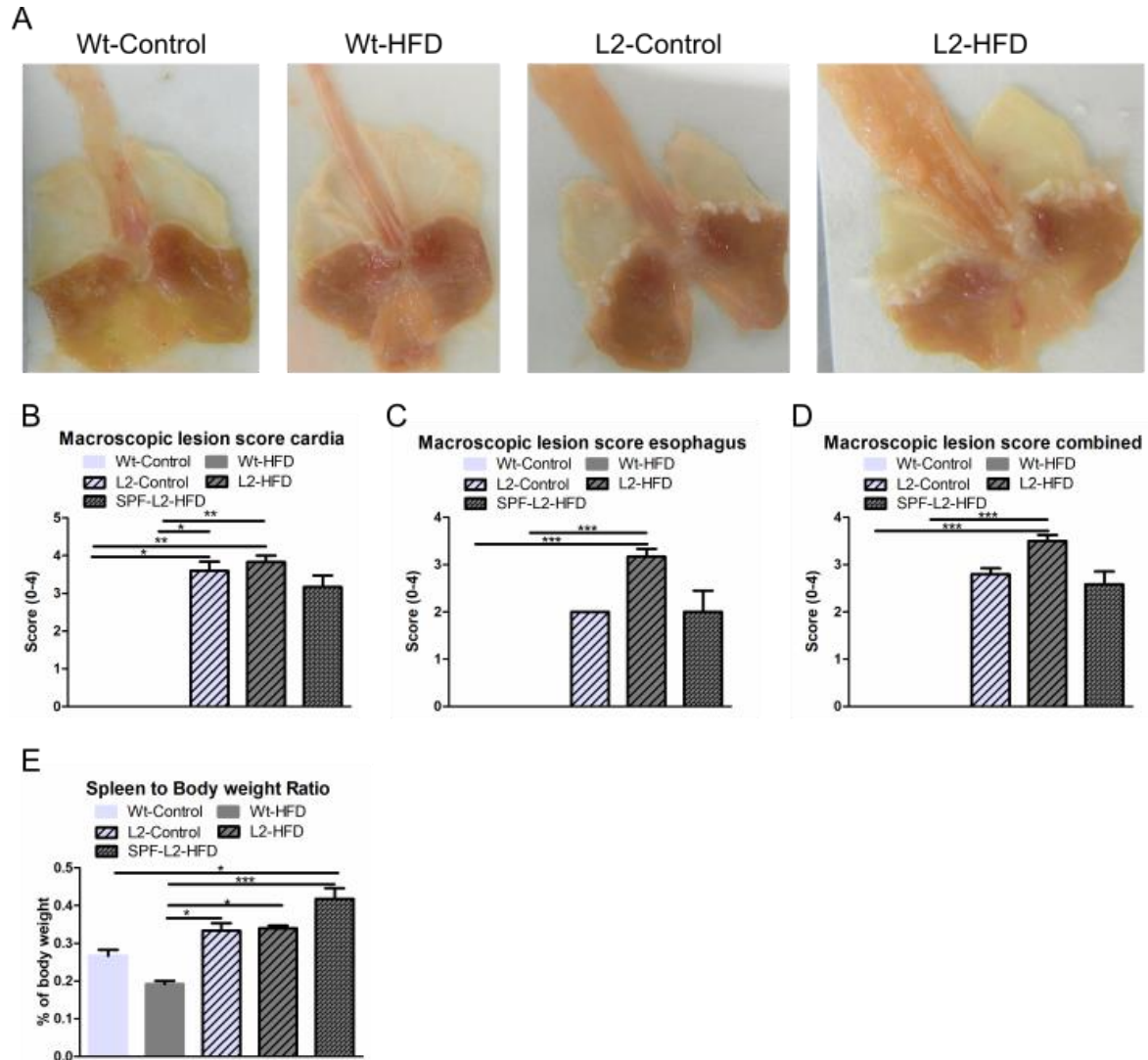


Figure 18: Macroscopic analysis of VAT mice

A: Representative images of the mouse cohorts stomachs **B:** Macroscopic scoring of the cardia lesions **C:** Macroscopic scoring of the esophagus lesions **D:** Average of the lesion score for esophagus and and cardia **E:** Spleen to body weight ratio as an indicator for splenomegaly. A Kruskal-Wallis test with Dunn post-hoc testing was performed to test for significant differences. Plotted is mean with SEM * $p < 0.05$, ** $p < 0.01$, *** $p < 0.001$ (HFD=high fat diet, Control=Control diet, L2=L2-IL-1 β , wt=wildtype)

The macroscopic analysis of the VAT mice is depicted in Figure 18. While the trend is similar to the previously reported SPF mice, the esophageal lesions show a trend towards a stronger phenotype of L2-IL-1 β mice in the VAT [88].

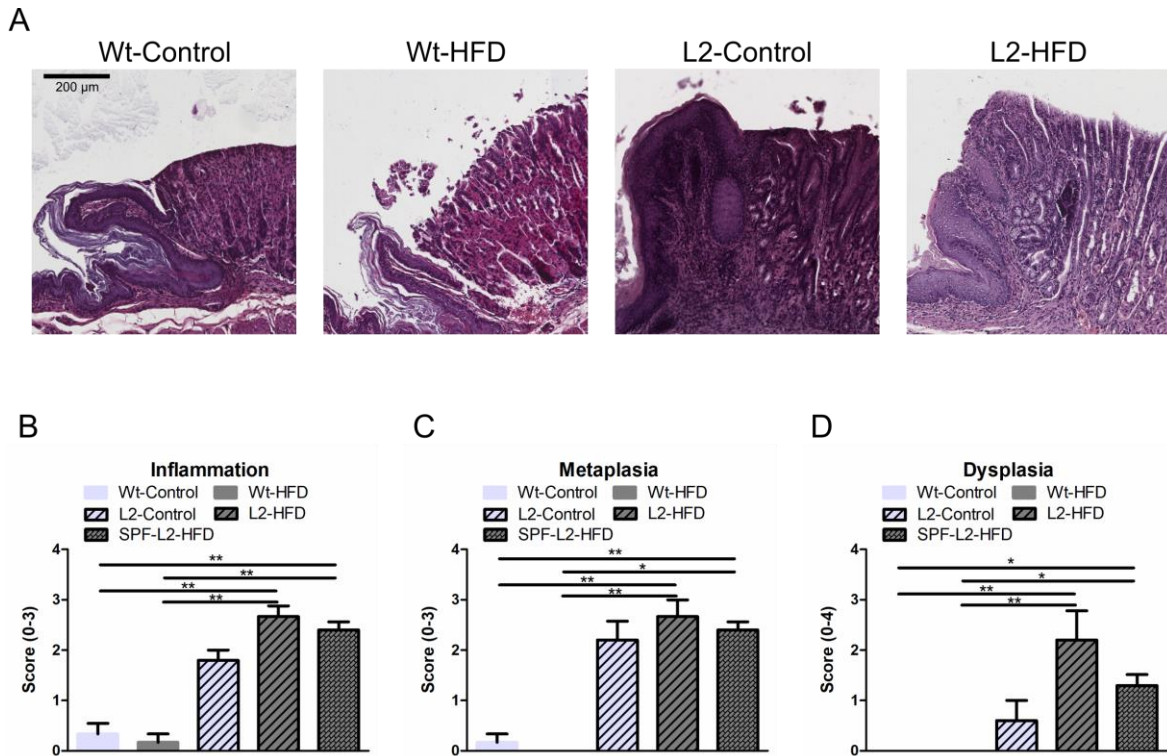


Figure 19: Histologic analysis of VAT samples using HE staining

A: Representative images of the squamous-columnar junction **B:** Inflammation score **C:** Metaplasia score **D:** Dysplasia score. A Kruskal-Wallis test with Dunn post-hoc testing was performed to test for significant differences. Plotted is mean with SEM * $p < 0.05$, ** $p < 0.01$ (HFD=high fat diet, Control=Control diet, L2=L2-IL-1 β , wt=wildtype)

Figure 19 shows increased inflammation, metaplasia and dysplasia in L2-IL-1 β mice compared to wildtype mice. Though not significant, the phenotype is stronger in HFD mice, matching results from the SPF cohorts. Interestingly the dysplasia score is higher in the VAT-L2-HFD mice compared to the SPF-L2-HFD mice.

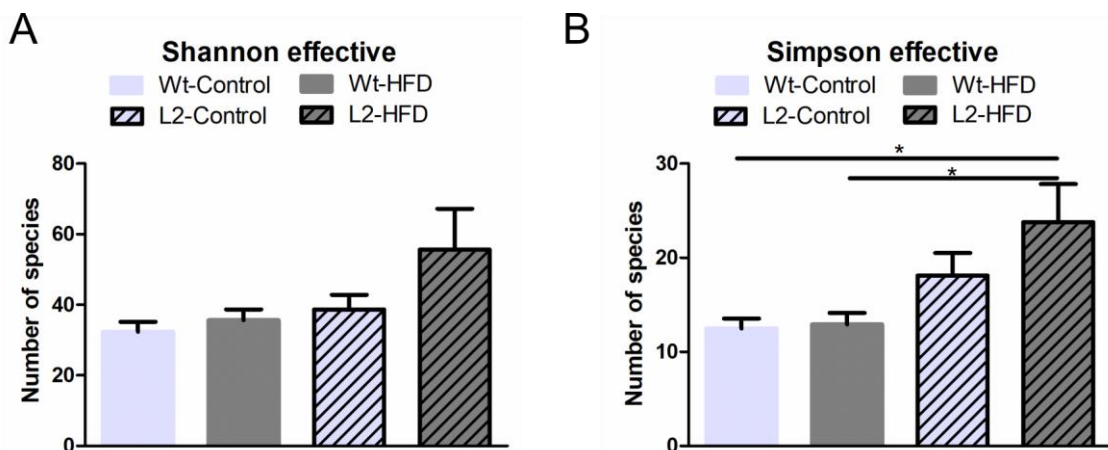


Figure 20: α -diversity of VAT samples

A: Number of Shannon effective species **B:** Number of Simpson effective species. An ANOVA with Tukey post-hoc testing was performed to test for significant differences. Plotted is mean with SEM * $p < 0.05$ (HFD=high fat diet, Control=Control diet, L2=L2-IL-1 β , wt=wildtype)

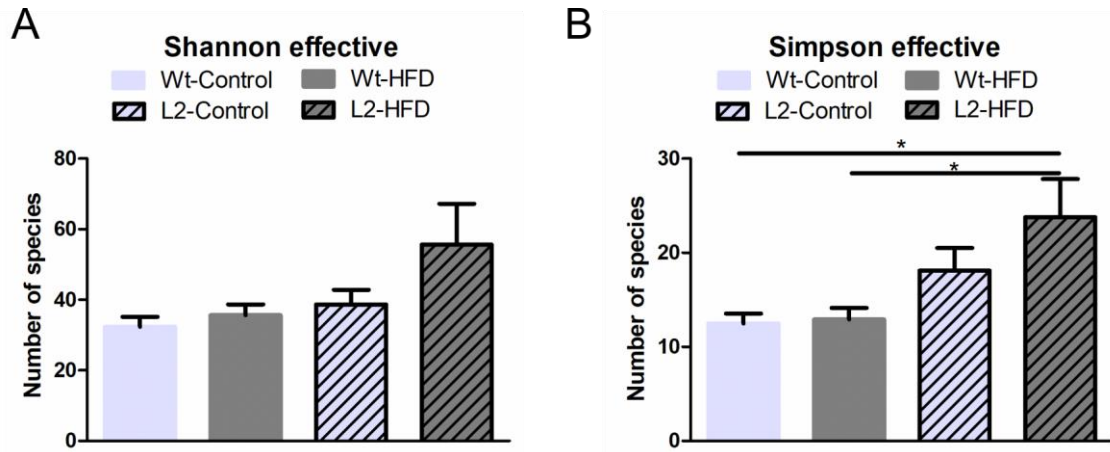


Figure 20 shows the α -diversity observed in the VAT samples, which was the highest in L2-HFD samples and for L2-HFD mice significantly increased compared to wildtype mice.

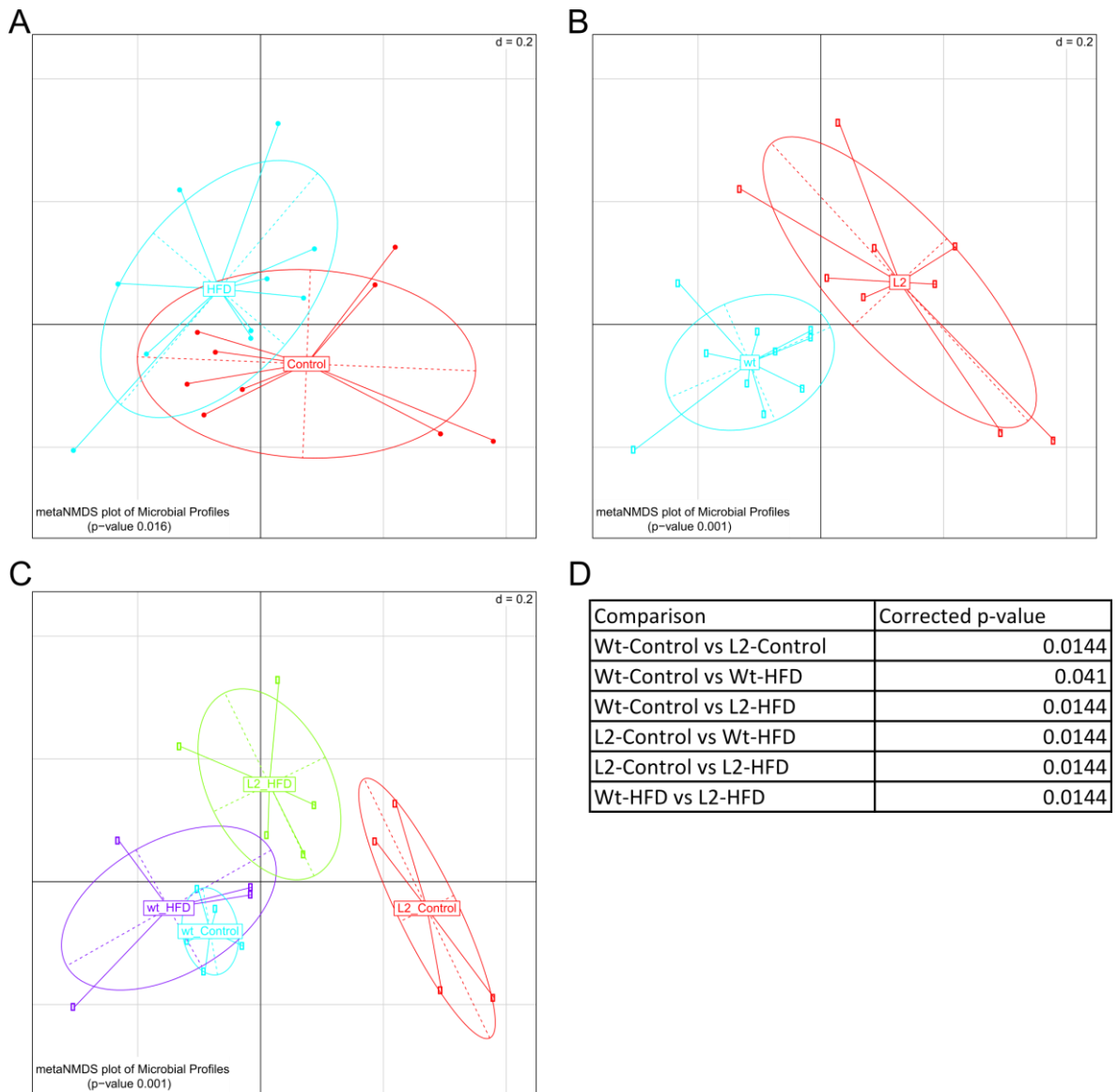


Figure 21: Generalized UniFrac using non-metric Multi-Dimensional Scaling of VAT samples

A: Separation by diet (turquoise=HFD, red=Control) **B:** Separation by genotype (turquoise=wt, red=L2) **C:** separation by diet and genotype (turquoise=wt-Control, red=L2-Control, purple=wt-HFD, green=L2-HFD) **D:** corrected p-values for pairwise comparisons in **C**. p-values were calculated after PERMANOVA with Bonferroni-Hochberg post-hoc testing (L2=L2-IL-1 β , wt=wildtype, HFD=high fat diet, Control=Control diet)

Figure 21 shows the different clustering in a generalized UniFrac. While diet and genotype alone are sufficient to cause significant differences between the microbial profiles, a clear and significant separation can be observed as well when testing for the interaction of diet and genotype. It is worth to note that L2-HFD and L2-Ctrl animals are clustering completely separately from the wildtype animals.

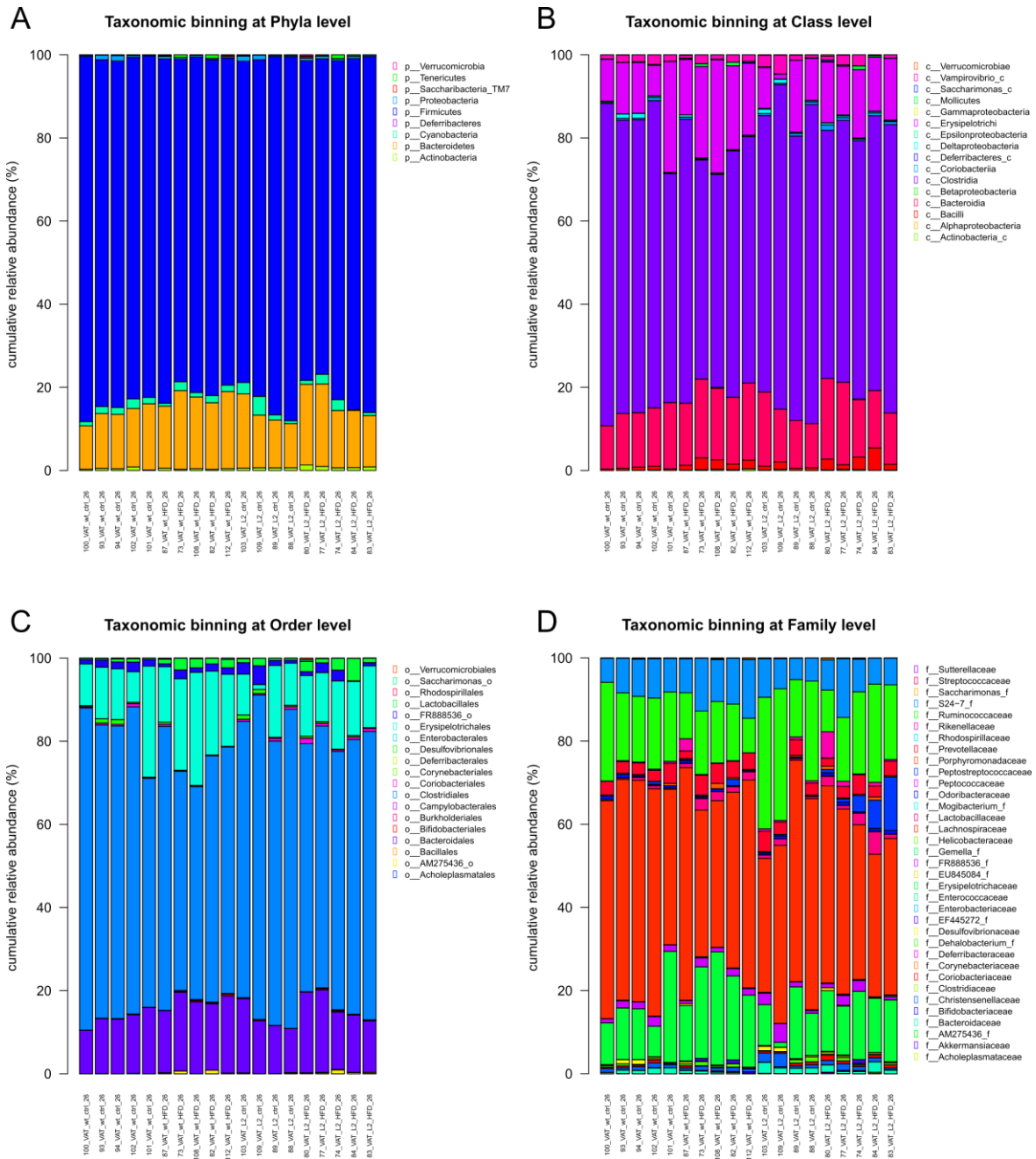


Figure 22: Taxonomic distribution of VAT samples

A: Taxonomy at phylum level **B:** Taxonomy at Class level **C:** Taxonomy at Order level **D:** Taxonomy at Family level

The taxonomic overview of the VAT samples in Figure 22 shows a similar distribution between all samples, with a small presence of Peptostreptococcaceae in L2-HFD mice.

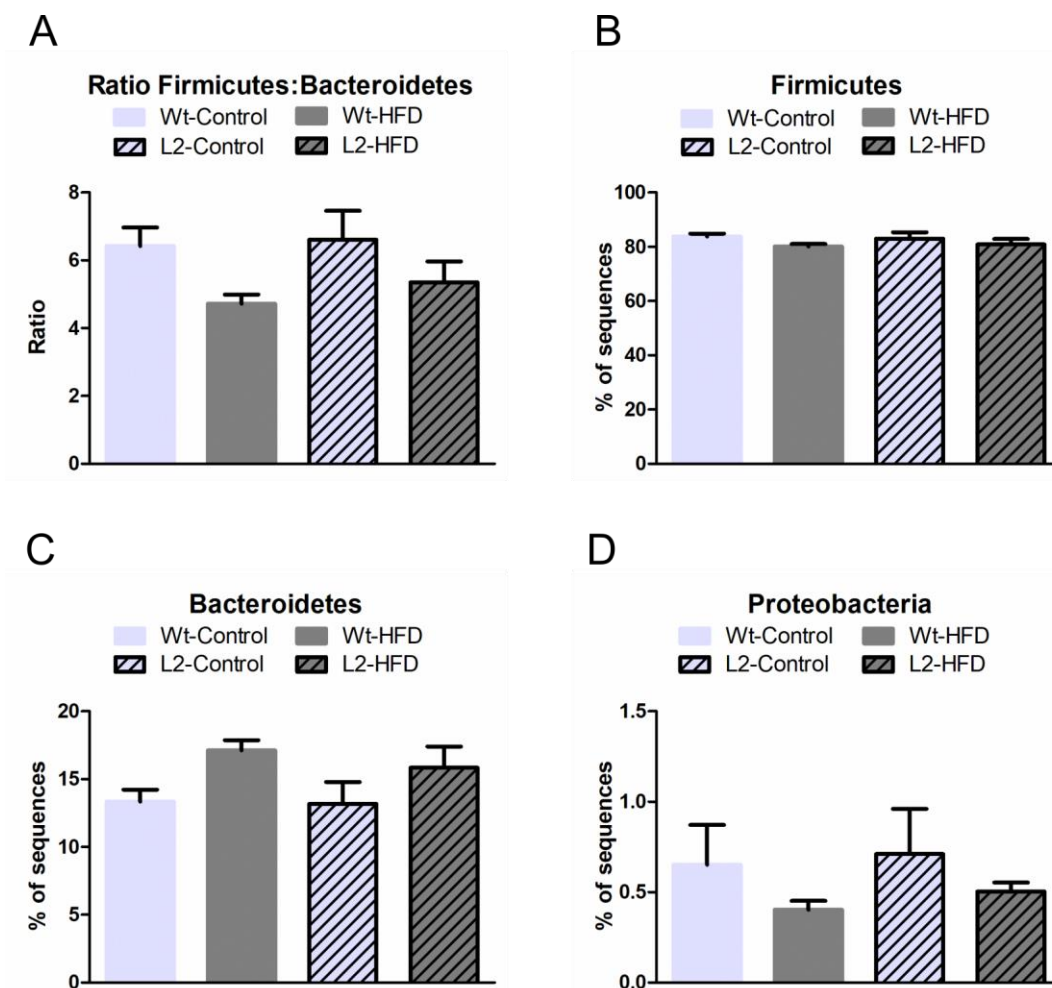


Figure 23: Common obesity associated phyla in VAT samples

A: Ratio of members of the phylum Firmicutes to the members of the phylum Bacteroidetes **B:** Relative abundance of the phylum Firmicutes **C:** Relative abundance of the phylum Bacteroidetes **D:** Relative abundance of the phylum Proteobacteria. An ANOVA with Tukey post-hoc testing was performed to test for significant differences. Plotted is mean with SEM. (HFD=high fat diet, Control=Control diet, L2=L2-IL-1 β , wt=wildtype)

Figure 23 shows bacterial phyla associated with obesity, which are not significantly different in the VAT cohort. There seems to be a trend of an increased Firmicutes:Bacteroidetes ratio in control diet fed mice which resembles more of an obesity phenotype.

3.1.2 Housing conditions define the phenotype, part II: SPF

The histology of the mice from the SPF has been presented in the thesis by Dr. Natasha Stephens Münch and our corresponding paper [2, 88]. Briefly L2-IL-1 β mice fed with a HFD present with more tumors and increased dysplasia compared to L2-IL-1 β on a chow diet and present with faster progression. In the following paragraph the 16S data from 6 month old mice from the SPF is analyzed.

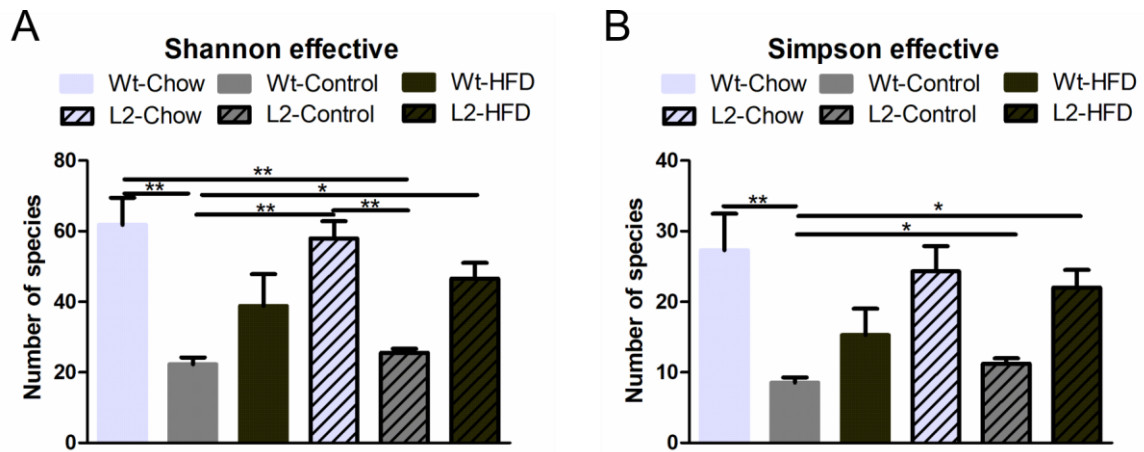


Figure 24: α -diversity of SPF samples

A: Number of Shannon effective species **B:** Number of Simpson effective species. A Kruskal-Wallis with Dunn's post-hoc testing was performed to test for significant differences. Plotted is mean with SEM * $p < 0.05$, ** $p < 0.01$ (HFD=high fat diet, Control=Control diet, L2=L2-IL-1 β , wt=wildtype)

Figure 24 shows the α -diversity observed in the SPF samples. Interestingly the highest diversity was observed in the chow samples, while the control diet samples had the lowest diversity. The effective count of species was intermediate in HFD mice. This holds true for wildtype and L2-IL-1 β mice, where the observed diversity is similar between the genotypes.

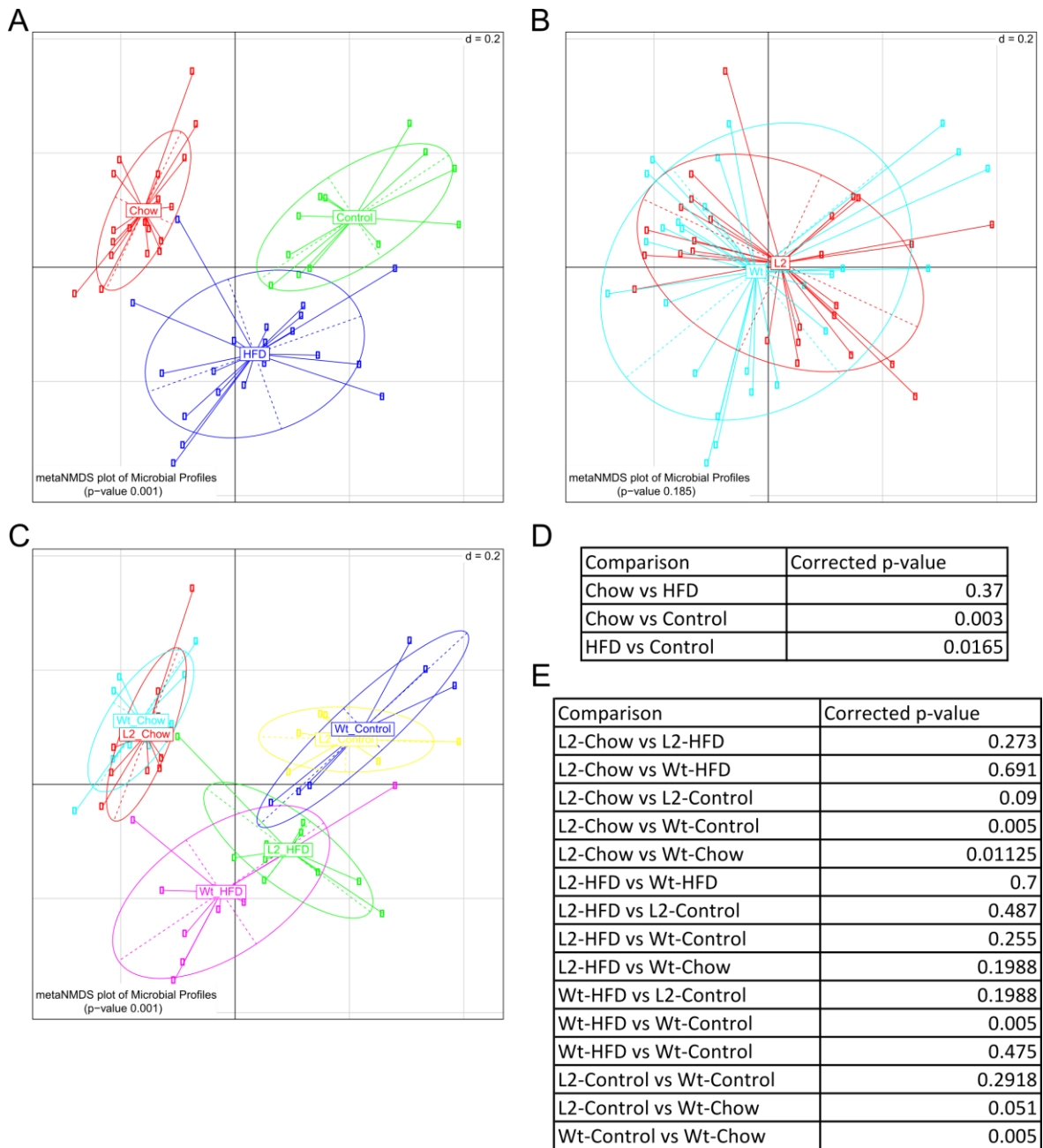


Figure 25: Generalized UniFrac using non-metric Multi-Dimensional Scaling of SPF samples

A: Separation by diet (red=Chow, blue=HFD, green=Control) **B:** Separation by genotype (turquoise=wt, red=L2) **C:** separation by diet and genotype (turquoise=wt-Chow, red=L2-Chow, purple=wt-HFD, green=L2-HFD, blue=wt-Control, yellow=L2-Control) **D:** corrected p-values for pairwise comparisons in **A** **E:** corrected p-values for pairwise comparisons in **C**. p-values were calculated after PERMANOVA with Bonferroni-Hochberg post-hoc testing (L2=L2-IL-1 β , wt=wildtype, HFD=high fat diet, Control=Control diet)

Figure 25 shows a clear separate clustering of samples according to the diet, however the difference between Chow and HFD samples is not significant, while Control samples are significantly different from both, Chow and HFD samples. Unlike in the VAT samples genotype alone is not leading to significantly different clustering in the UniFrac.

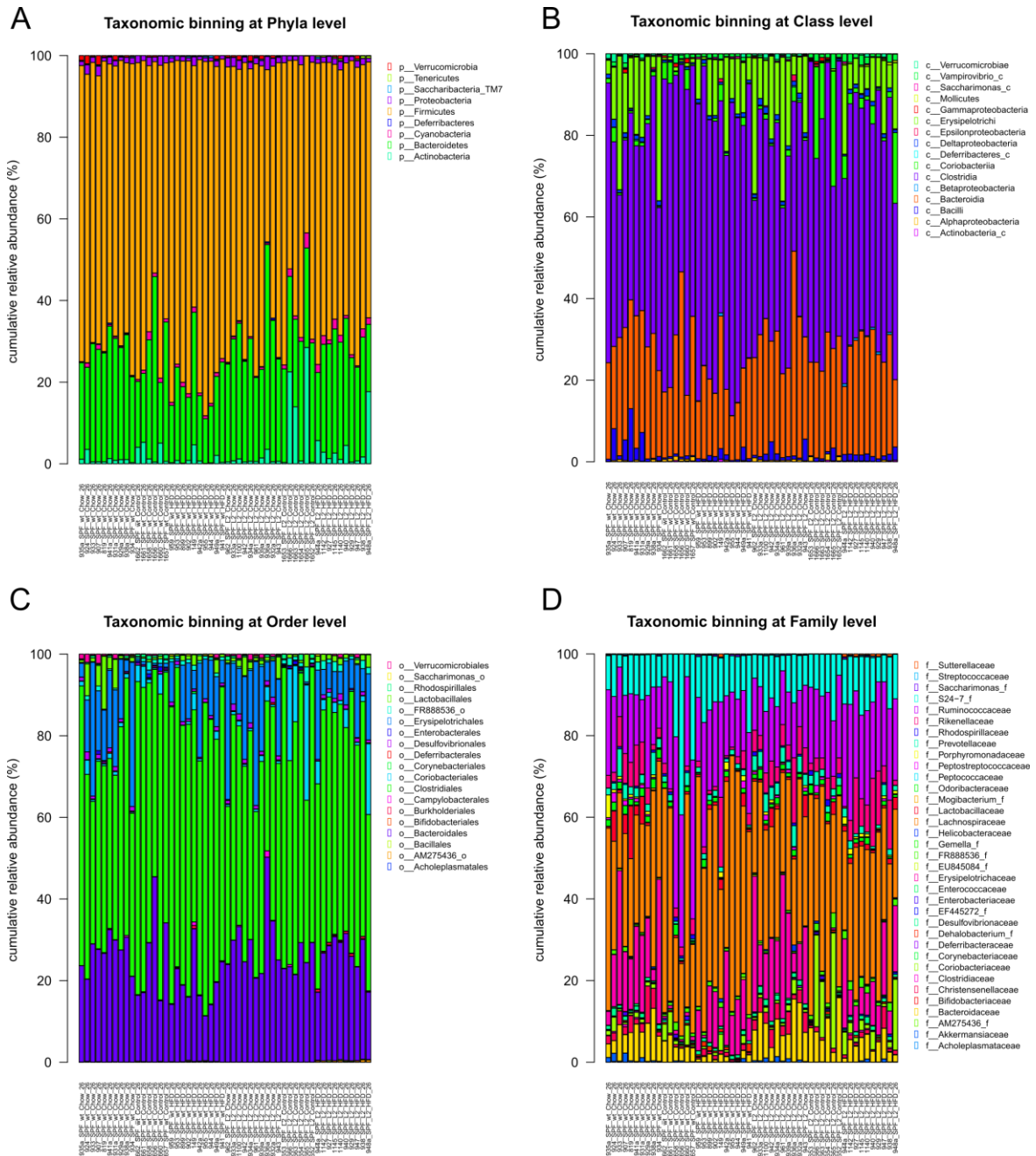


Figure 26: Taxonomic distribution of SPF samples

A: Taxonomy at phylum level **B:** Taxonomy at Class level **C:** Taxonomy at Order level **D:** Taxonomy at Family level

Figure 26 shows an overview of the taxa found in the SPF samples. It was not possible to identify taxa clearly associated with genotype or diet, possibly due to the large variety observed.

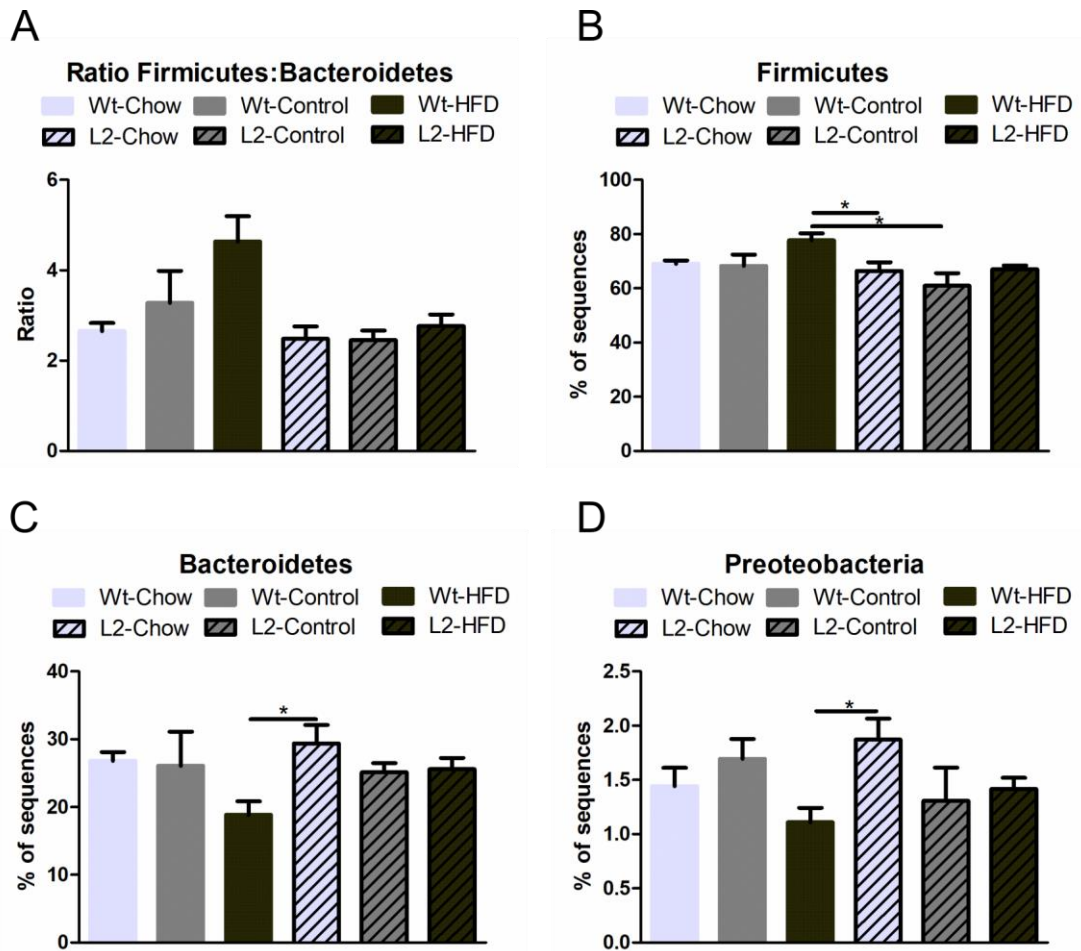


Figure 27: Common obesity associated phyla in SPF samples

A: Ratio of members of the phylum Firmicutes to the members of the phylum Bacteroidetes **B:** Relative abundance of the phylum Firmicutes **C:** Relative abundance of the phylum Bacteroidetes **D:** Relative abundance of the phylum Proteobacteria. An ANOVA with Tukey post-hoc testing was performed to test for significant differences. Plotted is mean with SEM. (HFD=high fat diet, Control=Control diet, L2=L2-IL-1 β , wt=wildtype)

Figure 27 shows bacterial phyla associated with obesity. There seems to be an increase of the Firmicutes:Bacteroidetes ratio in wt-HFD mice, which is mainly due to a decrease of Bacteroidetes. For all other mice the Firmicutes:Bacteroidetes ratio is unchanged. Especially in the L2 group the Firmicutes:Bacteroidetes ratio is not changed at all, only a small decrease in Proteobacteria is observable in L2-Control and L2-HFD mice.

3.1.3 Comparison of VAT and SPF housing of L2-IL-1 β mice

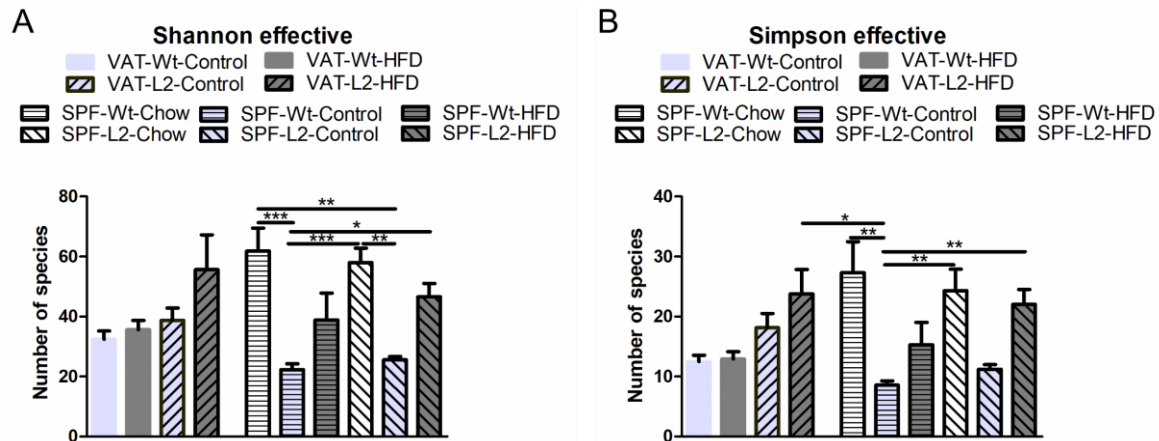


Figure 28: α -diversity of VAT and SPF samples

A: Number of Shannon effective species **B:** Number of Simpson effective species. A Kruskal-Wallis with Dunn's post-hoc testing was performed to test for significant differences. Plotted is mean with SEM * $p < 0.05$, ** $p < 0.01$, *** $p < 0.001$ (HFD=high fat diet, Control=Control diet, L2=L2-IL-1 β , wt=wildtype)

Figure 28 shows the combined α -diversity of 6 month old mice from both, VAT and SPF. In accordance to the VAT data, the diversity in SPF mice on a control is reduced in L2-IL-1 β and wildtype mice compared to the respective chow groups. The HFD mice present with an intermediate species number, located between Chow and Control in the SPF group. Interestingly, the VAT samples do not show many more species in comparison to the cleaner SPF mice.

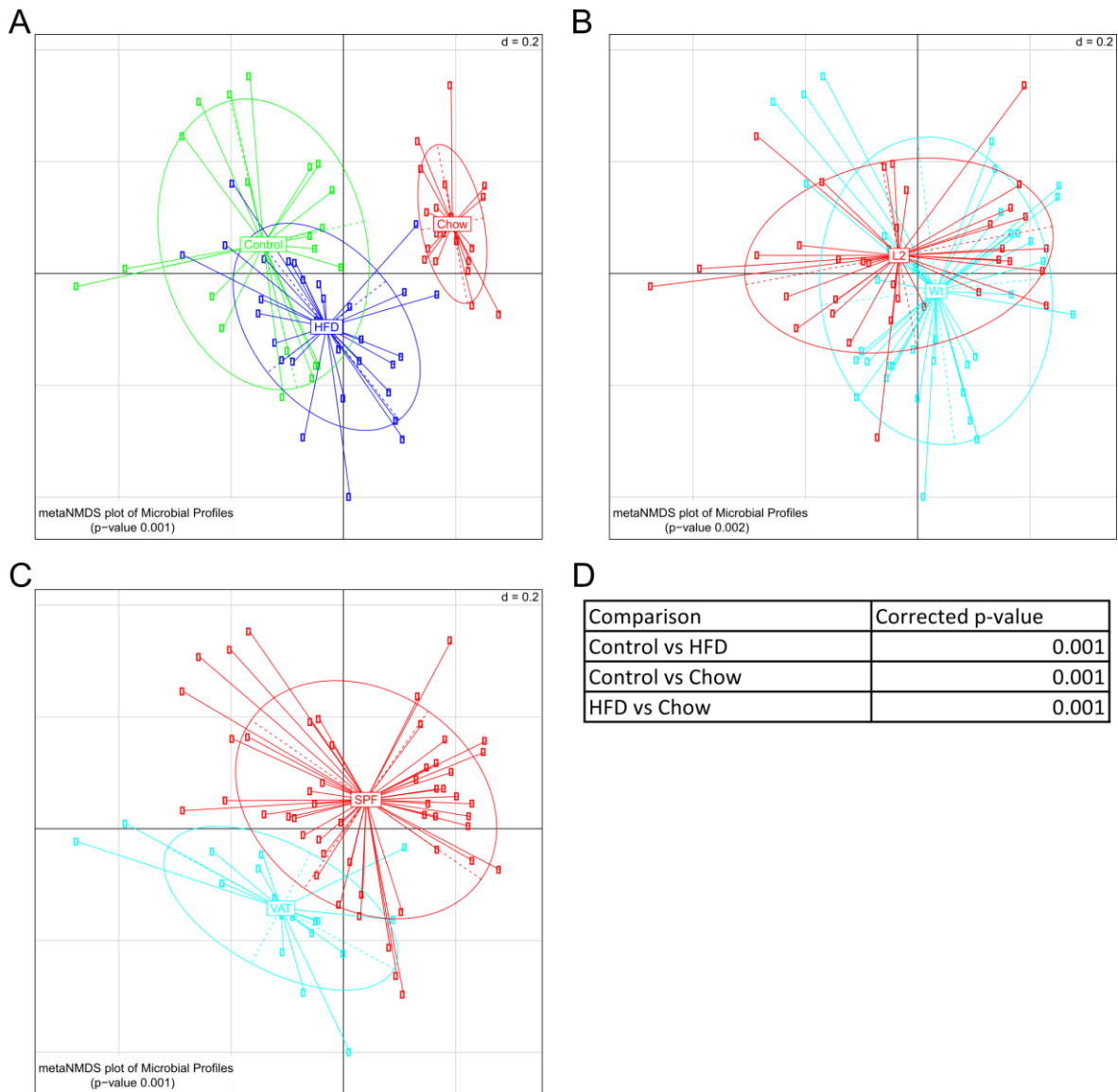


Figure 29: Generalized UniFrac using non-metric Multi-Dimensional Scaling of VAT and SPF samples
A: Separation by diet (blue=HFD, green=Control, red=Chow) **B:** Separation by genotype (turquoise=wt, red=L2) **C:** Separation by holding facility (turquoise=VAT, red=SPF) **D:** corrected p-values for pairwise comparisons in **A**. p-values were calculated after PERMANOVA with Bonferroni-Hochberg post-hoc testing (HFD=high fat diet, Control=Control diet, L2=L2-IL-1 β , wt=wildtype)

Figure 29 shows a highly significant clustering of samples according to the diet, even though the HFD and controls are overlapping considerably. The genotype alone is leading to significantly different values with a strong overlap of L2-IL-1 β and wildtype samples. The same is true for the separation based on the holding facility, were a significant difference is observable with overlapping clustering.

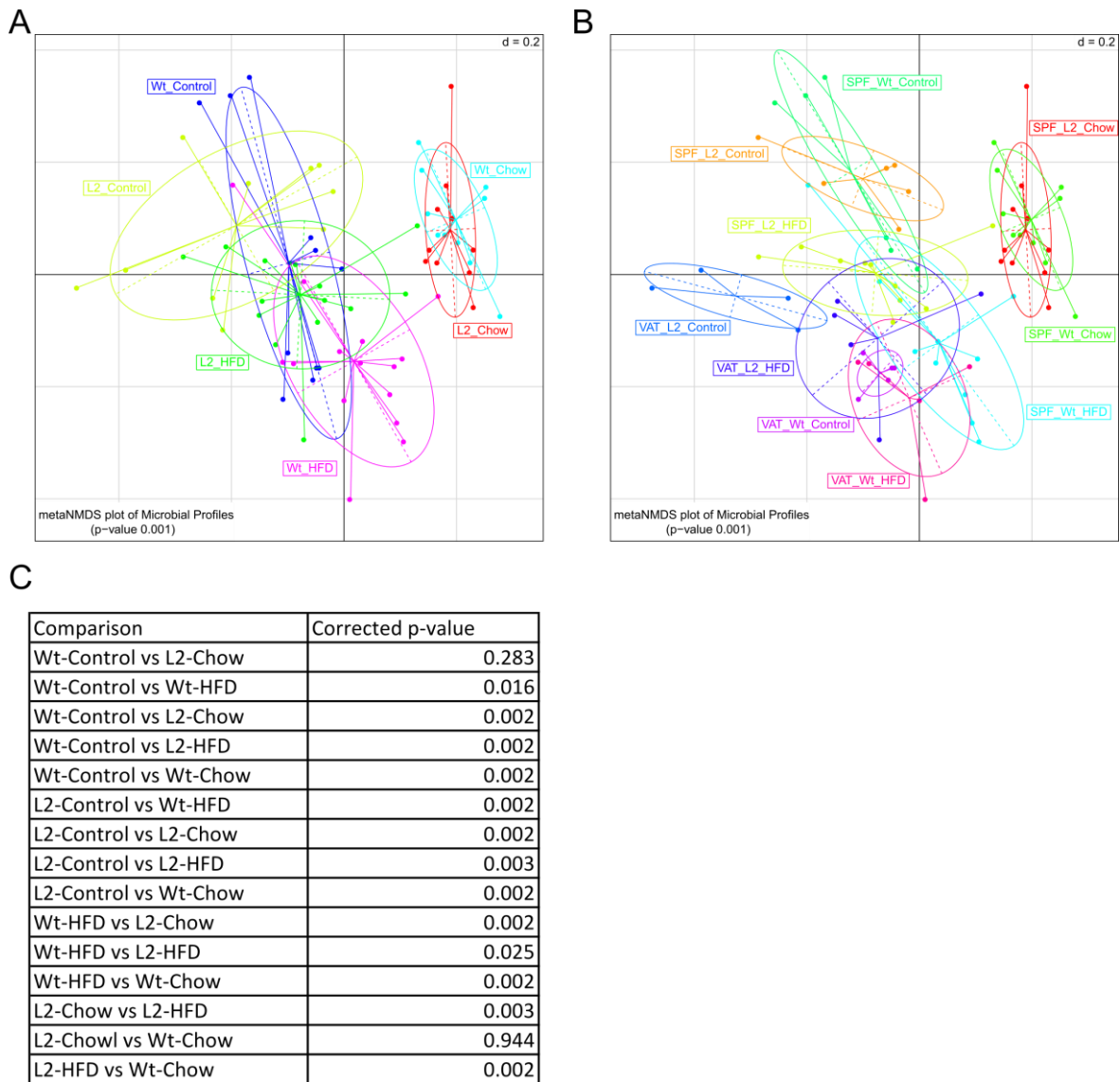


Figure 30: Generalized UniFrac using non-metric Multi-Dimensional Scaling of VAT and SPF samples
A: Separation by genotype and diet (turquoise=wt-Chow, red=L2-Chow, purple=wt-HFD, green=L2-HFD, blue=wt-control, lime=L2-Control) **B:** Separation by genotype, diet and holding facility (red=SPF-L2-Chow, green=SPF-wt-Chow, mint=SPF-wt-Control, orange=SPF-L2-Control, lime=SPF-L2-HFD, turquoise=SPF-wt-HFD, blue=VAT-L2-Control, purple=VAT-wt-Control, magenta=VAT-wt-HFD, lavender=VAT-L2-HFD)
C: corrected p-values for pairwise comparisons in **A**. p-values were calculated after PERMANOVA with Bonferroni-Hochberg post-hoc testing (HFD=high fat diet, Control=Control diet, L2=L2-IL-1 β , wt=wildtype)

Figure 30 shows highly significant separate clustering of generalized UniFrac data from the VAT and the SPF. It is noteworthy that the chow fed mice cluster most separately, regardless if they are separated by genotype and diet or separated by genotype, diet and holding. Figure 30A shows an overlapping clustering for HFD and Control mice, which nevertheless are significantly different from each other. In contrast to that the chow samples cannot be discriminated by genotype. Figure 30B shows the plot for separation by

diet, genotype and holding facility. Only 9 out of 45 pairwise comparisons yield a non-significant result, as depicted in the Appendix Table 13.

3.1.4 SPF during aging

To investigate potential changes over time within the cohorts, fecal samples from 13, 26, 39 and 52 week old L2 mice were analyzed. As a reference for a normal adult sample 26 week old wildtype mice on Chow and HFD were used.

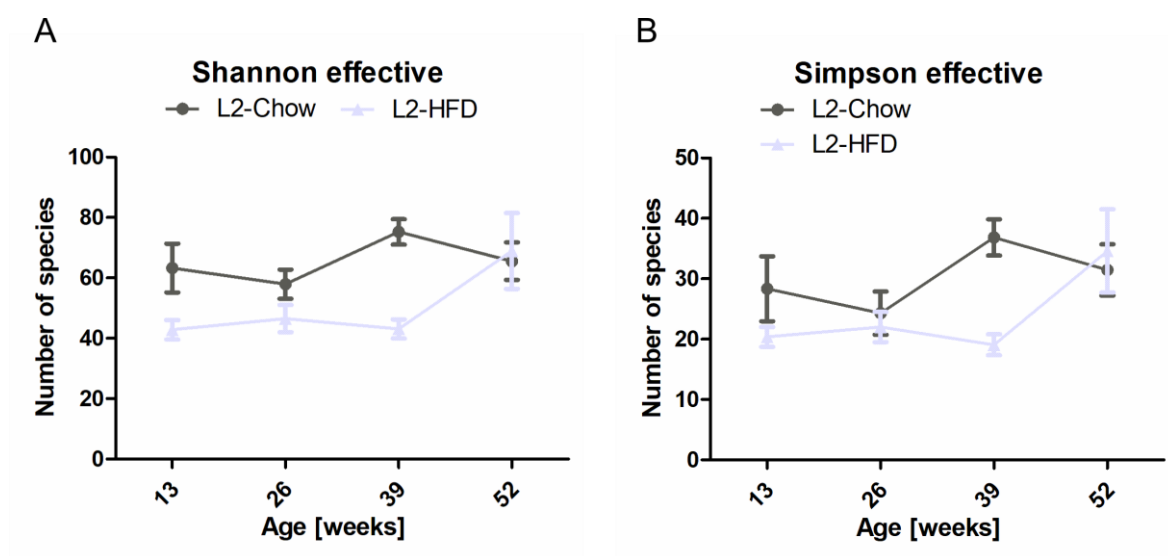


Figure 31: α -diversity of SPF samples during aging

A: Number of Shannon effective species **B:** Number of Simpson effective species. 2-way ANOVA showed that only the group (L2-Chow or L2-HFD) has a significant influence on diversity and not the age or an interacting term of group and age. Plotted is the mean with SEM (L2=L2-IL-1 β , wt=wildtype, HFD=high fat diet)

Figure 31 shows the diversity observed in the SPF samples in L2 mice at different ages, however only the diet is influencing the species number significantly. The curves seem to meet at the age of 52 weeks, indicating a very similar number of species in L2-Chow and L2-HFD mice at the age of 52 weeks.

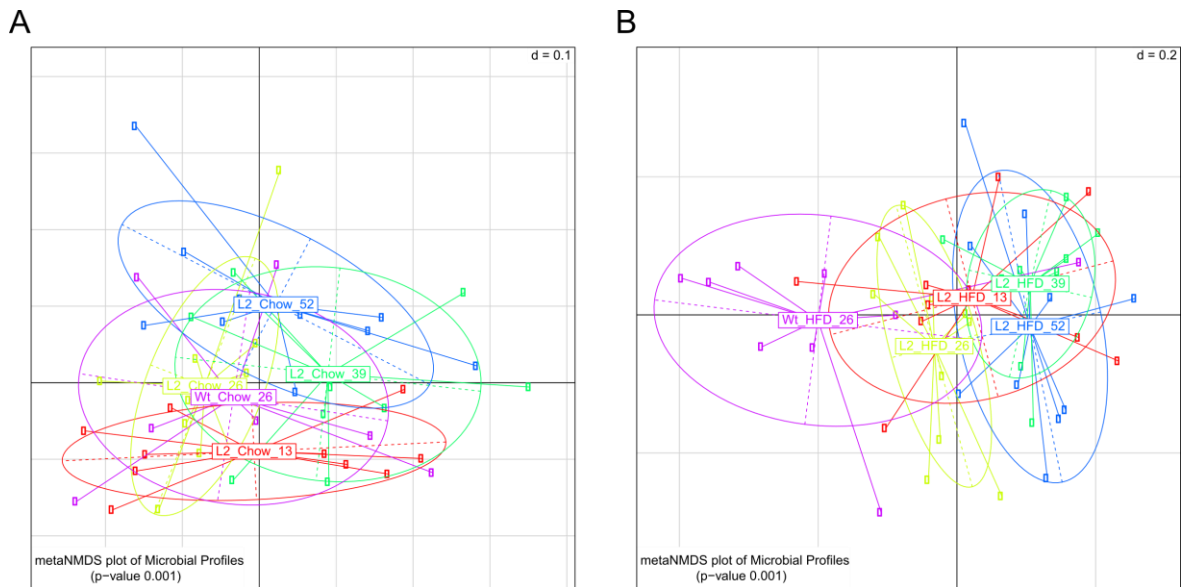


Figure 32: Generalized UniFrac using non-metric Multi-Dimensional Scaling of SPF samples during aging

A: Separation by age and genotype for Chow mice (purple=wt-Chow-26, red=L2-Chow-13, lime=L2-Chow-26, mint=L2-Chow-39, blue=L2-Chow-52) **B:** Separation by age and genotype for HFD mice (purple=wt-HFD-26, red=L2-HFD-13, lime=L2-HFD-26, mint=L2-HFD-39, blue=L2-HFD-52). p-values were calculated after PERMANOVA with Bonferroni-Hochberg post-hoc testing (L2=L2-IL-1 β , wt=wildtype, HFD=high fat diet)

Clustering of generalized UniFrac data shows an overall significant p-value, as depicted in Figure 32. The pairwise comparisons calculated show no significant differences between the timepoints. The older the L2-IL-1 β mice, the more distant they seem to cluster from the respective wildtype controls.

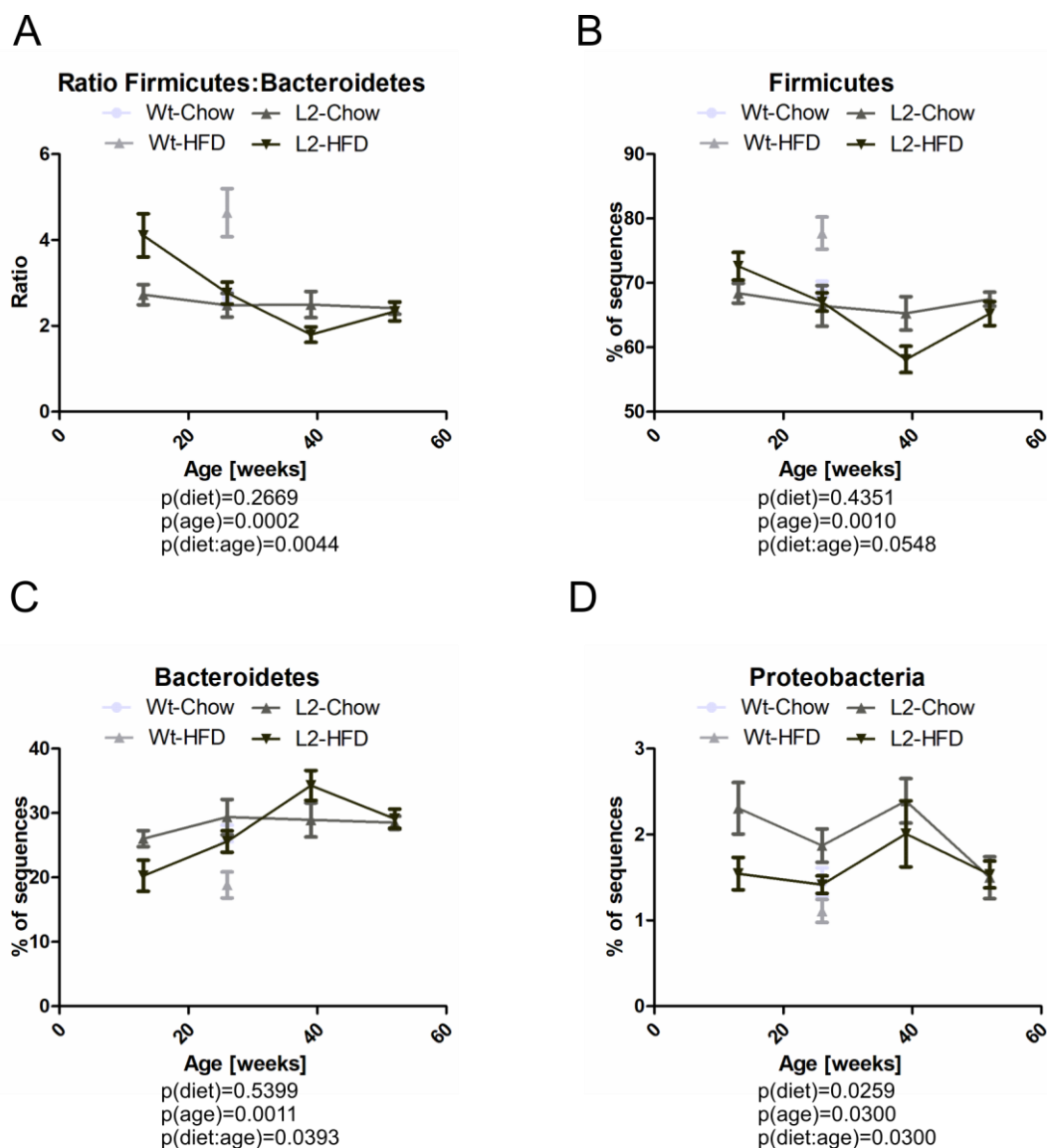


Figure 33: Common obesity associated phyla in SPF samples during aging

A: Ratio of members of the phylum Firmicutes to the members of the phylum Bacteroidetes, **B:** Relative abundance of the phylum Firmicutes **C:** Relative abundance of the phylum Bacteroidetes **D:** Relative abundance of the phylum Proteobacteria. 2-way ANOVA was performed to test for significant differences between L2-Chow and L2-HFD. Plotted is mean with SEM. (L2=L2-IL-1 β , wt=wildtype, HFD=high fat diet)

Figure 33 shows the abundances of phyla associated with obesity. Since the wildtype mice could not be integrated in the 2-way ANOVA due to the fact that there is only one timepoint, the 2-way ANOVA describes differences between L2-Chow and L2-HFD mice. Only the phylum Proteobacteria is significantly different, while the age is significant for the ratio Firmicutes:Bacteroidetes, Firmicutes, Bacteroidetes and Proteobacteria. The interacting term of diet and age is significant for the Firmicutes:Bacteroidetes ratio, Bacteroidetes and Proteobacteria. Interestingly the value for 26 weeks old wildtype mice is often similar to the L2-HFD values.

3.1.5 Germfree housing of L2-IL-1 β mice abrogates the inflammatory phenotype

Germfree L2-IL-1 β mice have been raised by the James G Fox laboratory at MIT (Cambridge, MA, USA) and analyzed in our laboratory.

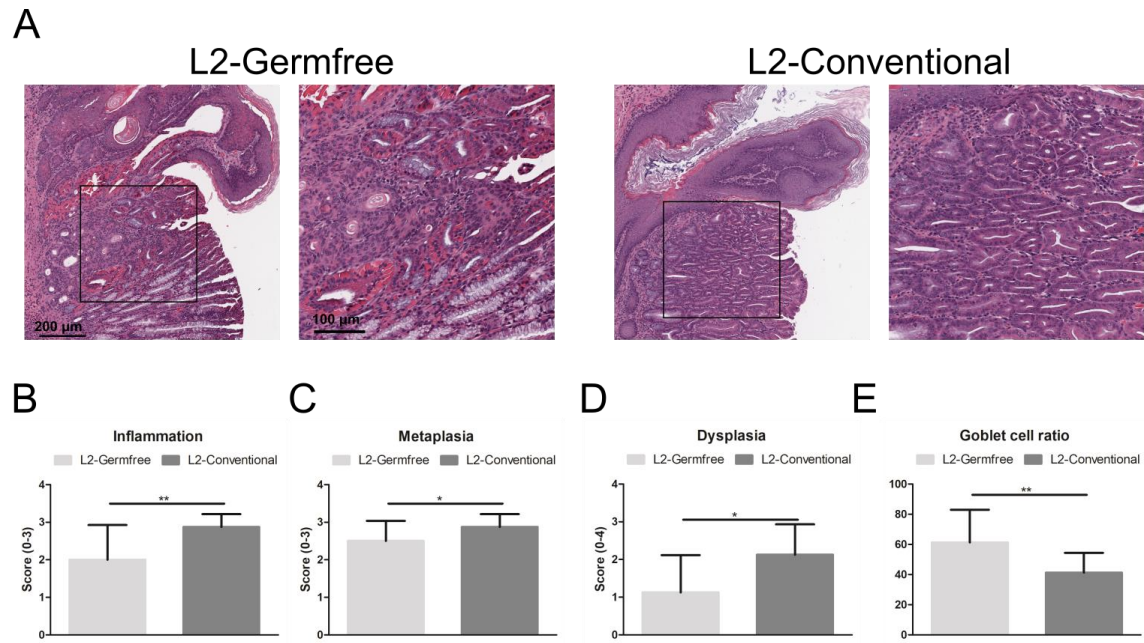


Figure 34: Histologic analysis of germfree and conventional L2-IL-1 β mice

A: Representative HE staining of the squamous-columnar junction **B:** Inflammation score **C:** Metaplasia score **D:** Dysplasia score **E:** Goblet cell ratio. A t-test was performed to test for significant differences. Plotted is mean with SEM * $p < 0.05$, ** $p < 0.01$ (L2=L2-IL-1 β)

As depicted in Figure 34 germfree L2-IL-1 β mice present with a different phenotype compared to L2-IL-1 β mice from a conventional facility. Germfree mice have significantly reduced inflammation, metaplasia and dysplasia meaning a reduced tumor phenotype. Additionally they have more goblet cells than the conventional mice, suggesting a more differentiated cell type found in the germfree mice.

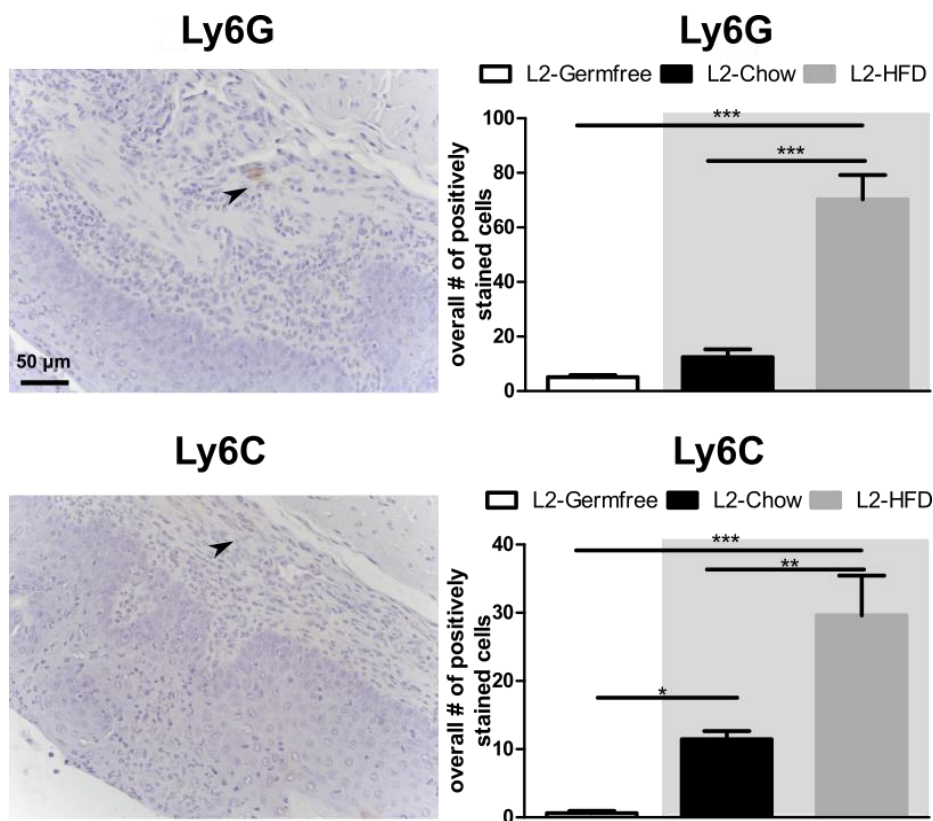


Figure 35: Representative Ly6G and Ly6C IHC staining and quantification

Ly6G staining for neutrophils and Ly6C staining for immature myeloid cells for germfree mice compared to the L2-Chow and L2-HFD mice generated by Dr. Münch (grey background) [88]. A 1-way ANOVA with Tukey post-hoc testing was performed to test for significant differences. Plotted is mean with SEM * $p < 0.05$, ** $p < 0.01$, *** $p > 0.001$ (L2=L2-IL-1 β , HFD=high fat diet)

IHC of neutrophils and immature myeloid cells shows a significantly reduced immune cell invasion in germfree mice as depicted in Figure 35, suggesting immune cell invasion as an important mechanism in tumor formation.

3.1.6 Bedding transfer is sufficient for a phenotype transfer

L2-IL-1 β mice in the VAT present with a significantly stronger dysplastic phenotype than age matched SPF mice while germfree mice present with reduced inflammation and reduced tumor formation. This is suggestive of a phenotype mediated by the observed differences in the microbiome. To investigate whether the L2-HFD phenotype can be transferred with the microbiome, a simple bedding transfer experiment was performed. Bedding from a cage of adult, female L2-IL-1 β mice on HFD (9-12 months old) was transferred weekly to L2-IL-1 β mice on control diet until the age of 9 months starting at the age of 6 weeks. 5 male and 5 female mice were treated this way to transfer the suspected dysbiotic L2-HFD microbiome.

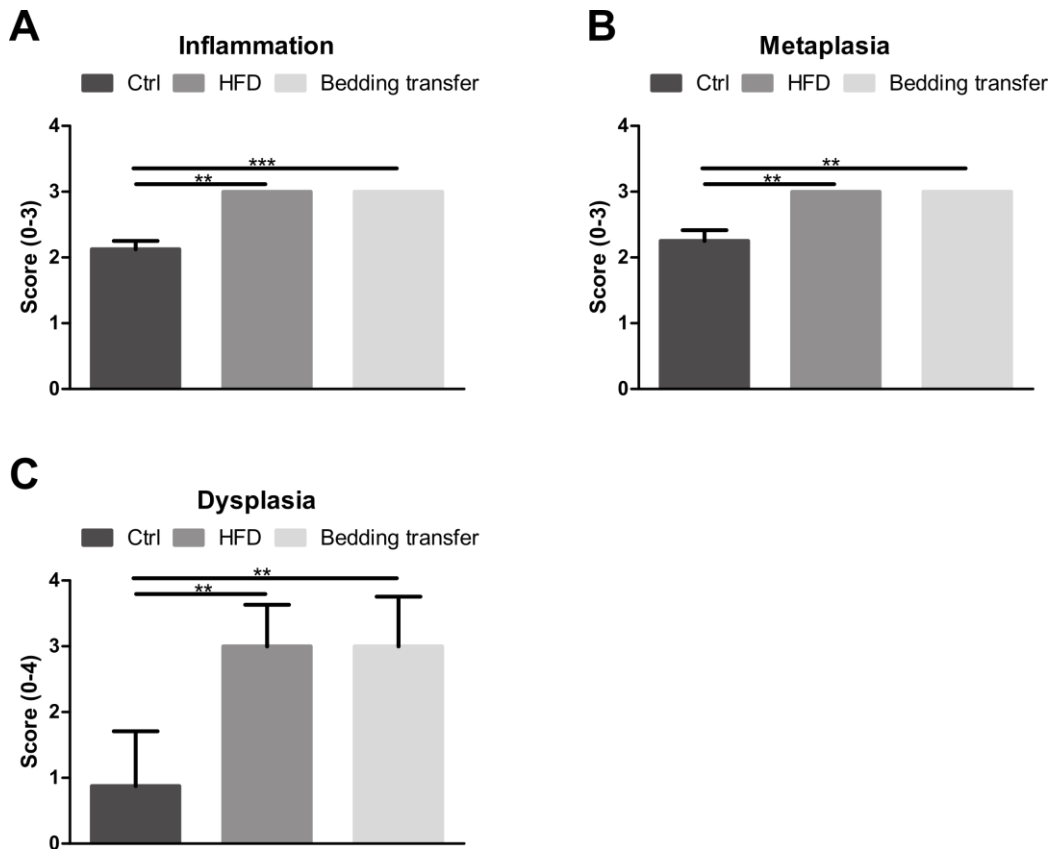


Figure 36: Histologic analysis of bedding transfer samples compared with L2-HFD and L2-Control mice

A: Inflammation score **B:** Metaplasia score **C:** Dysplasia score. A Kruskal-Wallis test with Dunn post-hoc testing was performed to test for significant differences. Plotted is mean with SEM ** $p < 0.01$, *** $p < 0.001$ (L2=L2-IL-1 β , HFD=high fat diet)

As depicted in Figure 36, the bedding transfer lead to significant change in the histologic phenotype. Inflammation, metaplasia and dysplasia scores of the mice who received the bedding are remarkably similar to the scores of L2-HFD mice and considerably stronger than in L2-Control mice.

3.1.7 Predictive functional profiling

The 16S data generated was analyzed in close collaboration with Dr. Sama Islam Sayin from the laboratory of Professor Timothy Cragin Wang at Columbia University using PICRUSt, a tool designed to predict the function of microbial communities based on 16S sequencing data [239]. This analysis was performed for the 6 months timepoint.

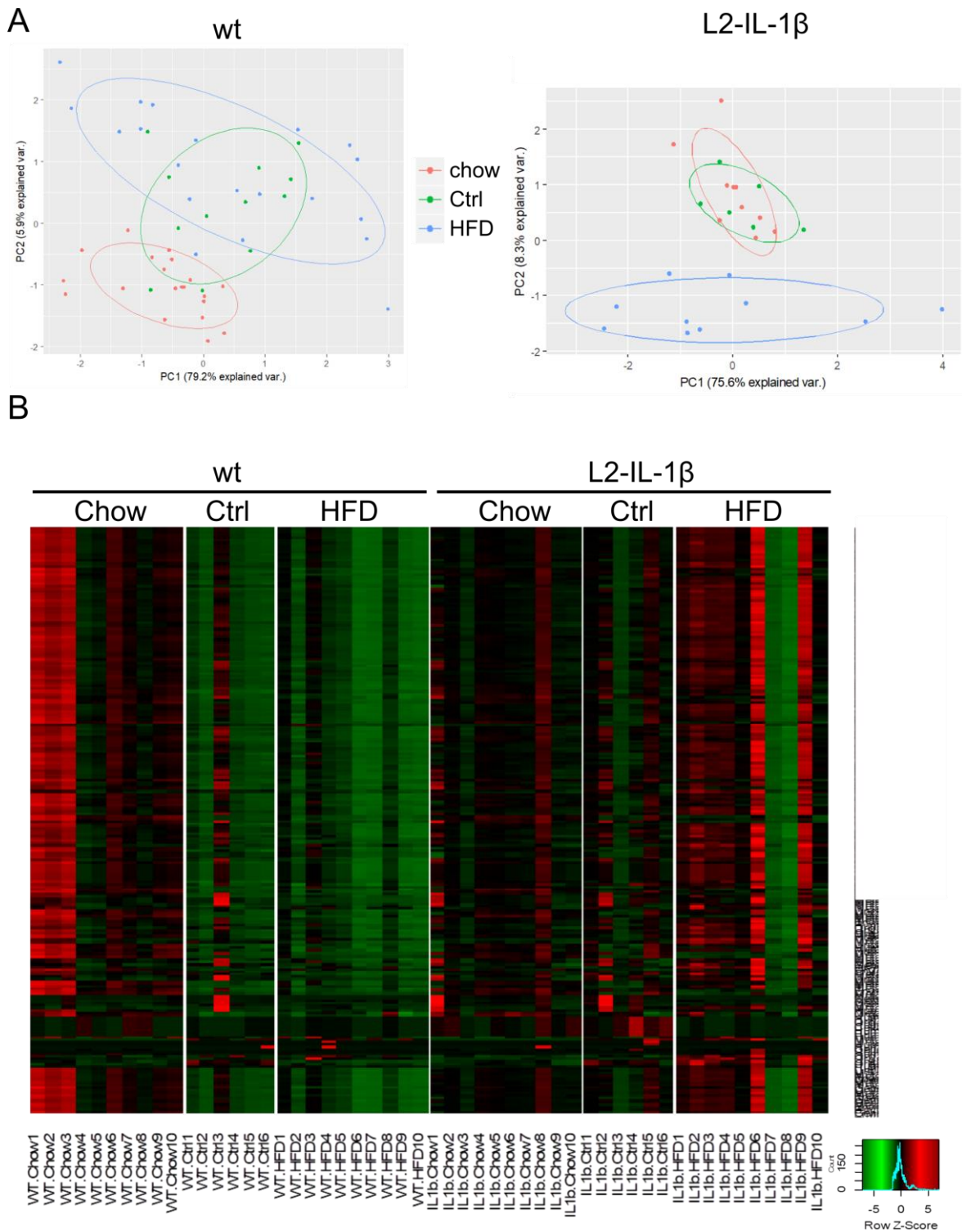


Figure 37: Predictive KEGG pathway enrichment of 16S data from wildtype and L2-IL-1 β mice on chow, control diet and HFD using PICRUST
A: Principal component analysis of the predicted KEGG pathways **B:** Heatmap showing differences in KEGG pathways (wt=wildtype, HFD=high fat diet)

Figure 37A shows the clustering of predicted KEGG pathways showing that there is no clear difference observable in the predicted function of the microbiome in wildtype mice, since they present with a strong scatter and overlapping clustering. In contrast the L2-HFD

mice cluster completely separately from the L2-IL-1 β mice on chow and control, suggesting a different functionality. The heatmap in Figure 37B shows that L2-IL-1 β mice seem to have a different KEGG profile compared to wildtype mice, suggesting an effect of the genotype on the function of the microbiome.

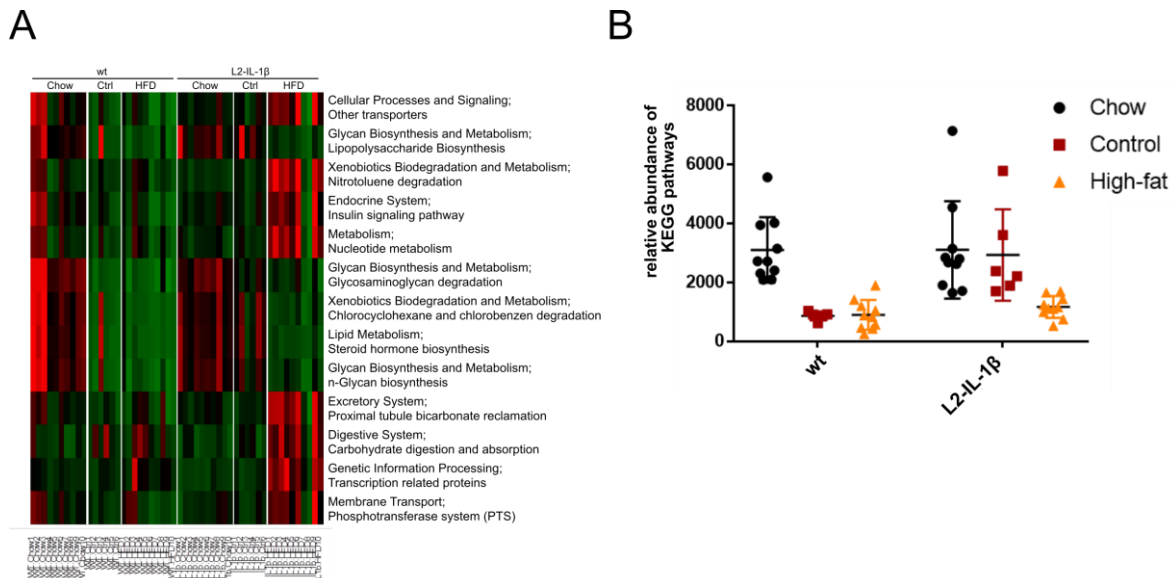


Figure 38: Significant predictive KEGG pathways of 16S data from wt and L2-IL-1 β mice on chow, control diet and HFD using PICRUSt

A: Heatmap of significantly regulated pathways **B:** KEGG pathways for lipopolysaccharides (wt=wildtype)

Figure 38A shows significantly regulated KEGG pathways, among which there are metabolic pathways potentially contributing to the non-obese phenotype of L2-HFD mice. The synthesis of lipopolysaccharides is highly downregulated in wildtype mice on the purified diets, while L2-Control mice seem to maintain a chow-like phenotype in contrast to L2-HFD mice where the synthesis of lipopolysaccharides is downregulated similarly as in the wildtype mice.

3.1.8 Potential indicator species associated with the L2-IL-1 β HFD phenotype could not be detected

LDA Effect Size (LEfSe) analysis was performed to identify indicator species potentially linked to tumor formation.

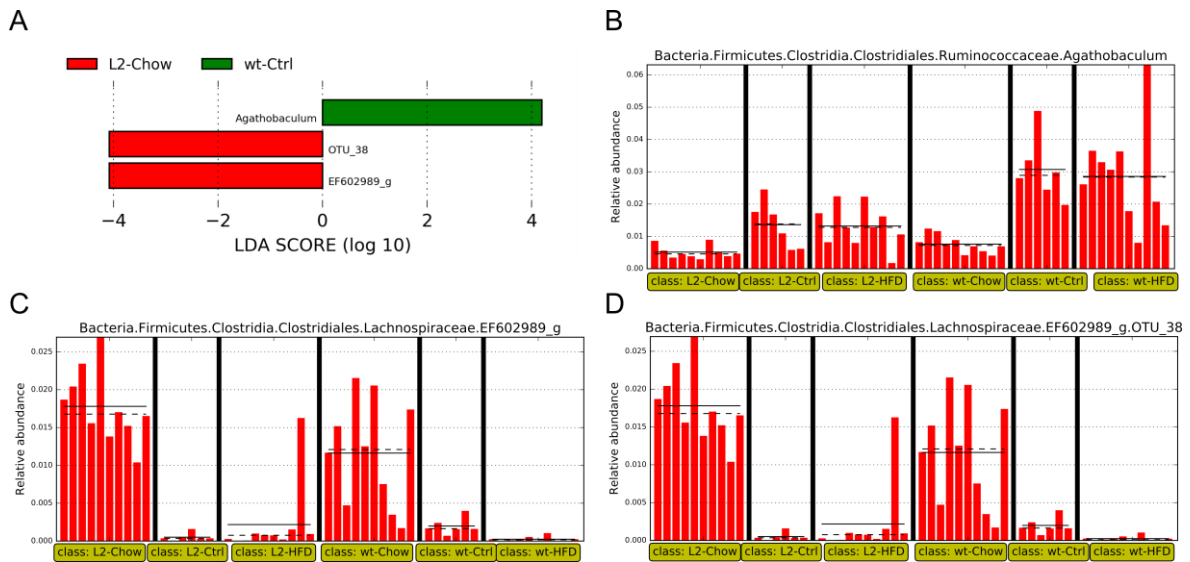


Figure 39: Results of the LDA Effect Size (LEfSe) analysis of the 26 weeks timepoint of the SPF cohort
A: Significantly different bacterial groups **B-C:** Relative abundances of the 3 significant results pointing towards the identity of OTU_38 (L2=L2-IL-1 β , wt=wildtype, Ctrl=Control diet, HFD= high fat diet)

As depicted in Figure 39, the only significant result was the differentiation between L2-Chow and wt-Control mice. It should be noted that OTU_38, a member of the *Lachnospiraceae* family is depicted twice, first as the OTU but also as a genus. No other effects could be detected indicating that there is no single bacterial species or strain associated with the genotype and the diet.

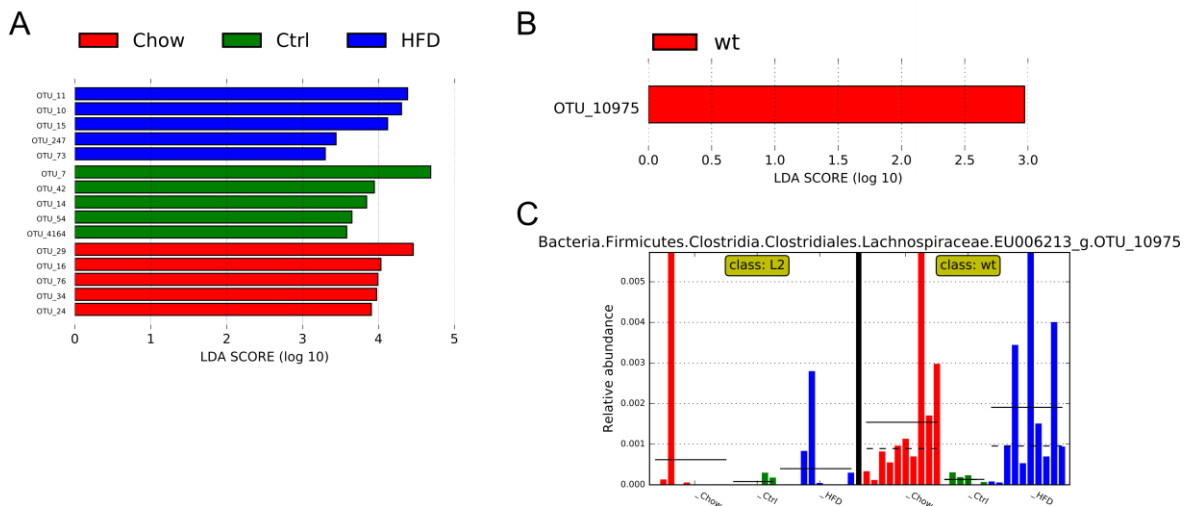


Figure 40: Results of the LDA Effect Size (LEfSe) analysis of the 26 weeks timepoint of the SPF cohort based on diet and genotype

A: Top 5 significantly different bacterial groups between the diets across genotypes **B:** Significantly different bacterial group between the genotypes across diets **C:** Relative abundance of the significantly different OTU between the genotypes across diets (L2=L2-IL-1 β , wt=wildtype, Ctrl=Control diet, HFD= high fat diet)

To verify if the analysis can be performed successfully the data was analyzed only based on the diet, which is a well-known influence on the microbiome composition. Figure 40A shows the most significant differences showing that the diet is associated with the microbiome across the genotypes. The full results are depicted in Appendix Figure 47. Figure 40B-C show the only OTU which is significantly different between wildtype and L2-IL-1 β mice across the diets with the control diet presenting different.

3.1.9 Inflammatory signaling leads to increased Lgr5+progenitor cells

The L2-HFD phenotype has been shown to be linked to IL8/KC signaling and an increase in Lgr5+ stem cells [88]. To investigate a mechanistic link between inflammation and stem cell proliferation CXCR2 expression was analyzed. L2/IL8Tg mice were used as a positive control for two reasons. L2/IL8Tg mice show a similar phenotype as L2-HFD mice regarding acceleration and strength of tumor development. CXCR2 is a receptor reacting to IL-8/KC and leads to proinflammatory signaling.

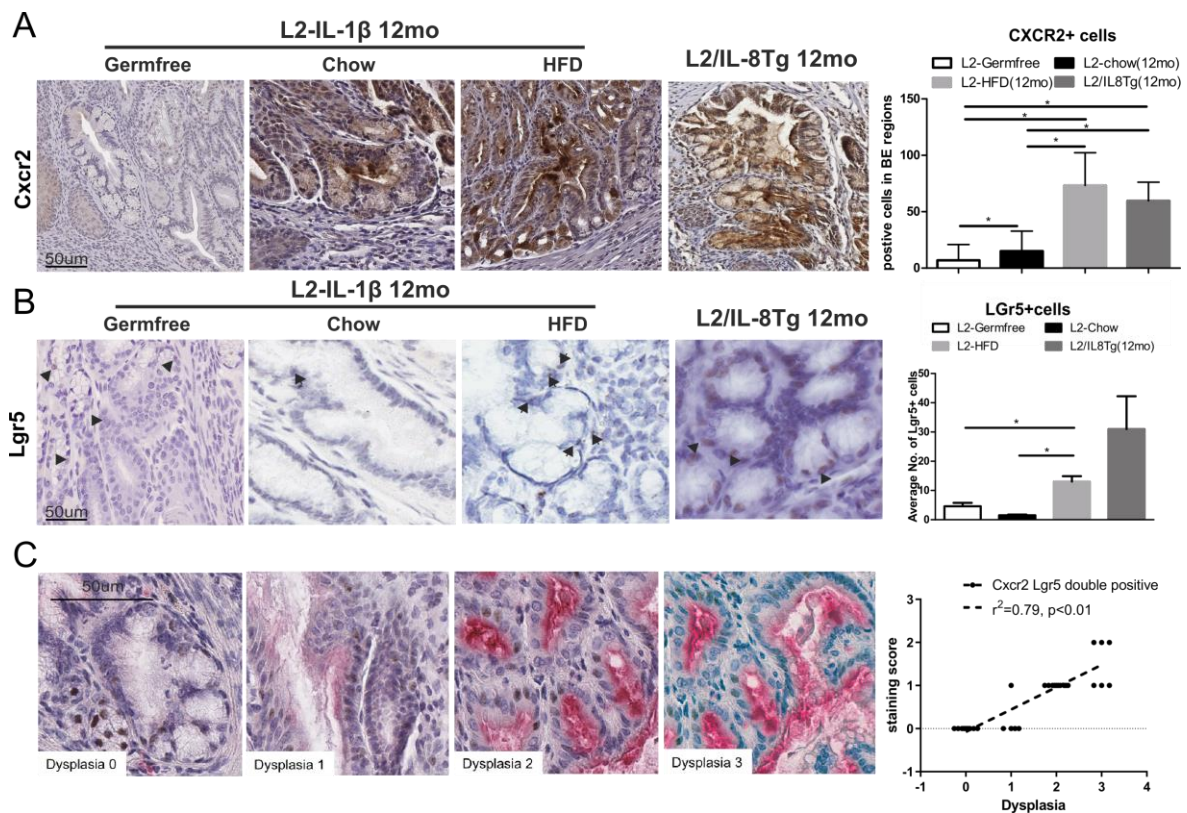


Figure 41: CXCR2 and Lgr5 expression

A: CXCR2 IHC in L2-IL-1 β mice **B:** Lgr5 ISH in L2-IL-1 β mice **C:** CXCR2 (red) and Lgr5 (brown) double staining and the correlation with the dysplasia score. An ANOVA with Tukey post-hoc testing was performed to test for significant differences. Plotted is mean with SEM. * $p<0.05$ (L2=L2-IL-1 β , L2/IL8tg=L2-IL-1 β +IL8Tg, HFD= high fat diet)

CXCR2 expression depends significantly on the hygiene/inflammation level, as depicted in Figure 41A. This is paralleled by an increase of Lgr5 positive cells as shown in Figure 41B. Figure 41C shows that CXCR2 expressing cells are also expressing Lgr5, linking inflammation to the expansion of progenitor cells. Interestingly the amount of CXCR2/Lgr5 double positive cells correlates with the dysplasia score, highlighting the importance of inflammation to tumor formation.

Taken together this data suggests that changes of the intestinal microbiome are associated with BE and EAC progression in mice. Since the HFD phenotype seems to be transferable with the microbiome, preventive approaches based on changing the microbiome (e.g. diet changes, antibiotic treatment or microbiome transfers) could be considered for further research. An alternative approach for prevention would be to target the inflammatory processes involved which seemingly influence the stem cell niche using anti-inflammatory treatment.

3.2 Anti-inflammatory treatment affects tumor progression

3.2.1 Anakinra attenuates the HFD phenotype

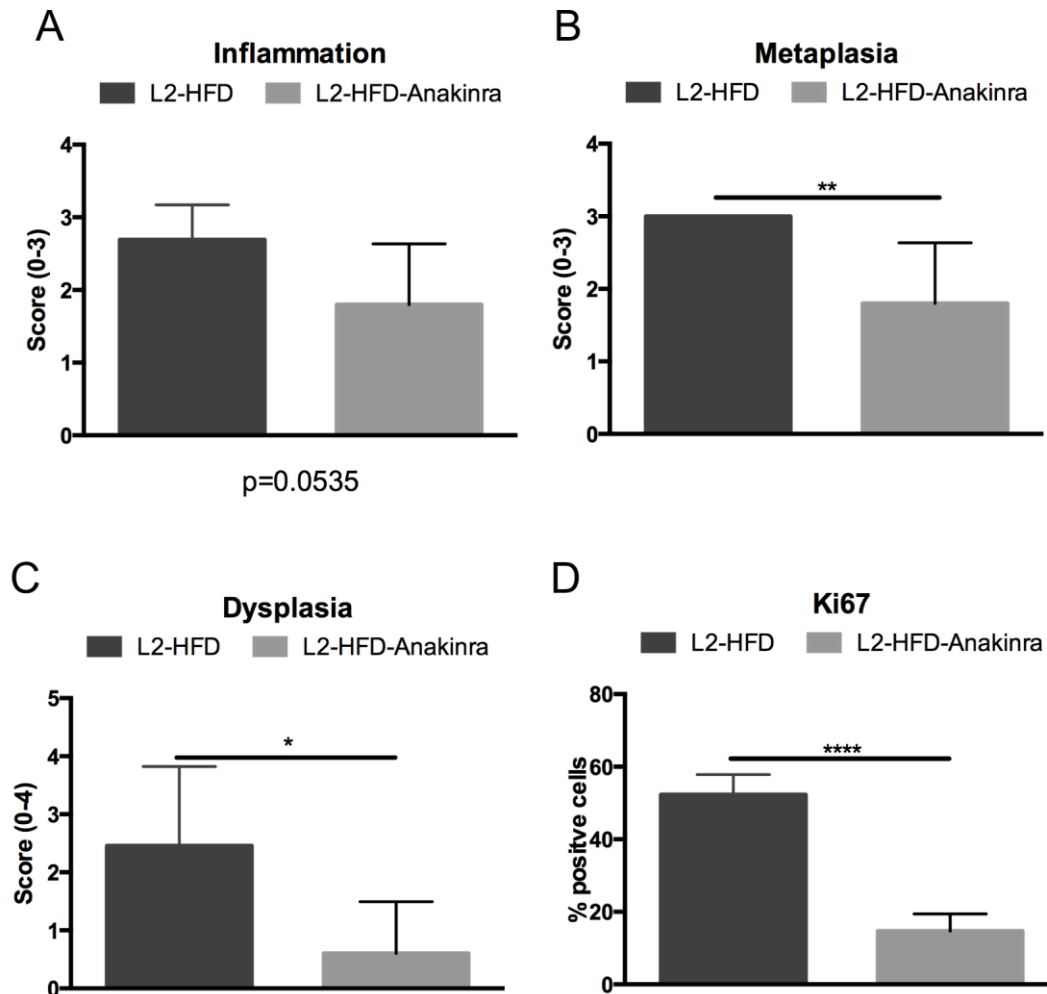


Figure 42: Histologic analysis of Anakinra treated mice samples using HE and Ki67 staining

A: Inflammation score B: Metaplasia score C: Dysplasia score D: Ki67 staining. A Mann Whitney test with was performed to test for significant differences. Plotted is mean with SEM *p<0.05, **p<0.01, ***p<0.001 (L2=L2-IL-1 β , HFD=high fat diet)

Figure 42 shows that the treatment with Anakinra attenuates the HFD-Phenotype in regard to metaplastic and dysplastic changes. A highly significant effect can be observed in regards to cell proliferation analyzed by Ki67 staining. This shows that Anakinra treatment has a significant effect on tumor development in L2-IL-1 β mice.

3.2.2 NSAIDs change the immune phenotype

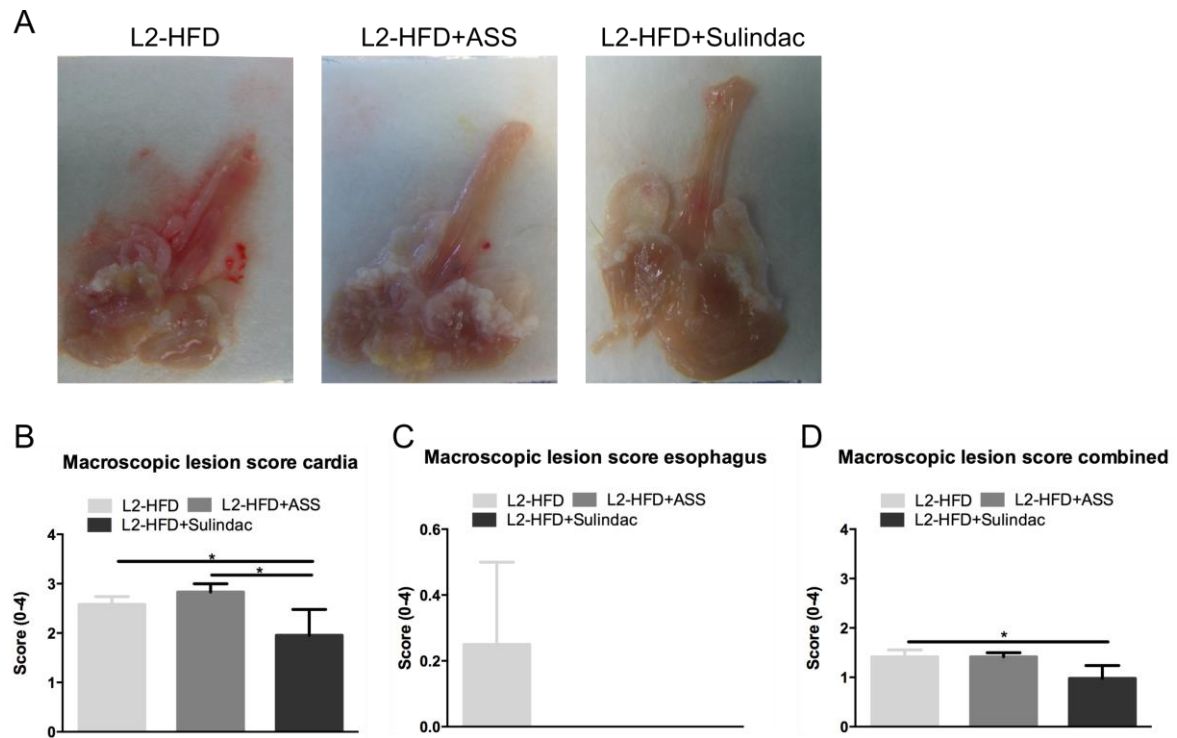


Figure 43: Macroscopic analysis of L2-IL-1 β mice treated with ASS or Sulindac

A: Representative images of the mouse cohorts stomachs **B:** Macroscopic scoring of the cardia lesions **C:** Macroscopic scoring of the esophagus lesions **D:** Average of the lesion score for esophagus and and cardia. A ANOVA test with Tukey post-hoc testing was performed to test for significant differences. Plotted is mean with SD * $p < 0.05$ (L2=L2-IL-1 β , HFD=high fat diet, ASS=Aspirin)

Figure 43 shows a weak, yet significant influence of the Sulindac treatment on tumor formation in the cardia, but not the esophagus while ASS doesn't seem to have an influence.

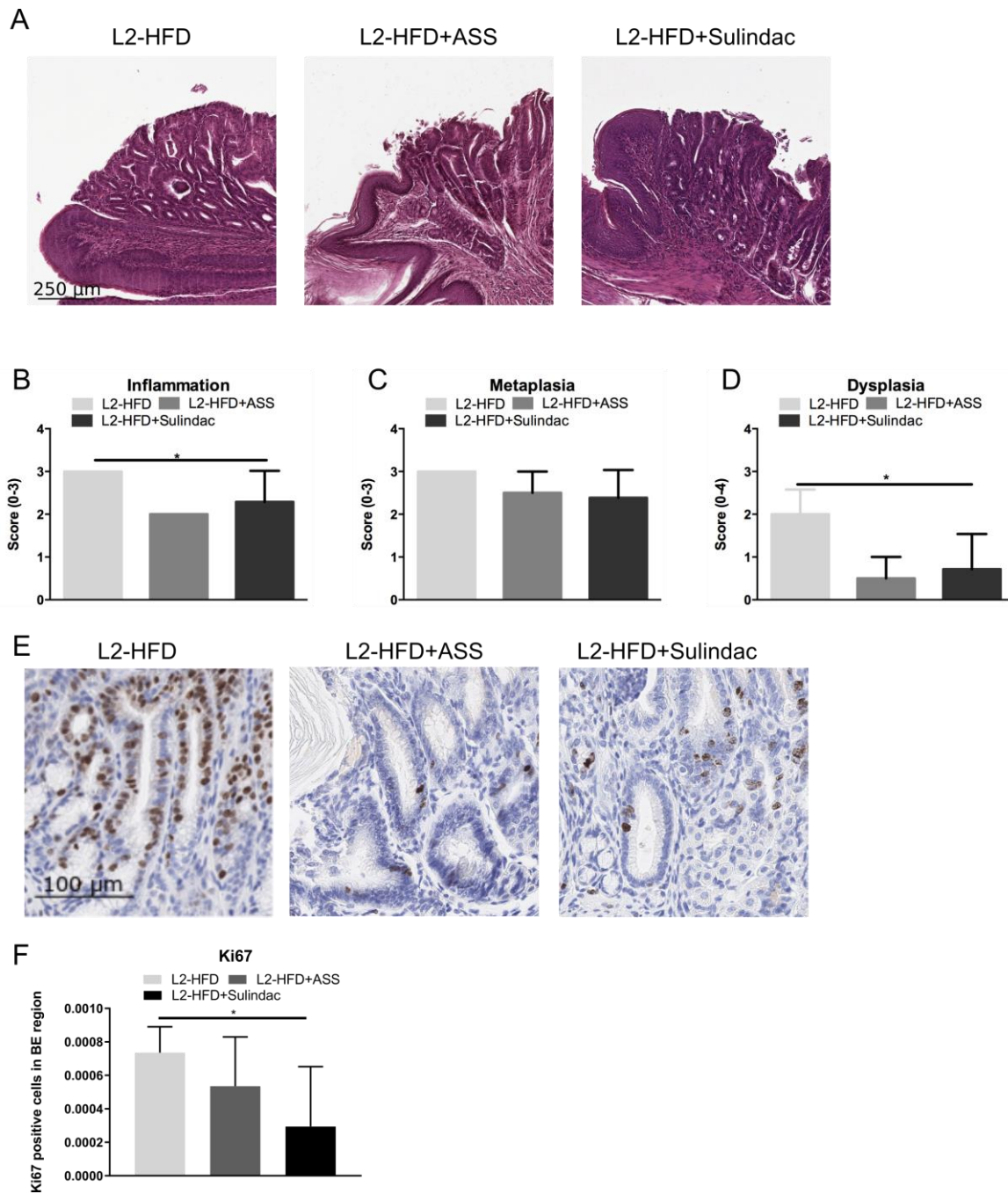


Figure 44: Histologic analysis of L2-IL-1 β mice treated with ASS or Sulindac

A: Representative HE stainings of the BE region **B:** Inflammation score **C:** Metaplasia score **D:** Dysplasia score **E:** Representative Ki67 staining in BE region **F:** Quantification of Ki67 positive cells in the BE region. A ANOVA test with Tukey post-hoc testing was performed to test for significant differences. Plotted is mean with SD * $p < 0.05$ (L2=L2-IL-1 β , HFD=high fat diet, ASS=Aspirin)

While the effect of Sulindac on the histologic scorings is significant as well for inflammation and dysplasia, as shown in Figure 44, ASS seems to have an effect on dysplasia development which fails to reach significance. It is worth to note that only Sulindac has a significant effect on proliferation quantified by Ki67 staining.

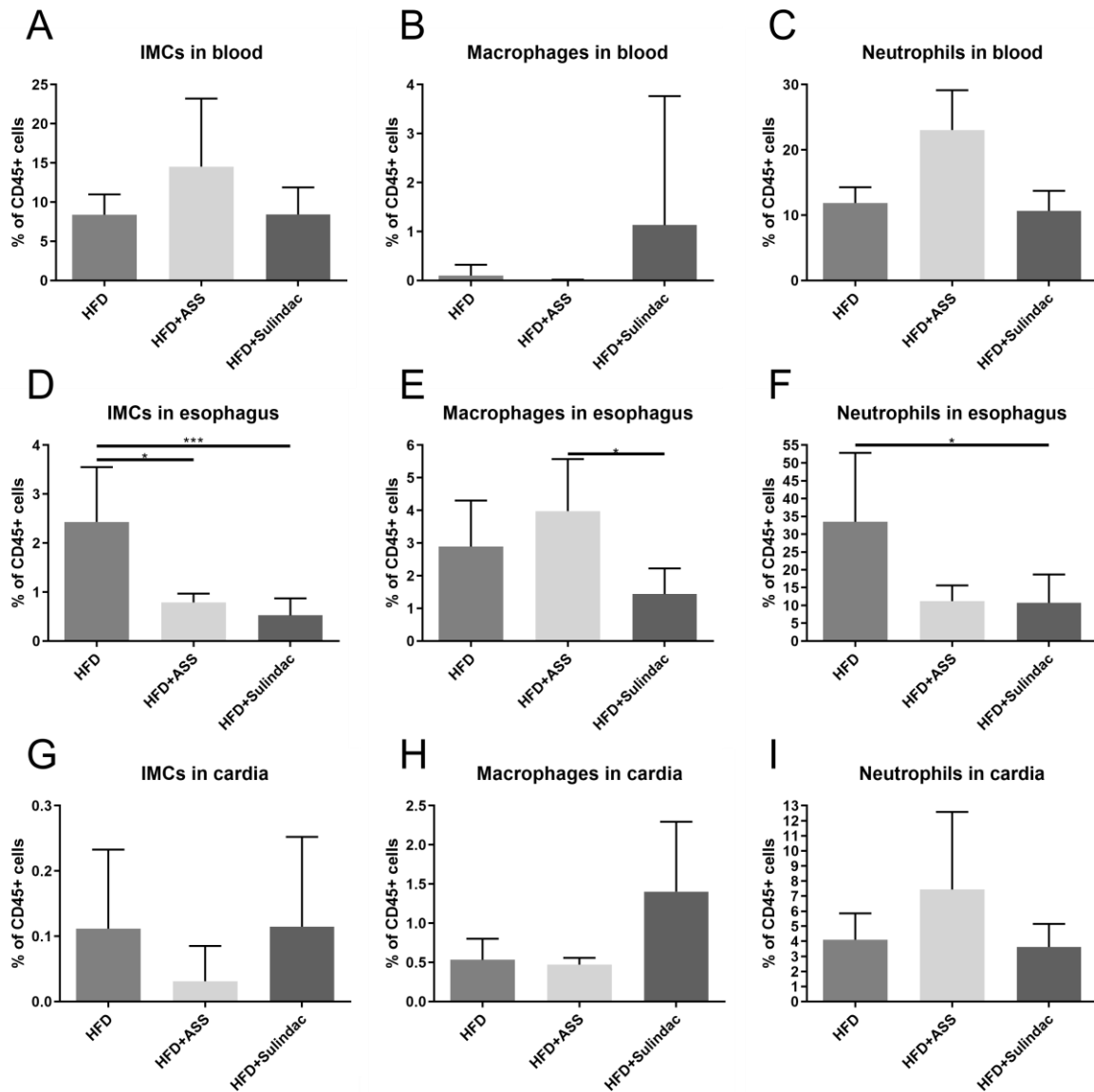


Figure 45: Analysis of immune cells of the myeloid lineage in L2-IL-1 β mice treated with ASS or Sulindac

Percentage of CD45 positive cells identified as immature myeloid cells (IMCs) (A, D, G), Macrophages (B, E, H) and Neutrophils (C, F, I) in the blood (A-C), esophagus (D-F) and the cardia region (G-I). A ANOVA test with Tukey post-hoc testing was performed to test for significant differences. Plotted is mean with SD * $p < 0.05$, *** $p < 0.001$ (HFD=high fat diet, ASS=Aspirin)

Figure 45 shows the influence of ASS and Sulindac on the immune cell profile of the myeloid lineage. Significant differences could only be observed in the esophagus of L2-IL-1 β mice, where ASS and Sulindac lead to a reduced invasion of immature myeloid cells (IMCs) and neutrophils. Interestingly the Sulindac treated animals present with decreased macrophage invasion in the esophagus and increased macrophage invasion in the cardia.

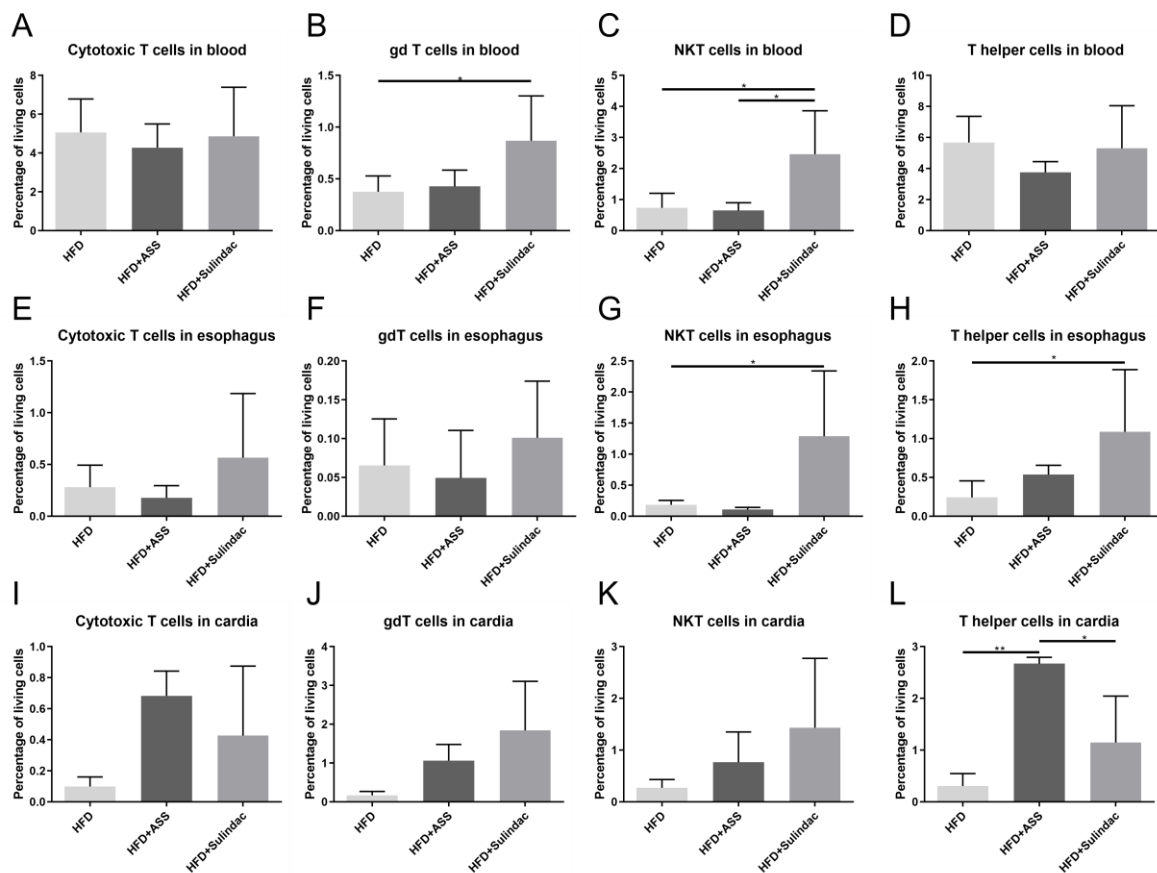


Figure 46: Analysis of immune cells of the T cell lineage in L2-IL-1 β mice treated with ASS or Sulindac Percentage of living cells identified as cytotoxic T cells (A, E, I), $\gamma\delta$ T cells (gdT cells) (B, F, J), NKT cells (C, G, H) and T helper cells (D, H, L) in the blood (A-D), esophagus (E-H) and the cardia region (I-L). A ANOVA test with Tukey post-hoc testing was performed to test for significant differences. Plotted is mean with SD * $p < 0.05$, ** $p < 0.01$ (HFD=high fat diet, ASS=Aspirin)

Figure 46 shows the influence of ASS and Sulindac on the immune cell profile of the T cell lineage. Interestingly there seems to be a systemic effect linked to the treatment with Sulindac leading to increased gdT and NKT cells in the blood, while ASS does not seem to have an influence on a systemic level. Apparently there is also an increased immigration of these two cell types in the cardia which fails to reach significance. NKT cells migrate significantly more into the esophagus of L2-IL-1 β mice treated with Sulindac, while there is an increase of T helper cells in the esophagus which is more pronounced in the cardia region with a stronger increase in ASS treated mice.

4. Discussion

EAC is a common form of esophageal cancer with rising incidence over the past decades but still a poor prognosis [42, 44]. BE and EAC are associated with age, male gender, Caucasian ethnicity, GERD, BE and obesity/dietary factors [44, 45]. While obesity was increasing in parallel, the increase of EAC incidence was rising about a decade earlier, suggesting other (environmental) factors as relevant actors [240]. It has been shown that L2-IL-1 β mice on a HFD present with an accelerated phenotype independent of obesity, suggesting that other mechanisms than obesity are responsible for the development of EAC [88]. This data leads to the hypothesis that the western diet/lifestyle is a driver for EAC development. Since nutritional behavior is highly associated with the composition of the gastrointestinal microbiome, the correlation of the microbiome shaped by diet and environment with tumor development in L2-IL-1 β mice was investigated. Since it remains unclear how the microbiome can be influenced in a protective way, anti-inflammatory treatment was investigated as preventive measure.

4.1 The gut microbiome is changed in tumor bearing mice

Until now no clear associations of BE and EAC with changes of the microbiome have been described [241]. Studies of the local microbiome at the gastroesophageal junction or at BE/EAC are limited in power due to the acidic environment caused by the commonly found reflux [242]. One prevalent association of the microbiome and BE/EAC association is with *Helicobacter pylori*. The eradication of *H. pylori* was found to be inversely associated with BE/EAC [243-245]. However it remains unclear whether *H. pylori* itself is protective or just a proxy for further microbiome changes [246]. In contrast *H. pylori* is well associated with and a well-established cause of gastric ulcers [247]. However it seems unlikely to find many instances of disease where a single bacterial species is responsible. Regarding complex gastrointestinal diseases it seems highly likely that changes in the microbiome composition play a bigger role than single species [248, 249]. It seems possible that systemic immune effects are linked to local inflammation in BE and EAC, which was investigated in the L2-IL-1 β mouse model.

Breeding the L2-IL-1 β mice in different hygiene levels ranging from a “dirty” open cage facility (VAT), a SPF facility and a germfree facility showed that tumor development increases in an inverse proportionally relationship to the hygiene level. Germfree L2-IL-1 β mice present with a reduced phenotype, corresponding to reduced inflammation which is well reported for germfree mice [250, 251]. This likely due to the reduced immune cell invasion compared to conventional L2-IL-1 β mice. Feeding L2-IL-1 β mice a HFD leads to increased tumor formation in both the SPF and the VAT facilities; to a stronger extent in the VAT. This phenotype was transferable by a simple bedding transfer from L2-HFD mice to L2-IL-1 β mice on a control diet, suggesting that the microbial composition is highly relevant. The L2-HFD mice have a distinct gut microbiome measured by 16S sequencing of feces. These results suggest an influence of the gut microbiome on the development of BE and tumors in the L2-IL-1 β mouse model. Taking together the evidence from the data presented here the association of changes in the gut microbiome with tumor development is highly plausible. While a traditional proxy of an obesity associated microbiome could not be observed in L2-HFD mice, the shift of the Bacteroidetes:Firmicutes ratio observed in obese mice could be reproduced in the wildtype mice in the SPF but not in the VAT [252, 253]. This suggests that it is not an obesity associated microbiome observed in the L-2-HFD mice but rather a distinct HFD associated microbiome and that the Bacteroidetes:Firmicutes ratio should be interpreted with care and depending on the hygiene level of the environment. This highlights the relevance of the hygiene level of a mouse facility regarding the characteristics of a microbiome. If one considers not only the hygiene level, but also other environmental variables, careful planning should be done before setting up experimental conditions in cancer models in mice. E.g. the ambient temperature, which is often below thermoneutrality for mice, is known to influence tumor growth and the regulation of the immune system, possibly by metabolic stress [254]. This adds to the evidence that the metabolism and its regulation are a central player in tumorigenesis and tumor development and is an additional link of cancer to nutrition. Overnutrition, ie. the intake of more energy than the energy spent, is associated with obesity and the metabolic syndrome, defined by increased BMI, insulin resistance/hyperinsulinemia, hyperglycemia, dyslipidemia and hypertension. It has become evident that the metabolic syndrome is associated with cancer development [255, 256]. Potential drivers include insulin dependent growth factor activation, adipokine secretion by adipose tissue and leptin induced angiogenesis via the VEGF pathway [257-260]. While obesity is clearly associated with metabolic syndrome, it seems highly likely that a

metabolic syndrome can be present even in patients without excessive body fat, expanding the potential of associated cancers developing in normal weight patients [261, 262].

While metabolic changes could be a cause or consequence of changes in the microbiome, little is known about the mechanisms behind. One relevant mechanism is FXR signaling, which reacts to bile acids metabolized by bacteria. It has been shown that FXR signaling is involved in obesity and bacterial community shifts associated with metabolic changes [263-265]. Recently it has been shown that FXR signaling in the context of a HFD can support intestinal tumor formation in mice [266]. While bile acids alone have been shown to be sufficient to accelerate tumor formation in L2-IL-1 β mice, a functional relevance of FXR signaling in L2-IL-1 β mice has been described highlighting the relevance of FXR signaling in BE and EAC in the L2-IL-1 β mouse model [72, 267]. A predictive functional analysis by using PICRUS_t however does not hint toward bile acid metabolism, but highlights metabolic pathways. The metabolic pathways could be a factor influencing the non-obese phenotype of L2-HFD mice, since the carbohydrate digestion seems to be influenced. On the other hand other pathways, e.g. the lipid metabolism pathway, seem to be similar to wt-HFD mice. These ambiguous results do not allow any further conclusions regarding the metabolic function of the microbiome in this model, but highlights its relevance. Interestingly there seems to be change regarding the pathways regulating lipopolysaccharide synthesis, which are known to bind to TLR which is also involved in inflammatory signaling [268]. Lipopolysaccharides can pass from the intestinal lumen to the circulatory system and are associated with inflammation [269]. TLR receptors can stimulate immune cells together with CD14 to progress into inflammatory signaling e.g. via NF- κ B signaling [251, 270]. TLR signaling has been shown to induce the expression of IL8 among other proinflammatory cytokines [271, 272]. Interestingly it has been shown that BE and EAC are associated with IL8 expression and that IL-1 β can lead to IL8 activation, suggesting a synergistic effect of IL-1 β driven inflammation and microbiome induced inflammatory processes in L2-HFD mice [120, 121, 273, 274]. Furthermore, it has been shown that the IL8 receptor CXCR2 is necessary for IL8 dependent proliferation in cancer and that CXCR2 is expressed in EAC and that CXCR2 inhibition leads to reduced invasion [119, 275-277]. While CXCR2 is mainly known as a receptor on immune cells, it has been reported that CXCR2 signaling can also support self-renewal of (cancer) stem cells [278-281]. Consequently the inflammatory phenotype found in L2-HFD mice mediates an increase in Lgr5/CXCR2 positive cells, directly linking inflammation and

progenitor cells at the SCJ. This is suggestive of an inflammatory, tumor promoting stem cell niche similar as described for skin lesions [282]. While these predictive results support the functionality of the microbiome regarding immune signaling in our mouse model, a causative connection has yet to be revealed. Further information could be gained by using complimentary techniques, such as metagenomic sequencing of the microbiome.

There are several limitations regarding these results. Even though the preliminary results of the 16S sequencing of the cardia region did not show a clear pattern, an influence of the local microbiome cannot be excluded. This is relevant due to the previously described microbial differences reported locally in BE and EAC patients [210-212]. A recently published study has shown that wildtype mice develop inflammation and metaplasia at the gastroesophageal junction when fed a HFD with DCA [283]. Interestingly HFD+DCA was correlated with an increased bacterial diversity in the esophagus, suggesting that the local microbiome might be involved. Additionally there are methodical drawbacks, such as the limited transferability of results of mouse microbiome studies to humans due to anatomical differences (e.g. stomach anatomy, mucosa layout), differences in the biorhythm (e.g. night-day activity), genetic heterogeneity and diet [284-286]. Furthermore, while it is known that 16S sequencing data from fecal samples is a proxy for luminal bacteria this does not allow any direct conclusions to be made about mucosal bacteria [287-289]. It has been described that the mucosal microbiome can regulate immunity, possibly linking it to inflammation [290-292]. While the functionality of the microbiome in our study is only predictive data, there could be a direct effect of fatty acids not investigated yet. It has been shown for the mouse intestine that a HFD per se is capable of enhancing stemness and tumor formation by increasing the amount of Lgr5 positive stem cells [293]. In mice treated with a HFD and DCA, a marked difference could be observed in the lipidome in the serum, highlighting the relevance of metabolic functions to esophageal inflammation [283]. Indeed it seems possible that not only obesity but more likely metabolic syndrome might be a driver of EAC [294]. In general 16S sequencing is limited in resolution, since only short fragments are analyzed which might be biased due to amplification biases and clustering issues [295-297]. While 16S analysis is still widely used, metagenomics sequencing might reduce biases and increase resolution and add information about the non-bacterial components of the microbiome [298, 299].

In summary, the influence of a HFD on the gut microbiome and an association of microbiome changes with the cancer phenotype in L2-IL-1 β mice is highly plausible

considering the data presented here and similar data reported on intestinal tumor formation [300]. The hypothesis is that a systemic influence of the intestinal microbiome on the inflammatory system is responsible for the acceleration than effects of the local microbiome possibly linked by TLR signaling that activates IL8/KC and influences the local stem cell niche. Clinical studies, such as BarrettNET, could analyze the microbiome to investigate the predictive value for human patients [301]. It could be speculated that, due to the existence of normal weight patients with metabolic syndrome and the changed microbiome in the normal weight L2-HFD mice, the collective of patients at risk for developing BE and EAC is larger than previously thought. However to date it remains unclear whether any preventive measures targeting the microbiome (e.g. changing nutritional behavior, antibiotics or microbiome transfers) could have a beneficial effect in BE/EAC patients. In contrast more is known about treatment with anti-inflammatory drugs, which directly act on the mechanism suspected for cancer development.

4.2 Anti-inflammatory treatment could be used for chemoprevention in BE/EAC

4.2.1 Anakinra reduces IL-1 β mediated inflammation

The IL-1 receptor antagonist (IL-1RA) is a member of the IL-1 family binding to the IL-1 receptor and competitively inhibiting IL-1 receptor activation [302, 303]. IL-1RA is thus able to reduce or inhibit inflammatory responses induced by IL-1 [304]. IL-1RA is a glycosylated 22 kDa protein which can be expressed as 3 isoforms with isoform 1 being the secreted one [305, 306]. The non-glycosylated recombinant IL-1RA is 17 kDa and keeps its antagonistic effect [302, 307]. Even though the affinities of IL-1 and IL-1RA for the IL-1 receptor are similar, the need for 10-100 fold molar excess seems to be necessary to block IL-1 signaling in cell culture experiments [308]. Interestingly experiments in rabbits and baboons suggest the need for 100-1000 fold molar excess in vivo [309, 310]. For mice 200 μ g of IL-1RA have been reported to be necessary to block the lethal effect of 1 μ g of IL-1 [311]. Treatment of patients with rheumatoid arthritis (a systemic autoimmune disorder with crucial IL-1 contribution) with recombinant IL-1RA showed promising results regarding safety and efficacy [312, 313]. This led to the approval of recombinant IL-1RA as Anakinra (tradename Kineret) as a treatment for patients with rheumatoid arthritis in 2002 in Germany [314]. While it remains unclear whether the efficacy of

Anakinra is due to IL-1 β or IL-1 α blocking, it has shown to be effective in a wide range of diseases such as (auto-)inflammatory diseases, bone diseases and metabolic diseases [315]. A phase II trial has shown that patients with smoldering or indolent multiple myeloma might benefit from the treatment with Anakinra possibly in combination with dexamethasone [316]. Trials are currently in progress regarding other cancers (e.g. pancreatic cancer, colon cancer) but none regarding EAC that are publicly known [317]. The treatment of L2-IL-1 β mice with Anakinra showed promising results, serving as a proof of concept that the inhibition of inflammation can reduce tumor formation. This method might not be feasible for prevention in patients due to possible side-effects and the high cost, so more common drugs should be considered for chemoprevention.

4.2.2 Sulindac inhibits tumor formation by a change in immune cell profiles

Sulindac and ASS seem to have a very similar effect on tumor formation regarding macroscopic scoring and the histology, even though ASS treatment repeatedly fails to reach significance. However, Sulindac treatment in L2-HFD mice changed the immunphenotype analyzed by flow cytometry significantly. The reduced invasion of neutrophils in the esophagus of L2-IL-1 β mice treated with Sulindac (and non-significantly in the mice treated with ASS) could be a potential mechanism that reduces tumor growth. While neutrophils can be tumor antagonizing, increased levels of neutrophils have been reported frequently in association with a higher tumor grade and poor prognosis [318-320]. While the increase of gdT cells is not significant, these cells may have antitumoral properties. Human gdT cells are capable of killing tumor cells in cell culture experiments [321]. gdT cell lacking mice present with increased tumor growth, however being limited in explanatory power due to the different functionality of gdT cells in mice and men [322]. While also having tumor-supporting properties, e.g. in cancers of the gall bladder, clinical trials have shown a weak to medium beneficial effect of gdT cells in different cancers [323-327]. There is a massive increase of NKT cells in the esophagus and blood of the Sulindac treated mice. NKT cells have been reported to have at least 2 subtypes and it should be noted that the NK1.1 marker used here is not necessarily expressed in non C57BL/6J mice strains [328]. Type I NKT cells have been reported to have cytotoxic and antitumorigenic properties mediated by IFN- γ and IL-2 signaling [329-331]. In contrast, type 2 NKT cells are capable of suppressing immune surveillance of the tumor [332-334].

It seems possible that type I NKT cells are activated by Sulindac and are suppressing tumor growth in L2-IL-1 β mice possibly assisted by T helper cells.

The changed immune cell invasion presents a plausible mechanism causing the reduced phenotype due to ASS and Sulindac treatment, with the later appearing more pronounced. Recently it has been suggested in a study analyzing GERD, BE and EAC patients that the severity of the disease is linked to reduced T-cell invasion and suggesting chemokine receptor antagonism as a preventive measure [335]. Additionally reduced T cell invasion has been reported with a poor prognosis in combination with PD-1/PD-L1 expression in EAC [336]. This is similar to the observed effect of Sulindac on the immune cell profile with an increased T cell influx into the esophagus linked with reduced tumor formation. In contrast, macrophage invasion has been reported with a poor prognosis in EAC, fitting the observation of reduced macrophage invasion into the esophagus in L2-HFD mice treated with Sulindac [337]. The increased invasion of macrophages at the cardia region of the Sulindac treated mice suggests different roles of macrophages at the main region of inflammation (the esophagus) and within the stem cell niche (the cardia).

This project was not designed to identify the subtypes of the detected immune cells, limiting the explanatory power on detailed immune mechanisms at work. ASS and Sulindac are both nonsteroidal anti-inflammatory drugs which reduce pain and inflammation. ASS is a commonly used drug which irreversibly inhibits COX-1 and to a lesser extent COX-2 [338]. ASS usage has been reported to have a protective effect regarding various cancers, e.g. colon cancer and prostate cancer [339-341]. Most of the cancer preventive effects of ASS are thought to be due to COX-2 inhibition which is rarely expressed under normal conditions, despite COX independent effects that have been reported [342]. COX-2 inhibition causes a reduction of pro-inflammatory prostaglandins, angiogenesis and increases apoptosis [343]. COX independent mechanism include the inhibition of IKK β and thus NF- κ B signaling [344]. These effects may be dose-dependent and thus have the potential to increase common side effects of ASS such as gastrointestinal bleeding [345]. It has been shown that TLR-4 is activated in BE and EAC tissue, activating COX-2 and highlighting the relevance of ASS in BE and EAC [346]. It is noteworthy that even though ASS is a very common drug, the mode of action so far is still not completely understood. The recently published AspECT trial investigated the influence of Esomeprazole and/or ASS on BE in patients and showed that ASS, especially in combination with Esomeprazole, could reduce the incidence of EAC [347]. Sulindac is

currently not approved in Germany. Sulindac is thought to act on COX-2, NF- κ B and STAT3 signaling [348-350]. Sulindac has been suggested to be preventive in colorectal cancer, another gastrointestinal cancer associated with inflammatory processes [351-353]. Studies in a mouse model of breast cancer have shown that Sulindac enhances survival and tumor regression and led to reduced influx of macrophages in the tumor environment, supporting the observation of a changed immune profile due to Sulindac [354]. In regard to COX-2 inhibition, it has been recently shown in a mouse model of esophageal squamous carcinoma, based on Krt5 driven KrasG12D expression and p53 knock-out, that tumor formation depends on COX-2 signaling [355].

In summary both, ASS and Sulindac are interesting candidates regarding chemoprevention in BE and EAC and need further (clinical) investigation. Since ASS and Sulindac show an effect on tumor formation in the L2-IL-1 β mice, the relevance of COX-2 signaling for tumor formation could be investigated by crossing in COX-2 knock-out mouse. Sulindac might be the more interesting candidate for chemoprevention due to the stronger effect on the immune cell profile and the markedly reduced proliferation it causes. It remains unclear if the observed immunophenotype and the presumed anti-tumorigenic effects are translatable to other cancers types in mice or have similar effects in patients. In the patient setting it seems likely that other factors adding to chronic inflammation may have an additional effect and that anti-inflammatory chemoprevention will only benefit a subgroup of patients or will need to be considered in combination with other interventions (i.e. changes of nutritional behavior, reflux management).

5. Conclusion and outlook

In summary, the tumor phenotype of L2-IL-1 β mice depends on the hygiene level of the holding facility and on the diet. These differences are accompanied by changes in the gut microbiome in these mice. While the microbiome analysis shows associations with tumor development, and computational predictions of the function of the microbiome suggest a functional impact on tumor formation and inflammation, this study is not able to prove the functional relevance of these microbiome changes. Notably, there was an increase in possibly inflammation induced progenitor cells. Additional experiments, like the investigation of functional properties of single bacteria or bacterial consortia could be performed in vitro (e.g. on gut or esophageal organoids) and in vivo (e.g. in germfree mice) could help to further investigate this association. Possibly colonizing mice with a humanized microbiome from either healthy controls or BE/EAC patients could support the idea of a systemic effect. It would be interesting to test the gut microbiome as a predictor of progression to EAC in BE patients to verify the medical relevance of the observed associations in patients. Additionally, it would be highly interesting to investigate the metabolic changes found by Dr. Münch in her doctoral thesis, since the level of metabolites in e.g. serum could influence inflammatory processes and thus could link the microbiome changes to inflammation and tumor development in L2-IL-1 β mice. Considering the link of bile acids, the microbiome and FXR signaling mentioned before, it would be worthwhile to further investigate this mechanism linking the microbiome to tumor formation. Currently work on this concept is performed in the laboratory of Dr. Michael Quante in mice and patients.

Chemoprevention using NSAIDS could be an easy and affordable preventive measure and since the ASPECT trial has shown that ASS could help BE patients it could be a worthwhile approach. Sulindac could be considered for chemoprevention in humans but large trials would be necessary to establish its efficiency in preventing EAC. Since the main problem of not knowing who to treat or survey persists, further research in the etiology of BE and EAC is needed.

6. References

1. Fang, H.Y., et al., *CXCR4 Is a Potential Target for Diagnostic PET/CT Imaging in Barrett's Dysplasia and Esophageal Adenocarcinoma*. Clin Cancer Res, 2018. **24**(5): p. 1048-1061.
2. Munch, N.S., et al., *High-Fat Diet Accelerates Carcinogenesis in a Mouse Model of Barrett's Esophagus via Interleukin 8 and Alterations to the Gut Microbiome*. Gastroenterology, 2019. **157**(2): p. 492-506 e2.
3. Kunze, B., et al., *Notch Signaling Mediates Differentiation in Barrett's Esophagus and Promotes Progression to Adenocarcinoma*. Gastroenterology, 2020.
4. Müller, W.A. and S. Frings, *Tier-und Humanphysiologie: eine Einführung*. 2009: Springer-Verlag.
5. National Institutes of Health - National Institute of Diabetes and Digestive and Kidney Diseases. *Gastrointestinal Tract (GI Tract)*. 29.08.2018]; Available from: <https://www.ncbi.nlm.nih.gov/pubmedhealth/PMHT0022855/>.
6. Kuo, B. and D. Urma, *Esophagus-anatomy and development*. GI Motility online, 2006.
7. Alpers, D.H., et al., *Textbook of gastroenterology*. 2011: John Wiley & Sons.
8. Tortora, G.J. and B.H. Derrickson, *Principles of anatomy and physiology*. 2008: John Wiley & Sons.
9. Feldman, M., L.S. Friedman, and L.J. Brandt, *Sleisenger and Fordtran's Gastrointestinal and Liver Disease E-Book: Pathophysiology, Diagnosis, Management*. 2015: Elsevier Health Sciences.
10. Kahrilas, P.J., et al., *American Gastroenterological Association Institute technical review on the management of gastroesophageal reflux disease*. Gastroenterology, 2008. **135**(4): p. 1392-1413, 1413 e1-5.
11. Vakil, N., et al., *The Montreal definition and classification of gastroesophageal reflux disease: a global evidence-based consensus*. Am J Gastroenterol, 2006. **101**(8): p. 1900-20; quiz 1943.
12. Ismail-Beigi, F., P.F. Horton, and C.E. Pope, 2nd, *Histological consequences of gastroesophageal reflux in man*. Gastroenterology, 1970. **58**(2): p. 163-74.
13. Souza, R.F., et al., *Gastroesophageal reflux might cause esophagitis through a cytokine-mediated mechanism rather than caustic acid injury*. Gastroenterology, 2009. **137**(5): p. 1776-84.
14. Hershovici, T. and R. Fass, *Pharmacological management of GERD: where does it stand now?* Trends Pharmacol Sci, 2011. **32**(4): p. 258-64.

15. Sigterman, K.E., et al., *Short-term treatment with proton pump inhibitors, H2-receptor antagonists and prokinetics for gastro-oesophageal reflux disease-like symptoms and endoscopy negative reflux disease*. Cochrane Database Syst Rev, 2013(5): p. CD002095.
16. Vaezi, M.F. and J.E. Richter, *Role of acid and duodenogastroesophageal reflux in gastroesophageal reflux disease*. Gastroenterology, 1996. **111**(5): p. 1192-9.
17. Nehra, D., et al., *Toxic bile acids in gastro-oesophageal reflux disease: influence of gastric acidity*. Gut, 1999. **44**(5): p. 598-602.
18. Barrett, N.R., *The lower esophagus lined by columnar epithelium*. Surgery, 1957. **41**(6): p. 881-94.
19. Barrett, N.R., *Chronic peptic ulcer of the oesophagus and 'oesophagitis'*. Br J Surg, 1950. **38**(150): p. 175-82.
20. Allison, P.R. and A.S. Johnstone, *The oesophagus lined with gastric mucous membrane*. Thorax, 1953. **8**(2): p. 87-101.
21. Bani-Hani, K.E. and B.K. Bani-Hani, *Columnar-lined esophagus: time to drop the eponym of "Barrett": Historical review*. J Gastroenterol Hepatol, 2008. **23**(5): p. 707-15.
22. Schmidt, F., *De Mammalian Oesophage Atque Ventriculo [dissertation]*. Halle: University of Halle, Germany, 1805.
23. Tileston, W., *PEPTIC ULCER OF THE OESOPHAGUS*. The American Journal of the Medical Sciences (1827-1924), 1906. **132**(2): p. 240.
24. Wang, K.K., R.E. Sampliner, and G. Practice Parameters Committee of the American College of, *Updated guidelines 2008 for the diagnosis, surveillance and therapy of Barrett's esophagus*. Am J Gastroenterol, 2008. **103**(3): p. 788-97.
25. Fitzgerald, R.C., et al., *British Society of Gastroenterology guidelines on the diagnosis and management of Barrett's oesophagus*. Gut, 2014. **63**(1): p. 7-42.
26. H. Koop, K.H.F., J. Labenz, P. Lynen Jansen, H. Messmann, S. Miehle, W. and T.W.u.d.M.d.L. Schepp. *S2k-Leitlinie 021/013 Gastroösophageale Refluxkrankheit*. 2014 [cited 2019 24.02.2019]; Available from: https://www.awmf.org/uploads/tx_szleitlinien/021-013l_S2k_Refluxkrankheit_2014-05.pdf.
27. Spechler, S.J., *Barrett esophagus and risk of esophageal cancer: a clinical review*. JAMA, 2013. **310**(6): p. 627-36.
28. Spechler, S.J. and R.F. Souza, *Barrett's esophagus*. N Engl J Med, 2014. **371**(9): p. 836-45.
29. Naini, B.V., et al., *Barrett's oesophagus diagnostic criteria: endoscopy and histology*. Best Pract Res Clin Gastroenterol, 2015. **29**(1): p. 77-96.

30. Thomas, T., et al., *Meta analysis: Cancer risk in Barrett's oesophagus*. *Aliment Pharmacol Ther*, 2007. **26**(11-12): p. 1465-77.
31. Yousef, F., et al., *The incidence of esophageal cancer and high-grade dysplasia in Barrett's esophagus: a systematic review and meta-analysis*. *Am J Epidemiol*, 2008. **168**(3): p. 237-49.
32. Hvid-Jensen, F., et al., *Incidence of adenocarcinoma among patients with Barrett's esophagus*. *N Engl J Med*, 2011. **365**(15): p. 1375-83.
33. Shaheen, N.J., et al., *Is there publication bias in the reporting of cancer risk in Barrett's esophagus?* *Gastroenterology*, 2000. **119**(2): p. 333-8.
34. Thota, P.N., et al., *Low Risk of High-Grade Dysplasia or Esophageal Adenocarcinoma Among Patients With Barrett's Esophagus Less Than 1 cm (Irregular Z Line) Within 5 Years of Index Endoscopy*. *Gastroenterology*, 2017. **152**(5): p. 987-992.
35. Peters, Y., et al., *Incidence of Progression of Persistent Nondysplastic Barrett's Esophagus to Malignancy*. *Clin Gastroenterol Hepatol*, 2019. **17**(5): p. 869-877 e5.
36. Gaddam, S., et al., *Persistence of nondysplastic Barrett's esophagus identifies patients at lower risk for esophageal adenocarcinoma: results from a large multicenter cohort*. *Gastroenterology*, 2013. **145**(3): p. 548-53 e1.
37. Moawad, F.J., et al., *Barrett's oesophagus length is established at the time of initial endoscopy and does not change over time: results from a large multicentre cohort*. *Gut*, 2015. **64**(12): p. 1874-80.
38. Singh, S., et al., *Acid-suppressive medications and risk of oesophageal adenocarcinoma in patients with Barrett's oesophagus: a systematic review and meta-analysis*. *Gut*, 2014. **63**(8): p. 1229-37.
39. Phoa, K.N., et al., *Radiofrequency ablation vs endoscopic surveillance for patients with Barrett esophagus and low-grade dysplasia: a randomized clinical trial*. *JAMA*, 2014. **311**(12): p. 1209-17.
40. van Vilsteren, F.G., et al., *Stepwise radical endoscopic resection versus radiofrequency ablation for Barrett's oesophagus with high-grade dysplasia or early cancer: a multicentre randomised trial*. *Gut*, 2011. **60**(6): p. 765-73.
41. Everhart, J.E. and C.E. Ruhl, *Burden of digestive diseases in the United States part I: overall and upper gastrointestinal diseases*. *Gastroenterology*, 2009. **136**(2): p. 376-86.
42. Hur, C., et al., *Trends in esophageal adenocarcinoma incidence and mortality*. *Cancer*, 2013. **119**(6): p. 1149-1158.
43. Pohl, H., B. Sirovich, and H.G. Welch, *Esophageal adenocarcinoma incidence: are we reaching the peak?* *Cancer Epidemiol Biomarkers Prev*, 2010. **19**(6): p. 1468-70.

44. Coleman, H.G., S.H. Xie, and J. Lagergren, *The Epidemiology of Esophageal Adenocarcinoma*. *Gastroenterology*, 2018. **154**(2): p. 390-405.
45. Brandtner, A.K. and M. Quante, *Risk prediction in Barrett's esophagus - aspects of a combination of molecular and epidemiologic biomarkers reflecting alterations of the microenvironment*. *Scand J Clin Lab Invest Suppl*, 2016. **245**(sup245): p. S63-9.
46. Aleman, J.O., et al., *Mechanisms of obesity-induced gastrointestinal neoplasia*. *Gastroenterology*, 2014. **146**(2): p. 357-373.
47. Cheng, K.K., et al., *A case-control study of oesophageal adenocarcinoma in women: a preventable disease*. *Br J Cancer*, 2000. **83**(1): p. 127-32.
48. Chow, W.H., et al., *Body mass index and risk of adenocarcinomas of the esophagus and gastric cardia*. *J Natl Cancer Inst*, 1998. **90**(2): p. 150-5.
49. Lagergren, J., et al., *Association between medications that relax the lower esophageal sphincter and risk for esophageal adenocarcinoma*. *Ann Intern Med*, 2000. **133**(3): p. 165-75.
50. Vaughan, T.L. and R.C. Fitzgerald, *Precision prevention of oesophageal adenocarcinoma*. *Nat Rev Gastroenterol Hepatol*, 2015. **12**(4): p. 243-8.
51. Jiang, M., et al., *Transitional basal cells at the squamous-columnar junction generate Barrett's oesophagus*. *Nature*, 2017. **550**: p. 529.
52. Tosh, D. and J.M. Slack, *How cells change their phenotype*. *Nat Rev Mol Cell Biol*, 2002. **3**(3): p. 187-94.
53. Yu, W.Y., J.M. Slack, and D. Tosh, *Conversion of columnar to stratified squamous epithelium in the developing mouse oesophagus*. *Dev Biol*, 2005. **284**(1): p. 157-70.
54. Milano, F., et al., *Bone morphogenetic protein 4 expressed in esophagitis induces a columnar phenotype in esophageal squamous cells*. *Gastroenterology*, 2007. **132**(7): p. 2412-21.
55. Kong, J., et al., *Ectopic Cdx2 expression in murine esophagus models an intermediate stage in the emergence of Barrett's esophagus*. *PLoS One*, 2011. **6**(4): p. e18280.
56. Shi, Q., et al., *Evidence for circulating bone marrow-derived endothelial cells*. *Blood*, 1998. **92**(2): p. 362-7.
57. Petersen, B.E., et al., *Bone marrow as a potential source of hepatic oval cells*. *Science*, 1999. **284**(5417): p. 1168-70.
58. LaBarge, M.A. and H.M. Blau, *Biological progression from adult bone marrow to mononucleate muscle stem cell to multinucleate muscle fiber in response to injury*. *Cell*, 2002. **111**(4): p. 589-601.

59. Krause, D.S., et al., *Multi-organ, multi-lineage engraftment by a single bone marrow-derived stem cell*. Cell, 2001. **105**(3): p. 369-77.
60. Houghton, J., et al., *Gastric cancer originating from bone marrow-derived cells*. Science, 2004. **306**(5701): p. 1568-71.
61. Sarosi, G., et al., *Bone marrow progenitor cells contribute to esophageal regeneration and metaplasia in a rat model of Barrett's esophagus*. Dis Esophagus, 2008. **21**(1): p. 43-50.
62. Hutchinson, L., et al., *Human Barrett's adenocarcinoma of the esophagus, associated myofibroblasts, and endothelium can arise from bone marrow-derived cells after allogeneic stem cell transplant*. Stem Cells Dev, 2011. **20**(1): p. 11-7.
63. Barbera, M. and R.C. Fitzgerald, *Cellular origin of Barrett's metaplasia and oesophageal stem cells*. Biochem Soc Trans, 2010. **38**(2): p. 370-3.
64. Gillen, P., et al., *Experimental columnar metaplasia in the canine oesophagus*. Br J Surg, 1988. **75**(2): p. 113-5.
65. Coad, R.A., et al., *On the histogenesis of Barrett's oesophagus and its associated squamous islands: a three-dimensional study of their morphological relationship with native oesophageal gland ducts*. J Pathol, 2005. **206**(4): p. 388-94.
66. Leedham, S.J., et al., *Individual crypt genetic heterogeneity and the origin of metaplastic glandular epithelium in human Barrett's oesophagus*. Gut, 2008. **57**(8): p. 1041-8.
67. Owen, R.P., et al., *Single cell RNA-seq reveals profound transcriptional similarity between Barrett's oesophagus and oesophageal submucosal glands*. Nat Commun, 2018. **9**(1): p. 4261.
68. Odze, R.D., *Unraveling the mystery of the gastroesophageal junction: a pathologist's perspective*. Am J Gastroenterol, 2005. **100**(8): p. 1853-67.
69. Zhao, C.M., et al., *Denervation suppresses gastric tumorigenesis*. Sci Transl Med, 2014. **6**(250): p. 250ra115.
70. Lavery, D.L., et al., *The stem cell organisation, and the proliferative and gene expression profile of Barrett's epithelium, replicates pyloric-type gastric glands*. Gut, 2014. **63**(12): p. 1854-63.
71. O'Neil, A., et al., *Unique Cellular Lineage Composition of the First Gland of the Mouse Gastric Corpus*. J Histochem Cytochem, 2017. **65**(1): p. 47-58.
72. Quante, M., et al., *Bile acid and inflammation activate gastric cardia stem cells in a mouse model of Barrett-like metaplasia*. Cancer Cell, 2012. **21**(1): p. 36-51.
73. Senoo, M., et al., *p63 Is essential for the proliferative potential of stem cells in stratified epithelia*. Cell, 2007. **129**(3): p. 523-36.

74. Wang, X., et al., *Residual embryonic cells as precursors of a Barrett's-like metaplasia*. Cell, 2011. **145**(7): p. 1023-1035.
75. Jaiswal, K.R., et al., *Characterization of telomerase-immortalized, non-neoplastic, human Barrett's cell line (BAR-T)*. Dis Esophagus, 2007. **20**(3): p. 256-64.
76. Rockett, J.C., et al., *Five newly established oesophageal carcinoma cell lines: phenotypic and immunological characterization*. Br J Cancer, 1997. **75**(2): p. 258-63.
77. Stoner, G.D., et al., *Establishment and characterization of SV40 T-antigen immortalized human esophageal epithelial cells*. Cancer Res, 1991. **51**(1): p. 365-71.
78. Huo, X., et al., *Deoxycholic acid causes DNA damage while inducing apoptotic resistance through NF-kappaB activation in benign Barrett's epithelial cells*. Am J Physiol Gastrointest Liver Physiol, 2011. **301**(2): p. G278-86.
79. Abdel-Latif, M.M., et al., *NF-kappaB activation in esophageal adenocarcinoma: relationship to Barrett's metaplasia, survival, and response to neoadjuvant chemoradiotherapy*. Ann Surg, 2004. **239**(4): p. 491-500.
80. Gotzel, K., et al., *In-depth characterization of the Wnt-signaling/beta-catenin pathway in an in vitro model of Barrett's sequence*. BMC Gastroenterol, 2019. **19**(1): p. 38.
81. Okawa, T., et al., *The functional interplay between EGFR overexpression, hTERT activation, and p53 mutation in esophageal epithelial cells with activation of stromal fibroblasts induces tumor development, invasion, and differentiation*. Genes Dev, 2007. **21**(21): p. 2788-803.
82. Kosoff, R.E., et al., *Development and characterization of an organotypic model of Barrett's esophagus*. J Cell Physiol, 2012. **227**(6): p. 2654-9.
83. Kalabis, J., et al., *Isolation and characterization of mouse and human esophageal epithelial cells in 3D organotypic culture*. Nat Protoc, 2012. **7**(2): p. 235-46.
84. Lancaster, M.A., et al., *Cerebral organoids model human brain development and microcephaly*. Nature, 2013. **501**(7467): p. 373-9.
85. Sato, T., et al., *Single Lgr5 stem cells build crypt-villus structures in vitro without a mesenchymal niche*. Nature, 2009. **459**(7244): p. 262-5.
86. Eicher, A.K., H.M. Berns, and J.M. Wells, *Translating Developmental Principles to Generate Human Gastric Organoids*. Cell Mol Gastroenterol Hepatol, 2018. **5**(3): p. 353-363.
87. Pastula, A., et al., *Three-Dimensional Gastrointestinal Organoid Culture in Combination with Nerves or Fibroblasts: A Method to Characterize the Gastrointestinal Stem Cell Niche*. Stem Cells Int, 2016. **2016**: p. 3710836.

88. Münch, N.S., *High fat diet accelerates esophageal dysplasia in a mouse model of Barrett Esophagus through IL-8 (KC) mediated inflammatory niche formation*. 2016, Technische Universität München: München.
89. Morizane, R., et al., *Nephron organoids derived from human pluripotent stem cells model kidney development and injury*. *Nat Biotechnol*, 2015. **33**(11): p. 1193-200.
90. Trisno, S.L., et al., *Esophageal Organoids from Human Pluripotent Stem Cells Delineate Sox2 Functions during Esophageal Specification*. *Cell Stem Cell*, 2018. **23**(4): p. 501-515 e7.
91. Sato, T., et al., *Long-term expansion of epithelial organoids from human colon, adenoma, adenocarcinoma, and Barrett's epithelium*. *Gastroenterology*, 2011. **141**(5): p. 1762-72.
92. Williamson, I.A., et al., *A High-Throughput Organoid Microinjection Platform to Study Gastrointestinal Microbiota and Luminal Physiology*. *Cell Mol Gastroenterol Hepatol*, 2018. **6**(3): p. 301-319.
93. Green, N.H., et al., *Production, Characterization and Potential Uses of a 3D Tissue-engineered Human Esophageal Mucosal Model*. *J Vis Exp*, 2015(99): p. e52693.
94. Gibson, C.J., et al., *Adenomatous polyp with intestinal metaplasia of the esophagus (Barrett esophagus) in a dog*. *Vet Pathol*, 2010. **47**(1): p. 116-9.
95. Chambers, J.K., et al., *Adenocarcinoma of Barrett's esophagus in a dog*. *J Toxicol Pathol*, 2017. **30**(3): p. 239-243.
96. Kawaura, Y., et al., *Immunohistochemical study of p53, c-erbB-2, and PCNA in barrett's esophagus with dysplasia and adenocarcinoma arising from experimental acid or alkaline reflux model*. *J Gastroenterol*, 2001. **36**(9): p. 595-600.
97. Bremner, C.G., V.P. Lynch, and F.H. Ellis, Jr., *Barrett's esophagus: congenital or acquired? An experimental study of esophageal mucosal regeneration in the dog*. *Surgery*, 1970. **68**(1): p. 209-16.
98. Kapoor, H., et al., *Animal Models of Barrett's Esophagus and Esophageal Adenocarcinoma-Past, Present, and Future*. *Clin Transl Sci*, 2015. **8**(6): p. 841-7.
99. Rubio, C.A., et al., *Mucous gland metaplasia in the esophagus and gastric mucosa in baboons*. *Anticancer Res*, 2011. **31**(6): p. 2187-90.
100. Glover, E.J., et al., *Gastroesophageal reflux disease in baboons (Papio sp.): a new animal model*. *J Med Primatol*, 2008. **37**(1): p. 18-25.
101. Phillips, K.A., et al., *Why primate models matter*. *Am J Primatol*, 2014. **76**(9): p. 801-27.
102. Abdulnour-Nakhoul, S., et al., *Characterization of esophageal submucosal glands in pig tissue and cultures*. *Dig Dis Sci*, 2007. **52**(11): p. 3054-65.

103. Groenen, M.A., et al., *Analyses of pig genomes provide insight into porcine demography and evolution*. Nature, 2012. **491**(7424): p. 393-8.
104. Principe, D.R., et al., *KRAS(G12D) and TP53(R167H) Cooperate to Induce Pancreatic Ductal Adenocarcinoma in Sus scrofa Pigs*. Sci Rep, 2018. **8**(1): p. 12548.
105. Hai, T., et al., *One-step generation of knockout pigs by zygote injection of CRISPR/Cas system*. Cell Res, 2014. **24**(3): p. 372-5.
106. Levrat, M., R. Lambert, and G. Kirshbaum, *Esophagitis produced by reflux of duodenal contents in rats*. Am J Dig Dis, 1962. **7**(6): p. 564-73.
107. Chen, X., et al., *Multilayered epithelium in a rat model and human Barrett's esophagus: similar expression patterns of transcription factors and differentiation markers*. BMC Gastroenterol, 2008. **8**: p. 1.
108. Su, Y., et al., *Phenotype of columnar-lined esophagus in rats with esophagogastrroduodenal anastomosis: similarity to human Barrett's esophagus*. Lab Invest, 2004. **84**(6): p. 753-65.
109. Fein, M., *Duodeno-esophageal reflux induces esophageal adenocarcinoma without exogenous carcinogen*. Journal of Gastrointestinal Surgery, 1998. **2**(3): p. 260-268.
110. Xu, X., et al., *Barrett's esophagus and associated adenocarcinoma in a mouse surgical model*. J Surg Res, 2000. **88**(2): p. 120-4.
111. Davelaar, A.L., et al., *Active matrix metalloproteases are expressed early on and are high during the Barrett's esophagus malignancy sequence*. Scand J Gastroenterol, 2015. **50**(3): p. 321-32.
112. Aikou, S., et al., *Columnar metaplasia in a surgical mouse model of gastro-esophageal reflux disease is not derived from bone marrow-derived cell*. Cancer Sci, 2013. **104**(9): p. 1154-61.
113. Pham, T.H., et al., *Development and characterization of a surgical mouse model of reflux esophagitis and Barrett's esophagus*. J Gastrointest Surg, 2014. **18**(2): p. 234-40; discussion 240-1.
114. Guy, N.C., et al., *A novel dietary-related model of esophagitis and Barrett's esophagus, a premalignant lesion*. Nutr Cancer, 2007. **59**(2): p. 217-27.
115. Hanahan, D., E.F. Wagner, and R.D. Palmiter, *The origins of oncomice: a history of the first transgenic mice genetically engineered to develop cancer*. Genes Dev, 2007. **21**(18): p. 2258-70.
116. Fein, M., et al., *Loss of function of Trp53, but not Apc, leads to the development of esophageal adenocarcinoma in mice with jejuno-esophageal reflux*. J Surg Res, 1999. **83**(1): p. 48-55.

117. Ellis, F.H., Jr., et al., *Malignant transformation of the esophageal mucosa is enhanced in p27 knockout mice*. J Thorac Cardiovasc Surg, 2001. **122**(4): p. 809-14.
118. Wang, D.H., et al., *Aberrant epithelial-mesenchymal Hedgehog signaling characterizes Barrett's metaplasia*. Gastroenterology, 2010. **138**(5): p. 1810-22.
119. Shrivastava, M.S., et al., *Targeting chemokine pathways in esophageal adenocarcinoma*. Cell Cycle, 2014. **13**(21): p. 3320-7.
120. Cook, M.B., et al., *Prediagnostic circulating markers of inflammation and risk of oesophageal adenocarcinoma: a study within the National Cancer Institute Cohort Consortium*. Gut, 2019. **68**(6): p. 960-968.
121. Fitzgerald, R.C., et al., *Inflammatory gradient in Barrett's oesophagus: implications for disease complications*. Gut, 2002. **51**(3): p. 316-22.
122. Hanahan, D. and R.A. Weinberg, *The hallmarks of cancer*. Cell, 2000. **100**(1): p. 57-70.
123. Hanahan, D. and R.A. Weinberg, *Hallmarks of cancer: the next generation*. Cell, 2011. **144**(5): p. 646-74.
124. Balkwill, F. and A. Mantovani, *Inflammation and cancer: back to Virchow?* Lancet, 2001. **357**(9255): p. 539-45.
125. Schmidt, A. and O.F. Weber, *In memoriam of Rudolf virchow: a historical retrospective including aspects of inflammation, infection and neoplasia*. Contrib Microbiol, 2006. **13**: p. 1-15.
126. Hussain, S.P. and C.C. Harris, *Inflammation and cancer: an ancient link with novel potentials*. Int J Cancer, 2007. **121**(11): p. 2373-80.
127. Medzhitov, R., *Origin and physiological roles of inflammation*. Nature, 2008. **454**(7203): p. 428-35.
128. Takeuchi, O. and S. Akira, *Pattern recognition receptors and inflammation*. Cell, 2010. **140**(6): p. 805-20.
129. Czerkies, M. and K. Kwiatkowska, *Toll-Like Receptors and their Contribution to Innate Immunity: Focus on TLR4 Activation by Lipopolysaccharide*. Advances in Cell Biology, 2014. **4**(1): p. 1-23.
130. Nathan, C., *Neutrophils and immunity: challenges and opportunities*. Nat Rev Immunol, 2006. **6**(3): p. 173-82.
131. Eming, S.A., T.A. Wynn, and P. Martin, *Inflammation and metabolism in tissue repair and regeneration*. Science, 2017. **356**(6342): p. 1026-1030.
132. Larsen, C.M., et al., *Interleukin-1-receptor antagonist in type 2 diabetes mellitus*. N Engl J Med, 2007. **356**(15): p. 1517-26.

133. Kubes, P. and W.Z. Mehal, *Sterile inflammation in the liver*. Gastroenterology, 2012. **143**(5): p. 1158-1172.
134. Wu, Y., et al., *Molecular mechanisms underlying chronic inflammation-associated cancers*. Cancer Lett, 2014. **345**(2): p. 164-73.
135. Gilmore, T.D., *Introduction to NF-kappaB: players, pathways, perspectives*. Oncogene, 2006. **25**(51): p. 6680-4.
136. Ben-Neriah, Y. and M. Karin, *Inflammation meets cancer, with NF-kappaB as the matchmaker*. Nat Immunol, 2011. **12**(8): p. 715-23.
137. Karin, M. and F.R. Greten, *NF-kappaB: linking inflammation and immunity to cancer development and progression*. Nat Rev Immunol, 2005. **5**(10): p. 749-59.
138. Greten, F.R., et al., *IKKbeta links inflammation and tumorigenesis in a mouse model of colitis-associated cancer*. Cell, 2004. **118**(3): p. 285-96.
139. Brocker, C., et al., *Evolutionary divergence and functions of the human interleukin (IL) gene family*. Hum Genomics, 2010. **5**(1): p. 30-55.
140. Bent, R., et al., *Interleukin-1 Beta-A Friend or Foe in Malignancies?* Int J Mol Sci, 2018. **19**(8).
141. Lu, Y.C., et al., *Differential role for c-Rel and C/EBPbeta/delta in TLR-mediated induction of proinflammatory cytokines*. J Immunol, 2009. **182**(11): p. 7212-21.
142. Zhang, Y. and W.N. Rom, *Regulation of the interleukin-1 beta (IL-1 beta) gene by mycobacterial components and lipopolysaccharide is mediated by two nuclear factor-IL6 motifs*. Mol Cell Biol, 1993. **13**(6): p. 3831-7.
143. Toda, Y., et al., *Autocrine induction of the human pro-IL-1beta gene promoter by IL-1beta in monocytes*. J Immunol, 2002. **168**(4): p. 1984-91.
144. Cogswell, J.P., et al., *NF-kappa B regulates IL-1 beta transcription through a consensus NF-kappa B binding site and a nonconsensus CRE-like site*. J Immunol, 1994. **153**(2): p. 712-23.
145. Marucha, P.T., R.A. Zeff, and D.L. Kreutzer, *Cytokine-induced IL-1 beta gene expression in the human polymorphonuclear leukocyte: transcriptional and post-transcriptional regulation by tumor necrosis factor and IL-1*. J Immunol, 1991. **147**(8): p. 2603-8.
146. Donnelly, R.P., et al., *IL-1 expression in human monocytes is transcriptionally and posttranscriptionally regulated by IL-4*. J Immunol, 1991. **146**(10): p. 3431-6.
147. Awad, F., et al., *Impact of human monocyte and macrophage polarization on NLR expression and NLRP3 inflammasome activation*. PLoS One, 2017. **12**(4): p. e0175336.
148. Boatright, K.M. and G.S. Salvesen, *Mechanisms of caspase activation*. Curr Opin Cell Biol, 2003. **15**(6): p. 725-31.

149. Boraschi, D., et al., *The family of the interleukin-1 receptors*. Immunol Rev, 2018. **281**(1): p. 197-232.
150. Nakamura, S., et al., *Antitumor effect of recombinant human interleukin 1 alpha against murine syngeneic tumors*. Jpn J Cancer Res, 1986. **77**(8): p. 767-73.
151. North, R.J., et al., *Interleukin 1-induced, T cell-mediated regression of immunogenic murine tumors. Requirement for an adequate level of already acquired host concomitant immunity*. J Exp Med, 1988. **168**(6): p. 2031-43.
152. Mullerad, J., et al., *Macrophage activation for the production of immunostimulatory cytokines by delivering interleukin 1 via biodegradable microspheres*. Cytokine, 2000. **12**(11): p. 1683-90.
153. Veltri, S. and J.W. Smith, *Interleukin 1 Trials in Cancer Patients: A Review of the Toxicity, Antitumor and Hematopoietic Effects*. Stem Cells, 1996. **14**(2): p. 164-176.
154. Mantovani, A., I. Barajon, and C. Garlanda, *IL-1 and IL-1 regulatory pathways in cancer progression and therapy*. Immunol Rev, 2018. **281**(1): p. 57-61.
155. Song, S., et al., *COX-2 induction by unconjugated bile acids involves reactive oxygen species-mediated signalling pathways in Barrett's oesophagus and oesophageal adenocarcinoma*. Gut, 2007. **56**(11): p. 1512-21.
156. Sihvo, E.I., et al., *Oxidative stress has a role in malignant transformation in Barrett's oesophagus*. Int J Cancer, 2002. **102**(6): p. 551-5.
157. Martin, R.C., et al., *Chemoprevention of carcinogenic progression to esophageal adenocarcinoma by the manganese superoxide dismutase supplementation*. Clin Cancer Res, 2007. **13**(17): p. 5176-82.
158. Wild, C.P. and L.J. Hardie, *Reflux, Barrett's oesophagus and adenocarcinoma: burning questions*. Nature Reviews Cancer, 2003. **3**(9): p. 676-684.
159. Corley, D.A., et al., *Abdominal obesity and body mass index as risk factors for Barrett's esophagus*. Gastroenterology, 2007. **133**(1): p. 34-41; quiz 311.
160. Sugerman, H., et al., *Intra-abdominal pressure, sagittal abdominal diameter and obesity comorbidity*. J Intern Med, 1997. **241**(1): p. 71-9.
161. Nelson, L.G., et al., *Amelioration of gastroesophageal reflux symptoms following Roux-en-Y gastric bypass for clinically significant obesity*. Am Surg, 2005. **71**(11): p. 950-3; discussion 953-4.
162. Park, H.S., J.Y. Park, and R. Yu, *Relationship of obesity and visceral adiposity with serum concentrations of CRP, TNF-alpha and IL-6*. Diabetes Res Clin Pract, 2005. **69**(1): p. 29-35.
163. Tselepis, C., et al., *Tumour necrosis factor-alpha in Barrett's oesophagus: a potential novel mechanism of action*. Oncogene, 2002. **21**(39): p. 6071-81.

164. Oka, M., et al., *The influence of interleukin-6 on the growth of human esophageal cancer cell lines*. J Interferon Cytokine Res, 1996. **16**(12): p. 1001-6.
165. Hardikar, S., et al., *Inflammation and oxidative stress markers and esophageal adenocarcinoma incidence in a Barrett's esophagus cohort*. Cancer Epidemiol Biomarkers Prev, 2014. **23**(11): p. 2393-403.
166. Garcia, J.M., et al., *Circulating inflammatory cytokines and adipokines are associated with increased risk of Barrett's esophagus: a case-control study*. Clin Gastroenterol Hepatol, 2014. **12**(2): p. 229-238 e3.
167. Isomoto, H., et al., *Elevated levels of chemokines in esophageal mucosa of patients with reflux esophagitis*. Am J Gastroenterol, 2003. **98**(3): p. 551-6.
168. Oh, D.S., et al., *Reduction of interleukin 8 gene expression in reflux esophagitis and Barrett's esophagus with antireflux surgery*. Arch Surg, 2007. **142**(6): p. 554-9; discussion 559-60.
169. Cheng, L., et al., *Acid-induced release of platelet-activating factor by human esophageal mucosa induces inflammatory mediators in circular smooth muscle*. J Pharmacol Exp Ther, 2006. **319**(1): p. 117-26.
170. Fitzgerald, R.C., et al., *Diversity in the oesophageal phenotypic response to gastro-oesophageal reflux: immunological determinants*. Gut, 2002. **50**(4): p. 451-9.
171. Rieder, F., et al., *Gastroesophageal reflux disease-associated esophagitis induces endogenous cytokine production leading to motor abnormalities*. Gastroenterology, 2007. **132**(1): p. 154-65.
172. Gruss, H.J., et al., *Human fibroblasts express functional IL-2 receptors formed by the IL-2R alpha- and beta-chain subunits: association of IL-2 binding with secretion of the monocyte chemoattractant protein-1*. J Immunol, 1996. **157**(2): p. 851-7.
173. Gomes, I., et al., *Eosinophil-fibroblast interactions induce fibroblast IL-6 secretion and extracellular matrix gene expression: implications in fibrogenesis*. J Allergy Clin Immunol, 2005. **116**(4): p. 796-804.
174. Vogel, J.D., et al., *CD40-mediated immune-nonimmune cell interactions induce mucosal fibroblast chemokines leading to T-cell transmigration*. Gastroenterology, 2004. **126**(1): p. 63-80.
175. Burge, M.N., *Fungi in biological control systems*. 1988, Manchester: Manchester University Press.
176. Turnbaugh, P.J., et al., *The human microbiome project*. Nature, 2007. **449**(7164): p. 804-10.
177. Whiteside, S.A., et al., *The microbiome of the urinary tract--a role beyond infection*. Nat Rev Urol, 2015. **12**(2): p. 81-90.

178. Tamboli, C.P., et al., *Dysbiosis in inflammatory bowel disease*. Gut, 2004. **53**(1): p. 1-4.
179. van Nood, E., et al., *Duodenal infusion of donor feces for recurrent Clostridium difficile*. N Engl J Med, 2013. **368**(5): p. 407-15.
180. Tvede, M. and J. Rask-Madsen, *Bacteriotherapy for chronic relapsing Clostridium difficile diarrhoea in six patients*. Lancet, 1989. **1**(8648): p. 1156-60.
181. Agrawal, M., et al., *The Long-term Efficacy and Safety of Fecal Microbiota Transplant for Recurrent, Severe, and Complicated Clostridium difficile Infection in 146 Elderly Individuals*. J Clin Gastroenterol, 2016. **50**(5): p. 403-7.
182. Segata, N., et al., *Metagenomic biomarker discovery and explanation*. Genome Biol, 2011. **12**(6): p. R60.
183. Dave, M., et al., *The human gut microbiome: current knowledge, challenges, and future directions*. Transl Res, 2012. **160**(4): p. 246-57.
184. Waldor, M.K., et al., *Where next for microbiome research?* PLoS Biol, 2015. **13**(1): p. e1002050.
185. Marques, F.Z., C.R. Mackay, and D.M. Kaye, *Beyond gut feelings: how the gut microbiota regulates blood pressure*. Nat Rev Cardiol, 2018. **15**(1): p. 20-32.
186. Mayer, E.A., et al., *Gut microbes and the brain: paradigm shift in neuroscience*. J Neurosci, 2014. **34**(46): p. 15490-6.
187. Vuong, H.E., et al., *The Microbiome and Host Behavior*. Annu Rev Neurosci, 2017. **40**: p. 21-49.
188. Allen, A.P., et al., *A psychology of the human brain-gut-microbiome axis*. Soc Personal Psychol Compass, 2017. **11**(4): p. e12309.
189. Le Chatelier, E., et al., *Richness of human gut microbiome correlates with metabolic markers*. Nature, 2013. **500**(7464): p. 541-6.
190. Chiller, K., B.A. Selkin, and G.J. Murakawa, *Skin microflora and bacterial infections of the skin*. J Investig Dermatol Symp Proc, 2001. **6**(3): p. 170-4.
191. Neish, A.S., *Microbes in gastrointestinal health and disease*. Gastroenterology, 2009. **136**(1): p. 65-80.
192. Sekirov, I., et al., *Gut microbiota in health and disease*. Physiol Rev, 2010. **90**(3): p. 859-904.
193. Rajilic-Stojanovic, M., et al., *Long-term monitoring of the human intestinal microbiota composition*. Environ Microbiol, 2012.
194. Faith, J.J., et al., *The long-term stability of the human gut microbiota*. Science, 2013. **341**(6141): p. 1237439.

195. Turnbaugh, P.J., et al., *An obesity-associated gut microbiome with increased capacity for energy harvest*. Nature, 2006. **444**(7122): p. 1027-31.
196. Turnbaugh, P.J., et al., *Diet-induced obesity is linked to marked but reversible alterations in the mouse distal gut microbiome*. Cell Host Microbe, 2008. **3**(4): p. 213-23.
197. Kubeck, R., et al., *Dietary fat and gut microbiota interactions determine diet-induced obesity in mice*. Mol Metab, 2016. **5**(12): p. 1162-1174.
198. De Vadder, F., et al., *Microbiota-generated metabolites promote metabolic benefits via gut-brain neural circuits*. Cell, 2014. **156**(1-2): p. 84-96.
199. Moskal, A., et al., *Main nutrient patterns and colorectal cancer risk in the European Prospective Investigation into Cancer and Nutrition study*. Br J Cancer, 2016. **115**(11): p. 1430-1440.
200. Feng, Q., et al., *Gut microbiome development along the colorectal adenoma-carcinoma sequence*. Nat Commun, 2015. **6**(1): p. 6528.
201. Wang, T., et al., *Structural segregation of gut microbiota between colorectal cancer patients and healthy volunteers*. ISME J, 2012. **6**(2): p. 320-9.
202. Yu, J., et al., *Metagenomic analysis of faecal microbiome as a tool towards targeted non-invasive biomarkers for colorectal cancer*. Gut, 2017. **66**(1): p. 70-78.
203. Goodwin, A.C., et al., *Polyamine catabolism contributes to enterotoxigenic Bacteroides fragilis-induced colon tumorigenesis*. Proc Natl Acad Sci U S A, 2011. **108**(37): p. 15354-9.
204. Wu, S., et al., *A human colonic commensal promotes colon tumorigenesis via activation of T helper type 17 T cell responses*. Nat Med, 2009. **15**(9): p. 1016-22.
205. Maloy, K.J. and F. Powrie, *Intestinal homeostasis and its breakdown in inflammatory bowel disease*. Nature, 2011. **474**(7351): p. 298-306.
206. Tjalsma, H., et al., *A bacterial driver-passenger model for colorectal cancer: beyond the usual suspects*. Nat Rev Microbiol, 2012. **10**(8): p. 575-82.
207. Pei, Z., et al., *Bacterial biota in the human distal esophagus*. Proc Natl Acad Sci U S A, 2004. **101**(12): p. 4250-5.
208. Gall, A., et al., *Bacterial Composition of the Human Upper Gastrointestinal Tract Microbiome Is Dynamic and Associated with Genomic Instability in a Barrett's Esophagus Cohort*. PLoS One, 2015. **10**(6): p. e0129055.
209. Amir, I., et al., *Gastric microbiota is altered in oesophagitis and Barrett's oesophagus and further modified by proton pump inhibitors*. Environ Microbiol, 2014. **16**(9): p. 2905-14.

210. Elliott, D.R.F., et al., *A non-endoscopic device to sample the oesophageal microbiota: a case-control study*. *Lancet Gastroenterol Hepatol*, 2017. **2**(1): p. 32-42.
211. Yamamura, K., et al., *Human Microbiome Fusobacterium Nucleatum in Esophageal Cancer Tissue Is Associated with Prognosis*. *Clin Cancer Res*, 2016. **22**(22): p. 5574-5581.
212. Zaidi, A.H., et al., *Associations of microbiota and toll-like receptor signaling pathway in esophageal adenocarcinoma*. *BMC Cancer*, 2016. **16**: p. 52.
213. Sanduleanu, S., et al., *Non-Helicobacter pylori bacterial flora during acid-suppressive therapy: differential findings in gastric juice and gastric mucosa*. *Aliment Pharmacol Ther*, 2001. **15**(3): p. 379-88.
214. Karmeli, Y., et al., *Conventional dose of omeprazole alters gastric flora*. *Dig Dis Sci*, 1995. **40**(9): p. 2070-3.
215. Winter, J.W., et al., *N-nitrosamine generation from ingested nitrate via nitric oxide in subjects with and without gastroesophageal reflux*. *Gastroenterology*, 2007. **133**(1): p. 164-74.
216. Bockler, R., H. Meyer, and P. Schlag, *An experimental study on bacterial colonization, nitrite and nitrosamine production in the operated stomach*. *J Cancer Res Clin Oncol*, 1983. **105**(1): p. 62-6.
217. Asfaha, S., et al., *Mice that express human interleukin-8 have increased mobilization of immature myeloid cells, which exacerbates inflammation and accelerates colon carcinogenesis*. *Gastroenterology*, 2013. **144**(1): p. 155-66.
218. Lofgren, J.L., et al., *Lack of commensal flora in Helicobacter pylori-infected INS-GAS mice reduces gastritis and delays intraepithelial neoplasia*. *Gastroenterology*, 2011. **140**(1): p. 210-20.
219. Lertpiriyapong, K., et al., *Gastric colonisation with a restricted commensal microbiota replicates the promotion of neoplastic lesions by diverse intestinal microbiota in the Helicobacter pylori INS-GAS mouse model of gastric carcinogenesis*. *Gut*, 2014. **63**(1): p. 54-63.
220. Mladenova, D., et al., *The NSAID sulindac is chemopreventive in the mouse distal colon but carcinogenic in the proximal colon*. *Gut*, 2011. **60**(3): p. 350-60.
221. Cyrus, T., et al., *Effect of low-dose aspirin on vascular inflammation, plaque stability, and atherogenesis in low-density lipoprotein receptor-deficient mice*. *Circulation*, 2002. **106**(10): p. 1282-7.
222. Corbach, S., *Untersuchung der CO2-Euthanasie bei Labormäusen auf Tierschutzgerechtigkeit*. 2006, Tierärztliche Hochschule Hannover.
223. Illumina. *16S Metagenomic Sequencing Library*

- Preparation.* [cited 2017 11.07.2017]; Available from: https://support.illumina.com/content/dam/illumina-support/documents/documentation/chemistry_documentation/16s/16s-metagenomic-library-prep-guide-15044223-b.pdf.
224. Lagkouravdos, I., et al., *IMNGS: A comprehensive open resource of processed 16S rRNA microbial profiles for ecology and diversity studies*. Sci Rep, 2016. **6**: p. 33721.
 225. Edgar, R.C., *UPARSE: highly accurate OTU sequences from microbial amplicon reads*. Nat Methods, 2013. **10**(10): p. 996-8.
 226. Edgar, R.C., *Search and clustering orders of magnitude faster than BLAST*. Bioinformatics, 2010. **26**(19): p. 2460-1.
 227. Edgar, R.C., et al., *UCHIME improves sensitivity and speed of chimera detection*. Bioinformatics, 2011. **27**(16): p. 2194-200.
 228. Wang, Q., et al., *Naive Bayesian classifier for rapid assignment of rRNA sequences into the new bacterial taxonomy*. Appl Environ Microbiol, 2007. **73**(16): p. 5261-7.
 229. Edgar, R.C., *MUSCLE: multiple sequence alignment with high accuracy and high throughput*. Nucleic Acids Res, 2004. **32**(5): p. 1792-7.
 230. Price, M.N., P.S. Dehal, and A.P. Arkin, *FastTree 2--approximately maximum-likelihood trees for large alignments*. PLoS One, 2010. **5**(3): p. e9490.
 231. Pruesse, E., J. Peplies, and F.O. Glockner, *SINA: accurate high-throughput multiple sequence alignment of ribosomal RNA genes*. Bioinformatics, 2012. **28**(14): p. 1823-9.
 232. Yoon, S.H., et al., *Introducing EzBioCloud: a taxonomically united database of 16S rRNA gene sequences and whole-genome assemblies*. Int J Syst Evol Microbiol, 2017. **67**(5): p. 1613-1617.
 233. Lagkouravdos, I., et al., *Rhea: a transparent and modular R pipeline for microbial profiling based on 16S rRNA gene amplicons*. PeerJ, 2017. **5**: p. e2836.
 234. Team, R., *RStudio: Integrated Development Environment for R*. 2016, RStudio, Inc.: Boston.
 235. R Core Development Team, *R: A language and environment for statistical computing*. 2018, R Foundation for Statistical Computing: Vienna.
 236. *Galaxy instance of the Huttenhower laboratory*. 30.12.2019]; Available from: <https://huttenhower.sph.harvard.edu/galaxy/>.
 237. *GraphPad Prism 6.0f for Mac OS X*. 2014, GraphPad Software: La Jolla.
 238. Caporaso, J.G., et al., *QIIME allows analysis of high-throughput community sequencing data*. Nat Methods, 2010. **7**(5): p. 335-6.

239. Langille, M.G., et al., *Predictive functional profiling of microbial communities using 16S rRNA marker gene sequences*. Nat Biotechnol, 2013. **31**(9): p. 814-21.
240. Abrams, J.A., et al., *Dating the rise of esophageal adenocarcinoma: analysis of Connecticut Tumor Registry data, 1940-2007*. Cancer Epidemiol Biomarkers Prev, 2011. **20**(1): p. 183-6.
241. Di, J., et al., *A Meta-Analysis of the Impact of Obesity, Metabolic Syndrome, Insulin Resistance, and Microbiome on the Diagnosis of Barrett's Esophagus*. Dig Dis, 2020. **38**(3): p. 165-177.
242. Yap, Y.A. and E. Marino, *An Insight Into the Intestinal Web of Mucosal Immunity, Microbiota, and Diet in Inflammation*. Front Immunol, 2018. **9**: p. 2617.
243. Whiteman, D.C., et al., *Association of Helicobacter pylori infection with reduced risk for esophageal cancer is independent of environmental and genetic modifiers*. Gastroenterology, 2010. **139**(1): p. 73-83; quiz e11-2.
244. Islami, F. and F. Kamangar, *Helicobacter pylori and esophageal cancer risk: a meta-analysis*. Cancer Prev Res (Phila), 2008. **1**(5): p. 329-38.
245. Anderson, L.A., et al., *Relationship between Helicobacter pylori infection and gastric atrophy and the stages of the oesophageal inflammation, metaplasia, adenocarcinoma sequence: results from the FINBAR case-control study*. Gut, 2008. **57**(6): p. 734-9.
246. Pei, Z., et al., *Bacterial biota in reflux esophagitis and Barrett's esophagus*. World J Gastroenterol, 2005. **11**(46): p. 7277-83.
247. Logan, R.P. and M.M. Walker, *ABC of the upper gastrointestinal tract: Epidemiology and diagnosis of Helicobacter pylori infection*. BMJ, 2001. **323**(7318): p. 920-2.
248. Meng, C., et al., *Human Gut Microbiota and Gastrointestinal Cancer*. Genomics Proteomics Bioinformatics, 2018. **16**(1): p. 33-49.
249. Wroblewski, L.E., R.M. Peek, Jr., and L.A. Coburn, *The Role of the Microbiome in Gastrointestinal Cancer*. Gastroenterol Clin North Am, 2016. **45**(3): p. 543-56.
250. Engle, S.J., et al., *Elimination of colon cancer in germ-free transforming growth factor beta 1-deficient mice*. Cancer Res, 2002. **62**(22): p. 6362-6.
251. Vijay-Kumar, M., et al., *Metabolic syndrome and altered gut microbiota in mice lacking Toll-like receptor 5*. Science, 2010. **328**(5975): p. 228-31.
252. Ley, R.E., et al., *Obesity alters gut microbial ecology*. Proc Natl Acad Sci U S A, 2005. **102**(31): p. 11070-5.
253. Ley, R.E., et al., *Microbial ecology: human gut microbes associated with obesity*. Nature, 2006. **444**(7122): p. 1022-3.

254. Kokolus, K.M., et al., *Baseline tumor growth and immune control in laboratory mice are significantly influenced by subthermoneutral housing temperature*. Proc Natl Acad Sci U S A, 2013. **110**(50): p. 20176-81.
255. Esposito, K., et al., *Metabolic syndrome and risk of cancer: a systematic review and meta-analysis*. Diabetes Care, 2012. **35**(11): p. 2402-11.
256. Russo, A., M. Autelitano, and L. Bisanti, *Metabolic syndrome and cancer risk*. Eur J Cancer, 2008. **44**(2): p. 293-7.
257. Ibrahim, Y.H. and D. Yee, *Insulin-like growth factor-I and cancer risk*. Growth Horm IGF Res, 2004. **14**(4): p. 261-9.
258. Trayhurn, P. and I.S. Wood, *Adipokines: inflammation and the pleiotropic role of white adipose tissue*. Br J Nutr, 2004. **92**(3): p. 347-55.
259. Braun, S., K. Bitton-Worms, and D. LeRoith, *The link between the metabolic syndrome and cancer*. Int J Biol Sci, 2011. **7**(7): p. 1003-15.
260. Miyazawa-Hoshimoto, S., et al., *Elevated serum vascular endothelial growth factor is associated with visceral fat accumulation in human obese subjects*. Diabetologia, 2003. **46**(11): p. 1483-8.
261. Saito, I., *Epidemiological evidence of type 2 diabetes mellitus, metabolic syndrome, and cardiovascular disease in Japan*. Circ J, 2012. **76**(5): p. 1066-73.
262. Despres, J.P., et al., *Abdominal obesity and the metabolic syndrome: contribution to global cardiometabolic risk*. Arterioscler Thromb Vasc Biol, 2008. **28**(6): p. 1039-49.
263. Sun, L., et al., *Gut microbiota and intestinal FXR mediate the clinical benefits of metformin*. Nat Med, 2018. **24**(12): p. 1919-1929.
264. Li, F., et al., *Microbiome remodelling leads to inhibition of intestinal farnesoid X receptor signalling and decreased obesity*. Nat Commun, 2013. **4**: p. 2384.
265. Zhang, L., et al., *Farnesoid X Receptor Signaling Shapes the Gut Microbiota and Controls Hepatic Lipid Metabolism*. mSystems, 2016. **1**(5): p. e00070-16.
266. Fu, T., et al., *FXR Regulates Intestinal Cancer Stem Cell Proliferation*. Cell, 2019. **176**(5): p. 1098-1112 e18.
267. Nuber, A.H., *Analysis of the function of Farnesoid X Receptor in a mouse model of Barrett's Esophagus and Adenocarcinoma* 2016, Technische Universität München: München.
268. Park, B.S. and J.O. Lee, *Recognition of lipopolysaccharide pattern by TLR4 complexes*. Exp Mol Med, 2013. **45**(12): p. e66.
269. Cani, P.D., et al., *Metabolic endotoxemia initiates obesity and insulin resistance*. Diabetes, 2007. **56**(7): p. 1761-72.

270. Neal, M.D., et al., *Enterocyte TLR4 mediates phagocytosis and translocation of bacteria across the intestinal barrier*. J Immunol, 2006. **176**(5): p. 3070-9.
271. Schaefer, T.M., et al., *Toll-like receptor (TLR) expression and TLR-mediated cytokine/chemokine production by human uterine epithelial cells*. Immunology, 2004. **112**(3): p. 428-36.
272. Ohta, K., et al., *Toll-like receptor (TLR) expression and TLR-mediated interleukin-8 production by human submandibular gland epithelial cells*. Mol Med Rep, 2014. **10**(5): p. 2377-82.
273. Kim, G.Y., et al., *Proinflammatory cytokine IL-1beta stimulates IL-8 synthesis in mast cells via a leukotriene B4 receptor 2-linked pathway, contributing to angiogenesis*. J Immunol, 2010. **184**(7): p. 3946-54.
274. Li, J., et al., *Regulation of IL-8 and IL-1beta expression in Crohn's disease associated NOD2/CARD15 mutations*. Hum Mol Genet, 2004. **13**(16): p. 1715-25.
275. Schinke, C., et al., *IL8-CXCR2 pathway inhibition as a therapeutic strategy against MDS and AML stem cells*. Blood, 2015. **125**(20): p. 3144-52.
276. Lee, Y.S., et al., *Interleukin-8 and its receptor CXCR2 in the tumour microenvironment promote colon cancer growth, progression and metastasis*. Br J Cancer, 2012. **106**(11): p. 1833-41.
277. Emadi, S., et al., *IL-8 and its CXCR1 and CXCR2 receptors participate in the control of megakaryocytic proliferation, differentiation, and ploidy in myeloid metaplasia with myelofibrosis*. Blood, 2005. **105**(2): p. 464-73.
278. Chen, M.C., et al., *CXCL2/CXCR2 axis induces cancer stem cell characteristics in CPT-11-resistant LoVo colon cancer cells via Galphai-2 and Galphaq/11*. J Cell Physiol, 2019. **234**(7): p. 11822-11834.
279. Sinclair, A., et al., *CXCR2 and CXCL4 regulate survival and self-renewal of hematopoietic stem/progenitor cells*. Blood, 2016. **128**(3): p. 371-83.
280. Infanger, D.W., et al., *Glioblastoma stem cells are regulated by interleukin-8 signaling in a tumoral perivascular niche*. Cancer Res, 2013. **73**(23): p. 7079-89.
281. Jung, J.H., et al., *CXCR2 and its related ligands play a novel role in supporting the pluripotency and proliferation of human pluripotent stem cells*. Stem Cells Dev, 2015. **24**(8): p. 948-61.
282. Alexeev, V., et al., *Pro-Inflammatory Chemokines and Cytokines Dominate the Blister Fluid Molecular Signature in Patients with Epidermolysis Bullosa and Affect Leukocyte and Stem Cell Migration*. J Invest Dermatol, 2017. **137**(11): p. 2298-2308.
283. Molendijk, J., et al., *Chronic High-Fat Diet Induces Early Barrett's Esophagus in Mice through Lipidome Remodeling*. Biomolecules, 2020. **10**(5).

284. Hugenholtz, F. and W.M. de Vos, *Mouse models for human intestinal microbiota research: a critical evaluation*. Cell Mol Life Sci, 2018. **75**(1): p. 149-160.
285. Pissetsky, D.S., *Of mice, men and microbes: the impact of the microbiome on immune responses*. Ann Rheum Dis, 2020. **79**(2): p. 167-169.
286. Nguyen, T.L., et al., *How informative is the mouse for human gut microbiota research?* Dis Model Mech, 2015. **8**(1): p. 1-16.
287. Gevers, D., et al., *The treatment-naive microbiome in new-onset Crohn's disease*. Cell Host Microbe, 2014. **15**(3): p. 382-392.
288. Lavelle, A., et al., *Spatial variation of the colonic microbiota in patients with ulcerative colitis and control volunteers*. Gut, 2015. **64**(10): p. 1553-61.
289. Reyman, M., et al., *Rectal swabs are a reliable proxy for faecal samples in infant gut microbiota research based on 16S-rRNA sequencing*. Sci Rep, 2019. **9**(1): p. 16072.
290. Mosconi, I., et al., *Intestinal bacteria induce TSLP to promote mutualistic T-cell responses*. Mucosal Immunol, 2013. **6**(6): p. 1157-67.
291. El Aidy, S., et al., *Temporal and spatial interplay of microbiota and intestinal mucosa drive establishment of immune homeostasis in conventionalized mice*. Mucosal Immunol, 2012. **5**(5): p. 567-79.
292. Mangifesta, M., et al., *Mucosal microbiota of intestinal polyps reveals putative biomarkers of colorectal cancer*. Sci Rep, 2018. **8**(1): p. 13974.
293. Beyaz, S., et al., *High-fat diet enhances stemness and tumorigenicity of intestinal progenitors*. Nature, 2016. **531**(7592): p. 53-8.
294. Duggan, C., et al., *Association between markers of obesity and progression from Barrett's esophagus to esophageal adenocarcinoma*. Clin Gastroenterol Hepatol, 2013. **11**(8): p. 934-43.
295. Quince, C., et al., *Removing noise from pyrosequenced amplicons*. BMC Bioinformatics, 2011. **12**: p. 38.
296. Quince, C., et al., *Accurate determination of microbial diversity from 454 pyrosequencing data*. Nat Methods, 2009. **6**(9): p. 639-41.
297. Huse, S.M., et al., *Ironing out the wrinkles in the rare biosphere through improved OTU clustering*. Environ Microbiol, 2010. **12**(7): p. 1889-98.
298. Shakya, M., et al., *Comparative metagenomic and rRNA microbial diversity characterization using archaeal and bacterial synthetic communities*. Environ Microbiol, 2013. **15**(6): p. 1882-99.
299. Burke, C., et al., *Bacterial community assembly based on functional genes rather than species*. Proc Natl Acad Sci U S A, 2011. **108**(34): p. 14288-93.

300. Schulz, M.D., et al., *High-fat-diet-mediated dysbiosis promotes intestinal carcinogenesis independently of obesity*. Nature, 2014. **514**(7523): p. 508-12.
301. Wiethaler, M., et al., *BarrettNET-a prospective registry for risk estimation of patients with Barrett's esophagus to progress to adenocarcinoma*. Dis Esophagus, 2019. **32**(8).
302. Eisenberg, S.P., et al., *Primary structure and functional expression from complementary DNA of a human interleukin-1 receptor antagonist*. Nature, 1990. **343**(6256): p. 341-6.
303. Arend, W.P., et al., *Interleukin-1 receptor antagonist: role in biology*. Annu Rev Immunol, 1998. **16**: p. 27-55.
304. McIntyre, K.W., et al., *Inhibition of interleukin 1 (IL-1) binding and bioactivity in vitro and modulation of acute inflammation in vivo by IL-1 receptor antagonist and anti-IL-1 receptor monoclonal antibody*. J Exp Med, 1991. **173**(4): p. 931-9.
305. Seckinger, P., et al., *A urine inhibitor of interleukin 1 activity that blocks ligand binding*. J Immunol, 1987. **139**(5): p. 1546-9.
306. Mazzei, G.J., et al., *Purification and characterization of a 26-kDa competitive inhibitor of interleukin 1*. Eur J Immunol, 1990. **20**(3): p. 683-9.
307. Carter, D.B., et al., *Purification, cloning, expression and biological characterization of an interleukin-1 receptor antagonist protein*. Nature, 1990. **344**(6267): p. 633-8.
308. Arend, W.P., et al., *Biological properties of recombinant human monocyte-derived interleukin 1 receptor antagonist*. J Clin Invest, 1990. **85**(5): p. 1694-7.
309. Fischer, E., et al., *Comparison between effects of interleukin-1 alpha administration and sublethal endotoxemia in primates*. Am J Physiol, 1991. **261**(2 Pt 2): p. R442-52.
310. Ohlsson, K., et al., *Interleukin-1 receptor antagonist reduces mortality from endotoxin shock*. Nature, 1990. **348**(6301): p. 550-2.
311. Mengozzi, M., et al., *Inhibition by interleukin 1 receptor antagonist of in vivo activities of interleukin 1 in mice*. Lymphokine Cytokine Res, 1991. **10**(5): p. 405-7.
312. Champion, G.V., et al., *Dose-range and dose-frequency study of recombinant human interleukin-1 receptor antagonist in patients with rheumatoid arthritis. The IL-1Ra Arthritis Study Group*. Arthritis Rheum, 1996. **39**(7): p. 1092-101.
313. Bresnihan, B., et al., *Treatment of rheumatoid arthritis with recombinant human interleukin-1 receptor antagonist*. Arthritis Rheum, 1998. **41**(12): p. 2196-204.
314. Rubbert-Roth, A. and A. Perniok, *[Interleukin-1 receptor antagonist anakinra (Kineret) for treatment of rheumatic arthritis]*. Z Rheumatol, 2003. **62**(4): p. 367-77.

315. Dinarello, C.A., A. Simon, and J.W. van der Meer, *Treating inflammation by blocking interleukin-1 in a broad spectrum of diseases*. *Nat Rev Drug Discov*, 2012. **11**(8): p. 633-52.
316. Lust, J.A., et al., *Reduction in C-reactive protein indicates successful targeting of the IL-1/IL-6 axis resulting in improved survival in early stage multiple myeloma*. *Am J Hematol*, 2016. **91**(6): p. 571-4.
317. Medicine, N.L.o. *ClinicalTrials.gov*. Available from: <https://clinicaltrials.gov/ct2/results?cond=cancer&term=Anakinra&cntry=&state=&city=&dist=&Search=Search>.
318. Jensen, H.K., et al., *Presence of intratumoral neutrophils is an independent prognostic factor in localized renal cell carcinoma*. *J Clin Oncol*, 2009. **27**(28): p. 4709-17.
319. Reid, M.D., et al., *Tumor-infiltrating neutrophils in pancreatic neoplasia*. *Mod Pathol*, 2011. **24**(12): p. 1612-9.
320. Fossati, G., et al., *Neutrophil infiltration into human gliomas*. *Acta Neuropathol*, 1999. **98**(4): p. 349-54.
321. Hebbeler, A.M., et al., *Individual Vgamma2-Jgamma1.2+ T cells respond to both isopentenyl pyrophosphate and Daudi cell stimulation: generating tumor effectors with low molecular weight phosphoantigens*. *Cancer Immunol Immunother*, 2007. **56**(6): p. 819-29.
322. Lanca, T., et al., *Protective role of the inflammatory CCR2/CCL2 chemokine pathway through recruitment of type 1 cytotoxic gammadelta T lymphocytes to tumor beds*. *J Immunol*, 2013. **190**(12): p. 6673-80.
323. Patil, R.S., et al., *IL17 producing gammadeltaT cells induce angiogenesis and are associated with poor survival in gallbladder cancer patients*. *Int J Cancer*, 2016. **139**(4): p. 869-81.
324. Dieli, F., et al., *Targeting human {gamma}delta T cells with zoledronate and interleukin-2 for immunotherapy of hormone-refractory prostate cancer*. *Cancer Res*, 2007. **67**(15): p. 7450-7.
325. Nakajima, J., et al., *A phase I study of adoptive immunotherapy for recurrent non-small-cell lung cancer patients with autologous gammadelta T cells*. *Eur J Cardiothorac Surg*, 2010. **37**(5): p. 1191-7.
326. Sakamoto, M., et al., *Adoptive immunotherapy for advanced non-small cell lung cancer using zoledronate-expanded gammadeltaTcells: a phase I clinical study*. *J Immunother*, 2011. **34**(2): p. 202-11.
327. Lang, J.M., et al., *Pilot trial of interleukin-2 and zoledronic acid to augment gammadelta T cells as treatment for patients with refractory renal cell carcinoma*. *Cancer Immunol Immunother*, 2011. **60**(10): p. 1447-60.

328. Godfrey, D.I., et al., *NKT cells: what's in a name?* Nat Rev Immunol, 2004. **4**(3): p. 231-7.
329. Cui, J., et al., *Requirement for Valpha14 NKT cells in IL-12-mediated rejection of tumors.* Science, 1997. **278**(5343): p. 1623-6.
330. Kitamura, H., et al., *The natural killer T (NKT) cell ligand alpha-galactosylceramide demonstrates its immunopotentiating effect by inducing interleukin (IL)-12 production by dendritic cells and IL-12 receptor expression on NKT cells.* J Exp Med, 1999. **189**(7): p. 1121-8.
331. Kawano, T., et al., *Antitumor cytotoxicity mediated by ligand-activated human V alpha24 NKT cells.* Cancer Res, 1999. **59**(20): p. 5102-5.
332. Terabe, M., et al., *NKT cell-mediated repression of tumor immunosurveillance by IL-13 and the IL-4R-STAT6 pathway.* Nat Immunol, 2000. **1**(6): p. 515-20.
333. Terabe, M., et al., *Transforming growth factor-beta production and myeloid cells are an effector mechanism through which CD1d-restricted T cells block cytotoxic T lymphocyte-mediated tumor immunosurveillance: abrogation prevents tumor recurrence.* J Exp Med, 2003. **198**(11): p. 1741-52.
334. Terabe, M., et al., *A nonclassical non-Valpha14Jalpha18 CD1d-restricted (type II) NKT cell is sufficient for down-regulation of tumor immunosurveillance.* J Exp Med, 2005. **202**(12): p. 1627-33.
335. Kavanagh, M.E., et al., *Altered T Cell Migratory Capacity in the Progression from Barrett Oesophagus to Oesophageal Adenocarcinoma.* Cancer Microenviron, 2019. **12**(1): p. 57-66.
336. Daster, S., et al., *Low Expression of Programmed Death 1 (PD-1), PD-1 Ligand 1 (PD-L1), and Low CD8+ T Lymphocyte Infiltration Identify a Subgroup of Patients With Gastric and Esophageal Adenocarcinoma With Severe Prognosis.* Front Med (Lausanne), 2020. **7**: p. 144.
337. Dutta, S., et al., *The relationship between tumour necrosis, tumour proliferation, local and systemic inflammation, microvessel density and survival in patients undergoing potentially curative resection of oesophageal adenocarcinoma.* Br J Cancer, 2012. **106**(4): p. 702-10.
338. Vane, J.R., *Inhibition of prostaglandin synthesis as a mechanism of action for aspirin-like drugs.* Nat New Biol, 1971. **231**(25): p. 232-5.
339. Muscat, J.E., S.D. Stellman, and E.L. Wynder, *Nonsteroidal antiinflammatory drugs and colorectal cancer.* Cancer, 1994. **74**(7): p. 1847-54.
340. Liu, Y., et al., *Effect of aspirin and other non-steroidal anti-inflammatory drugs on prostate cancer incidence and mortality: a systematic review and meta-analysis.* BMC Med, 2014. **12**: p. 55.
341. Tsoi, K.K.F., et al., *Long-term use of low-dose aspirin for cancer prevention: A 10-year population cohort study in Hong Kong.* Int J Cancer, 2019. **145**(1): p. 267-273.

342. Grosch, S., et al., *Cyclooxygenase-2 (COX-2)-independent anticarcinogenic effects of selective COX-2 inhibitors*. J Natl Cancer Inst, 2006. **98**(11): p. 736-47.
343. Alfonso, L., et al., *Molecular targets of aspirin and cancer prevention*. Br J Cancer, 2014. **111**(1): p. 61-7.
344. McCarty, M.F. and K.I. Block, *Preadministration of high-dose salicylates, suppressors of NF-kappaB activation, may increase the chemosensitivity of many cancers: an example of proapoptotic signal modulation therapy*. Integr Cancer Ther, 2006. **5**(3): p. 252-68.
345. Sorensen, H.T., et al., *Risk of upper gastrointestinal bleeding associated with use of low-dose aspirin*. Am J Gastroenterol, 2000. **95**(9): p. 2218-24.
346. Verbeek, R.E., et al., *Toll-like receptor 4 activation in Barrett's esophagus results in a strong increase in COX-2 expression*. J Gastroenterol, 2014. **49**(7): p. 1121-34.
347. Jankowski, J.A.Z., et al., *Esomeprazole and aspirin in Barrett's oesophagus (AspECT): a randomised factorial trial*. Lancet, 2018. **392**(10145): p. 400-408.
348. Singh, J. and B.S. Reddy, *Molecular markers in chemoprevention of colon cancer. Inhibition of expression of ras-p21 and p53 by sulindac during azoxymethane-induced colon carcinogenesis*. Ann N Y Acad Sci, 1995. **768**: p. 205-9.
349. Samaha, H.S., et al., *Modulation of apoptosis by sulindac, curcumin, phenylethyl-3-methylcaffeate, and 6-phenylhexyl isothiocyanate: apoptotic index as a biomarker in colon cancer chemoprevention and promotion*. Cancer Res, 1997. **57**(7): p. 1301-5.
350. Suh, N., et al., *Combination of atorvastatin with sulindac or naproxen profoundly inhibits colonic adenocarcinomas by suppressing the p65/beta-catenin/cyclin D1 signaling pathway in rats*. Cancer Prev Res (Phila), 2011. **4**(11): p. 1895-902.
351. Rao, C.V., et al., *Chemoprevention of colon carcinogenesis by sulindac, a nonsteroidal anti-inflammatory agent*. Cancer Res, 1995. **55**(7): p. 1464-72.
352. Skinner, S.A., A.G. Penney, and P.E. O'Brien, *Sulindac inhibits the rate of growth and appearance of colon tumors in the rat*. Arch Surg, 1991. **126**(9): p. 1094-6.
353. Takayama, T., et al., *Randomized double-blind trial of sulindac and etodolac to eradicate aberrant crypt foci and to prevent sporadic colorectal polyps*. Clin Cancer Res, 2011. **17**(11): p. 3803-11.
354. Yin, T., et al., *Sulindac, a non-steroidal anti-inflammatory drug, mediates breast cancer inhibition as an immune modulator*. Sci Rep, 2016. **6**(1): p. 19534.
355. Moon, H., et al., *Krt5(+)/Krt15(+) foregut basal progenitors give rise to cyclooxygenase-2-dependent tumours in response to gastric acid stress*. Nat Commun, 2019. **10**(1): p. 2225.

7. Appendix

7.1 p-values Unifrac VAT SPF

Table 13: p-values for generalized UniFrac using non-metric Multi-Dimensional Scaling of VAT and SPF samples

Samples are separated by genotype, diet and holding facility. p-values were calculated after PERMANOVA with Bonferroni-Hochberg post-hoc testing and are rounded to 4 digits.

Comparison	Corrected p-value	Comparison	Corrected p-value
SPF-L2-Control vs SPF-Wt-Chow	0.0038	SPF-L2-Chow vs VAT-L2-HFD	0.0094
SPF-Wt-Control vs SPF-Wt-Chow	0.0038	VAT-L2-Control vs SPF-L2-Chow	0.0108
VAT-L2-HFD vs SPF-Wt-Chow	0.0038	VAT-L2-Control vs SPF-Wt-Chow	0.0113
VAT-Wt-Control vs SPF-L2-Chow	0.0038	VAT-Wt-HFD vs VAT-L2-HFD	0.0113
VAT-L2-Control vs SPF-Wt-HFD	0.0038	SPF-L2-HFD vs VAT-L2-HFD	0.0113
VAT-Wt-HFD vs SPF-L2-HFD	0.0038	VAT-Wt-Control vs SPF-Wt-Control	0.0120
VAT-Wt-HFD vs SPF-Wt-Chow	0.0038	SPF-Wt-HFD vs VAT-L2-HFD	0.0120
SPF-L2-Chow vs SPF-Wt-HFD	0.0038	VAT-L2-Control vs SPF-L2-HFD	0.0203
SPF-L2-Chow vs SPF-Wt-Control	0.0038	VAT-L2-Control vs SPF-Wt-Control	0.0225
SPF-L2-HFD vs SPF-L2-Control	0.0038	VAT-Wt-Control vs SPF-L2-HFD	0.0286
SPF-L2-HFD vs SPF-Wt-Control	0.0038	VAT-Wt-Control vs SPF-Wt-Chow	0.0357
SPF-Wt-HFD vs SPF-L2-Control	0.0038	VAT-L2-Control vs SPF-L2-Control	0.0399
VAT-Wt-HFD vs SPF-Wt-Control	0.0056	VAT-Wt-Control vs VAT-L2-HFD	0.0463
SPF-L2-Chow vs SPF-L2-Control	0.0056	VAT-Wt-Control vs VAT-Wt-HFD	0.0715
SPF-Wt-HFD vs SPF-Wt-Chow	0.0056	VAT-Wt-Control vs SPF-Wt-HFD	0.0715
SPF-L2-Control vs VAT-L2-HFD	0.0056	VAT-L2-Control vs VAT-Wt-HFD	0.0715
VAT-Wt-Control vs SPF-L2-Control	0.0075	VAT-Wt-HFD vs SPF-Wt-HFD	0.0776
SPF-L2-HFD vs SPF-Wt-Chow	0.0075	VAT-L2-Control vs VAT-L2-HFD	0.0790
SPF-Wt-Control vs VAT-L2-HFD	0.0082	VAT-Wt-Control vs VAT-L2-Control	0.1628
VAT-Wt-HFD vs SPF-L2-Chow	0.0082	SPF-L2-Control vs SPF-Wt-Control	0.1643
VAT-Wt-HFD vs SPF-L2-Control	0.0082	SPF-L2-HFD vs SPF-Wt-HFD	0.1718
SPF-Wt-HFD vs SPF-Wt-Control	0.0082	SPF-L2-Chow vs SPF-Wt-Chow	0.9470
SPF-L2-Chow vs SPF-L2-HFD	0.0094		

7.2 Indicator species

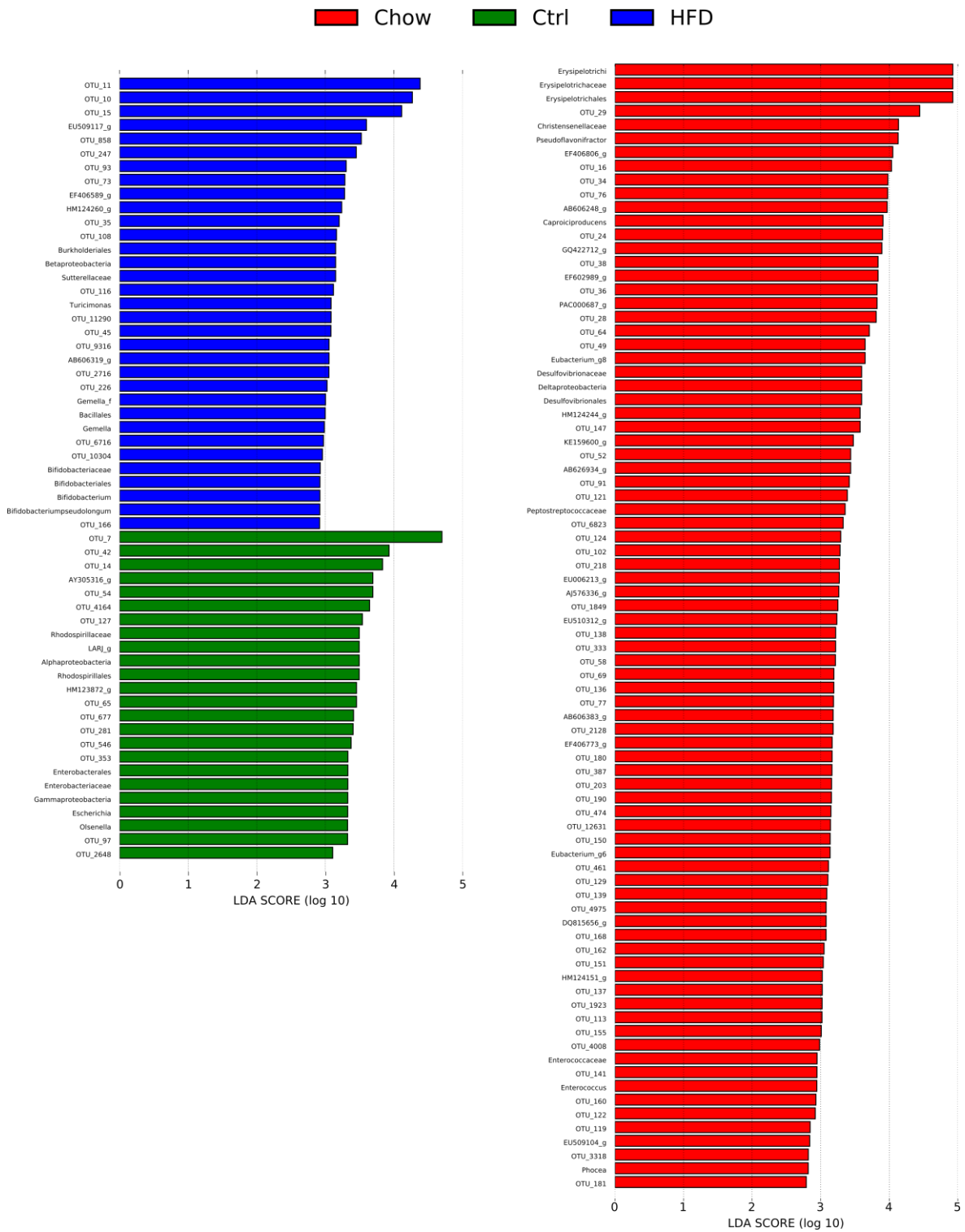


Figure 47: Results of the LDA Effect Size (LEfSe) analysis of the 26 weeks timepoint of the SPF cohort based on the diet

Curriculum vitae

Jonas Ingermann

Dauthendeystraße 30

81377 München

jonas.ingermann@gmx.net

Beruflicher Werdegang

- | | |
|-----------------|----------------------------------------------------------------------------------------------------------------------------|
| 12/2018-heute | Wissenschaftlicher Mitarbeiter in der gynäkologischen Tumorgenetik am Klinikum Rechts der Isar der Technischen Universität |
| 04/2014-12/2018 | Doktorand am Klinikum Rechts der Isar der Technischen Universität München im Graduiertenkolleg 1482 der DFG, AG Quante |

Schule&Studium

- | | |
|-----------------|-------------------------------------------------------------------------------------------------------------------|
| 10/2011-09/2013 | Studium der Biologie an der Ludwigs-Maximilians-Universität München, Schwerpunkt Humanbiologie, Master of Science |
| 10/2008-09/2011 | Studium der Biologie an der Technischen Universität München, Bachelor of Science |
| 06/2007 | Allgemeine Hochschulreife |

Acknowledgments

First I would like to thank Dr. Michael Quante, who always supported me and whose lab has always been an exciting place to work at. Without his support and understanding this thesis would never have been finished. Thanks to Professor Dr. Dirk Haller and Prof. Dr. Martin Klingenspor who enriched the GRK 1482 with their knowledge and were always willing to help and shared knowledge and equipment with us.

Thanks to all the lablings! You guys made the lab like a second home where colleagues are also friends. Special thanks go to Natasha, who took me under her wings and introduced me into lab work and Freising SPF. I'd also like to thank all the other "Old" people at the lab, who helped me and have been a lot of fun to work with: Thanks Hsin-Yu, Tina, Steffi, Andi, Julia H., Marina, Vincenz, Carlo, Anna and Moritz! Thank you Maria for your help and dealing with a supervisor who wasn't around for most of the time! And also a big thank you to the "new" Quante lab: Thanks Akanksha, Theresa and Julia! You guys helped me a lot over the last years!

Special thanks goes to Anja, Mathilde and Thorsten as well! It almost felt like I was a part of your lab, but only for the fun.

And of course thanks to my family who had to deal with me panicking every once in a while, especially Moni and Nikki!